ATMOSPHERIC FORCING OF WAVE STATES IN THE SOUTHEAST CHUKCHI SEA

By

Oceana Puananilei Francis

RECOMMENDED: _____

_____

_____

_____

_____
Advisory Committee Chair

_____
Chair, Department of Atmospheric Sciences

APPROVED: _____
Dean, College of Natural Science and Mathematics

_____
Dean of the Graduate School

_____
Date

ATMOSPHERIC FORCING OF WAVE STATES IN THE SOUTHEAST CHUKCHI SEA

A

DISSERTATION

Presented to the Faculty

of the University of Alaska Fairbanks

In Partial Fulfillment of the Requirements

for the Degree of

DOCTOR OF PHILOSOPHY

By

Oceana P. Francis, P.E., M.Sc.

Fairbanks, Alaska

May 2012

Abstract

The objective of this study was to assess the impact that the ocean state, particularly ocean waves, have on coastal communities and operations in the Western Alaska region. *In situ* measurements and one-dimensional spectra models, were used to link observed wave activity – wind-sea and swells – to their synoptic drivers. Bottom-mounted Recording Doppler Current Profilers (RDCPs) were placed at offshore and nearshore locations in the southeast Chukchi Sea, Alaska, during 2007 and 2009-2010. The highest significant wave height (SWH) "events" were defined as wave heights above 2m and 3m for a duration of 6h or more. Results show that SWH events appeared to be driven by three types of systems, 1) cyclonic systems that moved into the eastern Bering Sea and then stalled there, 2) cyclonic systems that moved into the eastern Chukchi Sea and then loitered there, and 3) a cyclonic system over the Brooks Range, a less common occurrence. Results also show the offshore region having highest SWHs with an east wind and wave direction, and classified as a wind-sea state. For the nearshore region, highest SWHs with south and west wind and wave directions, generally showed a swell state. Agreement between one-dimensional spectral models and in situ measurements was greatest for the higher wind-sea state in the offshore region, while discrepancies arose for the lower swell state in the nearshore region.

Cross-validation of *in situ* measurements with satellite altimeter radar measurements were also conducted. Good correlation was found for the offshore regions

but not for the nearshore regions. Satellite observations were also used to assess wave conditions in the Arctic during the years 1993-2011. A 0.020m/year increase of SWH for the SE Chukchi Sea and a 0.025m/year increase for the Pacific-Arctic, was found which correlates well with diminishing sea ice and the heighted wind speed, also shown in this study.

Dedication

This dissertation is dedicated to one of the earliest ocean navigators in the World, Polynesians, who used only the stars, ocean currents and swells to guide them across the Pacific Ocean.

Table of Contents

Page

List of Figures

Page

List of Tables

Page

List of Appendices

Page

Acknowledgements

The people and institutions I have come in contact with during my PhD have either added to my work, my dissertation, or my life into what it is today. With this, I would like to first and foremost thank Dr. David Atkinson, my former PhD advisor, who has guided me through my PhD work from 2005-2010 at the University of Alaska Fairbanks (UAF), who provided his expertise in describing synoptic conditions qualitatively, helped me with *SAS* Business Analytics software (used on another project), and who I have continued to work on publications with after he accepted a position at University of Victoria, BC. I also want to especially thank Dr. Uma Bhatt, who took over as my PhD advisor from 2010-present whose leadership, moral support, and guidance has helped me finish my PhD. I would like to thank the other committee members Dr. John Walsh (atmospheric sciences), Dr. Andrew Metzger (civil engineering), Dr. Tom Weingartner (physical oceanography) for taking their time out to be on my committee and provide me with their ideas on how to make my dissertation better with their recommendations.

For technical assistance, I want to thank Dr. Gleb Panteleev, International Arctic Research Center (IARC), and Dr. Robert Jensen, Engineering Research and Development Center - Coastal and Hydraulics Laboratory, Vicksburg, MS for their enormous help with satellite data (part of this dissertation), and the WAM wave model (a separate

publication). I have learned so much and continue to learn from their enormous knowledge in data processing, modeling, physical oceanography, and ocean engineering.

I would also like to acknowledge my co-authors which whose work is listed in Appendix A.

This dissertation was sponsored by the Cooperative Institute for Arctic Research (CIFAR) with funds from the National Oceanic and Atmospheric Administration (NOAA) under cooperative agreement NA17RJ1224 with the University of Alaska. Funding also provided by NOAA projects, NA06OAR4600179 and NA08OAR4600856. I am grateful to NCAR and AVISO for providing their data sets in the public domain.

All logistic support for gathering *in situ* measurements came from Teck and Foss Maritime, whose support made this project possible. So many personnel went into making this a success both the crewmen on the Foss tugboats who retrieved and deployed the instruments, and the personnel at Teck who I interacted with and responsible for storing, handling and shipping the equipment safely. I would especially like to thank Jim Kulas, Ted Zigarlick, Bill Willis, John Terry, Kie Curtis, Scott Olson, Paul Wooden, and Eric Skewis. Without their assistance in making things happen, this project would not have been possible. I also want to thank the UAF personnel who assisted me with the field work of the RDCPs and High Frequency Radars (used for another project) who were Julie Malingowski, Rachel Potter, and Hank Skatewich, and Rob Chadwell (former). Rob Chadwell (former) was especially helpful in teaching me his vast knowledge of retrieval and deployment of oceanographic instruments, and IARC shipping/handling procedures.

I also want to thank Dr. Igor Polykov for allowing me to use the assistance of two of his mooring technicians.

At Aanderaa Data Instruments (AADI) I would like to thank Richard Butler, Brandon Rieff, Ivan Victoria, Helge Minken, Jarle Heltne, and Emilie Dorgeville who hosted me during my factory visits, spent their time talking to me, and shared their technical knowledge of the Recording Doppler Current Profiler instrument.

I would also like to thank David Atkinson's family, his wife Kathy Atkinson, and his two children Kenny and Emma for their hospitality.

For getting me the facts about PhD deadlines I would like to thank, from UAF, Dr. Nicole Mölders, Barbara Day, and Laura Bender.

My colleagues/friends at the International Arctic Research Center and Geophysical Institute were a great support. I thank Dr. Martha Shulski (former), Dr. Michel Mesquita (former), Rebecca Legatt (former), Rena Bryan (former), Peter Bienek, D. Oliver Dammann (former), Jeanie Talbot, Dr. Jenny Hutchings, Dr. Harper Simmons (former), Tohru Saito, Dr. Jessie Cherry, Dr. Taro Nakai, Dr. Vladimir Alexeev, Dr. Dmitry Nicolsky, and Dr. Javier Fochesatto.

I want to thank the IARC IT personnel Christopher Swingley (former), Jim Long, and Matt Barkdull for their computing help. I want to especially thank Jim Long for helping me with technical computing issues and retrieving data off a completely a failed hard drive. Without all of their amazing IT support to keep things running, my computers (a Linux, a Windows, and a Mac) would have gone to "computer heaven" a long time

ago. I also want to thank all of the administrative support at IARC, who were both very helpful and kind, but especially Sarah Garcia and Kim Cox for their extra help in handling and processing equipment purchases and taking care of my PhD funding in the end after the departure of my former PhD adviser. I also want to thank Dr. Syun-Ichi Akasofu and Dr. Larry Hinzman for their support.

I would also like to acknowledge the people who inspired me the most while I worked at Alyeska Pipeline Service Company (APSC) doing engineering for the summer during a break from my PhD, Greg Kinney, Greg Coombs, Michael Pestrikoff, and Lorena Hegdal.

I would also like to thank MSPHDS (Minority Striving and Pursuing Higher Degrees of Success), and ANSEP (Alaska Native Science and Engineering Program), and ASCE (American Society of Civil Engineers) whose organizations I was closely affiliated with during my years as a PhD student and who helped shape my future.

I would also like to thank from the Fairbanks civil engineering community for their friendship during my service as an officer for the American Society of Civil Engineers in Fairbanks, Dr. Andrew Metzger, Dr. Bob Perkins, Mark Sherman, and Quentin Gehring. From ANSEP (Alaska Native Science and Engineering Program), I would like to thank Dr. Bill Schnabel, Dr. Tom Clausen, Robin Weinant, and Dr. Herb Schroeder.

I would also like to thank Frank Chythlook, a close family friend, who encouraged me to move to Fairbanks to pursue my PhD. I am also grateful to have his

family in my life who live in Fairbanks, Grete Chythlook, Rose Beth Levno, and John Chythlook.

I want to especially thank my sister, Jen, who took care of my father while I pursued my PhD, encouraged me to complete my PhD, and who I know will always be there for me both emotionally and while I pursue my career. She has also always been my role model. I also want to thank my father (living) and mother (deceased) who always encouraged me to work hard and follow my ambition in getting a PhD. My parents have always been there for me, and I am truly grateful.

Oceana Puananilei Francis

October 2011

Chapter 1 Introduction

The impact of the ocean state, particularly ocean waves, is greatly influenced by environmental parameters. The Arctic region is especially vulnerable to these environmental parameters (ACIA, 2005). Predicting extreme wave states from sea ice, teleconnection patterns, synoptic activity, and winds have been performed for numerous studies (Wang et al., 2004; Caires et al., 2006; Wang and Swail, 2006; Grabemann and Weisse, 2008; Lowe et al., 2010; Vanem, 2010; Le Cozannet et al., 2011). Le Cozannet et al. (2011) used teleconnection patterns to describe wave states. In comparison, Wang and Swail (2006) used mean sea level pressure to describe wave states. Lowe et al. (2010) describes predicting extreme wave states. Vanem (2010) and Caires et al. (2006) use different modeling processes, such as stochastic and Poisson processes to model extreme wave states. Grabemann and Weisse (2008) use the numerical wave model WAM and wind fields to predict extreme wave conditions. A consistent finding of these studies is that wave states are predicted to change, that is, generally increase, in the future. These studies also demonstrate that scenarios of wave states can be successfully predicted using a variety of models and input forcing.

Ocean wave states greatly influence the coastal communities and industrial operations in the Western Alaska region. In particular, the Southeast Chukchi Sea region is a key area for the Alaska economy since the Delong Mountain Terminal (DMT) (Figure 1.1), the largest shipping port in Western Alaska, is the only large marine terminal in the Arctic Western Alaska deep enough to handle large ships. This area is also

the region of the Bering Strait – Pacific gateway to the Arctic and already an area traversed by ships from many countries, something that will only continue to grow as sea ice continues to retreat.

Figure 1.1 - Delong Mountain Terminal
Wave action during an August 2008 storm at Delong Mountain Terminal (Red Dog Port site), Alaska. Taken by: Scott Olson, Red Dog Port Captain, Foss Maritime Company, Seattle WA on August 5, 2008.

The DMT is used by businesses, such as Teck Alaska Inc. and Foss Maritime for shipping mining materials, and also by the US government for research and/or operations, such as National Oceanic and Atmospheric Administration (NOAA), the US Army Corps of Engineers (USACE), and the US Coast Guard (USCG). There is also interest by

USCG to develop the DMT further in order to accommodate further infrastructure development in Western Alaska. With the decrease of multi-year sea ice, the presence of open water is increasing the navigable period for ships so there is an interest in developing the DMT further as the key port site for the Arctic Region.

The present state of understanding wave characteristics in the Southeast Chukchi Sea region has come through the Wave Information Study (WIS) (Jensen et al., 2002). WIS uses the numerical wave model WAM to estimate swell and wind-sea for various grid points along the Alaskan coastline. WAM was developed by the WAMDI Group (1988) and solves energy balance equation, $S = S_{wind} + S_{nonlin} + S_{dissip}$ (Hasselmann et al., 1973). Using wind forcing, it shows wind-sea and swell for the different grid points, with an additional feature of generating directional wave spectra (compared to one-dimensional wave spectra in our study).

The studies outlined above have several shortcomings for the region of the southeast Chukchi Sea. First, defining the wave state for this region has never been done before. The wave state (or sea state) is the typical condition of the water surface with respect to wind-sea and swell at a certain time interval and location. The wave state is statistically characterized and is defined by wave height, period, and wave spectrum. The sea state varies with time, and can be measured with instruments or estimated through analytical or numerical solutions using wind forcing. From the previous study done in this region (Jensen et al., 2002), it had been speculated that some wave energy is transmitted through the Bering Sea. However, an explicit linkage between observed wave

states with its synoptic drivers was never conducted. This study explores the storms that create this wave energy and where that wave energy is directed using *in situ* observations and one-dimensional models.

A second element missing from wave studies in this region is a quantitative description of the wave states using simple one-dimensional models. Although not a complete description of wave state, it is used in many forecasting and engineering applications due to its ease of use in distinguishing wind-sea and swell without wave direction. Parameters such as the peak enhancement factor of the JONSWAP, which is presently unknown for this region, have been estimated here by using one-dimensional models. The peak enhancement factor is the ratio of maximum spectral energy to the maximum Pierson-Moskowitz (PM) spectrum (Pierson and Moskowitz, 1964). In the JONSWAP spectrum (Hasselmann et al., 1973), the peak enhancement factor ranges from 1.6 to 6. This parameter varies depending on the conditions of the ocean region under consideration; thus, performing a detailed wave analysis will add to the knowledge of one-dimensional wave spectral models in this region.

A third important unknown for this region is documenting possible trends in significant wave heights. Although studies have been performed which investigate the trend of significant wave heights in lower latitude and global regions, the Chukchi Sea has to date not been investigated. The time is right to evaluate trends since 17 years of remote sensing data is available. In this study, wind speed and sea ice trends are explored

in conjunction with significant wave height trends to provide additional insight on the relations between sea ice decline and storm activity affecting waves in the Chukchi Sea.

The Southeast Chukchi Sea area is a complex environment. It is important to define local meteorological events since these events define the wave climate of the region. This region comes under frequent influence of storms that have moved in from formation regions in the North Pacific, along trajectories that take them into the Bering Strait and Gulf of Alaska, and sometimes through the Strait into the Chukchi Sea itself (Mesquita et al., 2010). A secondary storm pathway runs roughly east-west across the north Russian/Alaska coast. These storm pathways are also examined in this study. Further details on atmospheric processes related to these storms can be found in Appendix B.

Some wave energy generated in the North Pacific and Bering Sea does pass through the Bering Strait. However, the highest locally generated wind-seas are often created by extra-tropical storms, which create meso-scale winds that originate from the Kotzebue Sound, not through the Bering Strait, which was found in this study. The fetch available over the Chukchi Sea and Arctic Ocean to the north also play a role in wave generation in late summer/early autumn. The multi-year sea ice in the Arctic influences the active wave growth domain in the Chukchi Sea and Arctic Ocean (Young et al., 2011). However, with the decline of sea ice, resulting in longer open water seasons, fetch has increased allowing longer distance for wave generation. Thus, there is a rapidly growing need to improve understanding of the specific linkages between atmospheric

forcing and the resultant sea state. An overview of basic wind-wave theory is provided in Appendix C.1.

Past studies have been performed using one-dimensional models (Hasselmann et al., 1976; Lewis and Allos, 1990; Young, 1992) and further studies of these one-dimensional models are used to separate wind-sea and swell (Ewing, 1980; Mitsuyasu et al., 1980; Wang and Hwang, 2001). The method used in this study for determining wind-sea versus swell is currently used by the US National Data Buoy Center (Wang and Hwang, 2001). Further quantitative information on wind-sea versus swell is given in Appendix C.2.

One-dimensional wave spectra are useful for describing wave characteristics generated by a storm. There are two types of one-dimensional wave spectral models, the Joint North Sea Wave Project (JONSWAP) spectrum (Hasselmann et al., 1973), and the TEXEL storm, MARSEN, ARSLOE (TMA) spectrum (Bouws et. al., 1985) which can be used to show the frequency distribution of waves. The JONSWAP, a fetch-limited deep water model and the TMA, a fetch-limited depth-limited model, were adequate in this study to describe the conditions due to several features. These features included: 1) the enclosed embayment of shoreline surrounding the southeast Chukchi Sea region, 2) the direction from which winds and wave propagated – from the enclosed shoreline which created fetch-limited conditions, and 3) the shallow water environment of the nearshore *in situ* wave measurements. Appendix D gives a description of the basic wave spectra formulation.

Airy (1845) wave theory is also used for the modeling of random sea states. The Airy wave theory gives a good estimate of wave characteristics and their effects for purposes in ocean and coastal engineering (Goda, 2000, Dean and Dalrymple, 1991). Further, several second-order nonlinear properties of surface gravity waves (i.e. Stokes, 1847) can be estimated from the results of the Airy waves (Phillips, 1977).

Satellite altimeter radar observations offer homogeneous and global coverage of the surface sea state compared to *in situ* observations, which only provide localized coverage. Satellite altimeter radar observations of significant wave heights have been compared to *in situ* observations in many studies (e.g. Janssen et al., 2007; Li and Holt, 2007; Zieger et al., 2009; Young, 1994). These studies show that satellite altimeter radar observations are highly accurate and *in situ* observations were not always accurate due to an unstable mounting system used, or system calibration of the instrument. In comparison, satellite observations are continuously recalibrated and maintained. Because of the high level of accuracy of satellite observations, using satellite data allows performing a cross-validation between *in situ* observations and satellite observations.

1.1. Project motivation

From the preceding, four main needs may be drawn: 1) Sea states in the Arctic are becoming increasingly severe, damaging infrastructure (e.g. houses, schools) in the southeast Chukchi Sea, so understanding these processes is important toward preparedness, 2) the Delong Mountain Terminal located in this region, is the only port in the western US Arctic (above the Arctic Circle) that can support shipping activities of significant size. Since there is so little infrastructure in this region, and due to the fact that it is anticipated there will be a substantial increase in activity in the coming years, especially with increased shipping traffic in the Arctic due to anticipated continued sea ice decline, makes the Delong Mountain Terminal a valuable asset, 3) the lack of measured wave data in the Chukchi Sea also prompted our experimental design to gather *in situ* wave measurements for this study, and 4) with the sea ice decline, the need to document trends over the past few decades and explore trends of future wave states becomes even more necessary.

In situ wave measurements (RDCP wave data) provided wave information for three different regions in the southeast Chukchi Sea, an offshore location - north of Shishmaref, Alaska in 2007 (34m), and two nearshore locations – one near Cape Krusenstern, Alaska (18m) and the other between DMT and Kivalina (17m), Alaska in 2009-2010. These sites were considered optimal locations for gathering wave data in terms of shallow bathymetry for acoustic signals, no sea ice scouring the ocean floor (since they were deployed on the ocean floor), and the availability of Foss Maritime

tugboats to deploy and retrieve the instruments. It must be noted that support for the observational portion of this project came from Teck and Foss Maritime who generously provided room-and-board, deployment and retrievals costs. This was essential to project success.

Another motivation was to investigate the wave state in the Arctic due to the decline in sea ice in recent years. The Arctic Ocean has always been covered by multi-year sea ice throughout the year. The multi-year sea ice covers a vast expanse of the central Arctic Ocean basin which retreats in late summer/early autumn to more or less leave open shallow areas along the continental shelves of Eurasia and North America – the Arctic Marginal Seas (e.g. Chukchi Sea, Laptev Sea). But with the decline of sea ice due to global warming in recent years (Comiso et al., 2008; Screen and Simmonds, 2010; Perovich and Richter-Menge, 2009; Zhang, 2010) could come a change in wave states. Although the waves in the Arctic Ocean never develop to the extent observed in the open ocean regions of the Pacific or Indian Oceans, there is a point at which waves can be considered swell even for a shallow, enclosed environment like the southeast Chukchi Sea. The southeast Chukchi Sea has a shallow uniform continental shelf and is dominated by shorter period waves (i.e. 4-5 sec wave period for a 1-3m significant wave height). For an enclosed seas with shallow bathymetry, such as the Chukchi Sea, shorter period swell are normally generated as opposed to the longer period swell waves which dominate the World's Oceans. As with all swell, these waves, which are generated from storm activity, move away from the generating area and are no longer influenced by winds. An

additional influence to fetch is a longer Arctic open water season due to the decline of sea ice. Therefore swell conditions occur when the conditions dictate, even for shallow regions.

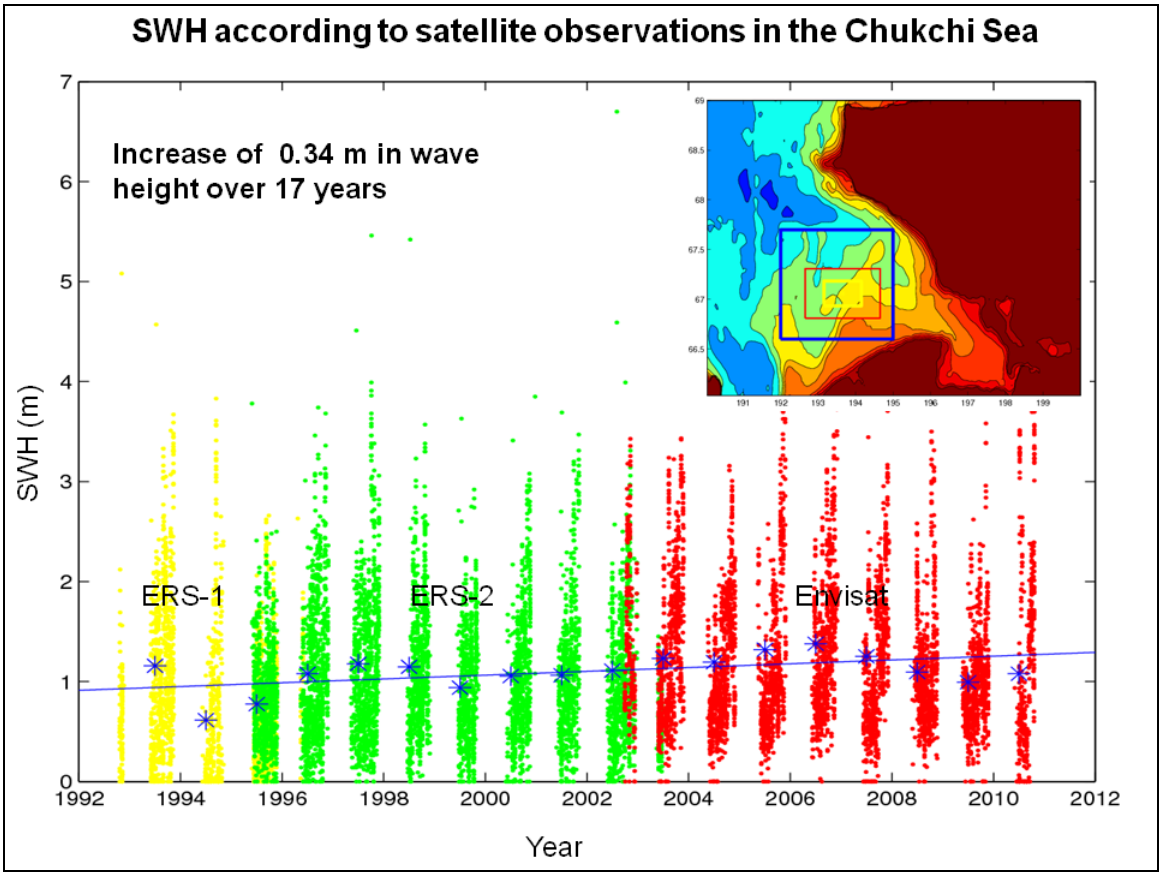

Figure 1.2 – Satellite trend over Chukchi Sea
Satellite significant wave height (SWH) measurements from ERS-1/2 and Envisat in the southeast Chukchi Sea from 1993-2010. The mean average SWH for each year are also shown (blue stars). Inset (top right) figure shows three domains. The domain (largest blue square) shows all satellite SWH observations for each year (yellow/green/red dots) shown in Figure 1.2. The smaller domains (red and yellow squares) are used for satellite SWHs described in Chapter 5. The color contours show the bathymetry in 10m increments.

Another motivation for this study was to determine the trend of the wave state in this region by using satellite analysis of significant wave heights which had never been

performed. From the satellite trend over the southeast Chukchi Sea performed for this study, the trend shows that the estimated mean significant wave height has increased 0.34m over the past 17 years (Figure 1.2). This significant wave height increase was assessed to be statistically significant as will be shown in Chapter 5, with the correlation to sea ice concentration. The motivation for studying wave states by means of satellite analysis in this region then becomes clearer: to help predict future wave states. The closest study of significant wave height trends performed near this region was for the North Pacific region by Young et al. (2011) who showed a slight decrease in the wind speed and wave height trend. Their study area excluded the Chukchi Sea, prompting this analysis of significant wave height trends for the Chukchi Sea and Pacific-Arctic sectors. In addition, the RDCP data provided an opportunity to validate and analyze satellite estimates of significant wave heights for this region, which had also not been performed before.

1.2. Project Goals

Therefore, from the motivations discussed, one of the main overarching goals for this PhD dissertation was to develop an ocean wave synthesis for the southeast Chukchi Sea, Alaska through investigation of *in situ* measurements, modeling, and long term satellite data. The ocean wave synthesis performed in this study can be summarized by region (Figure 1.3). These areas of focus are as follows: a) Synoptic scale meteorological events in the Bering and Chukchi Seas/Pacific-Arctic Ocean (Fig 1.3 – upper and lower dashed boxes), b) One-dimensional wave spectral modeling and satellite wave analysis in the southeast Chukchi Sea (Fig 1.3 – solid box), and c) Satellite wave analysis in the Pacific-Arctic Ocean (Fig 1.3 – upper dashed box).

The tools used for this study include: 1) *In situ* measurements gathered with Recording Doppler Current Profilers (RDCP) to collect observational wave measurements and validation of all analyses performed in this study, 2) Satellite altimeter radar measurements which include Envisat, ERS 1 and 2 for evaluating past wave trend and estimating future wave trend, and 3) Phase-resolving models which include Stoke's wave theory to classify waves, and one-dimensional wave spectral models which include the JONSWAP (Hasselmann et al., 1973), TMA (Bouws et. al., 1985) to produce wind-sea versus swell identification. Phase-resolving models are fully deterministic models based on hydrodynamics conservation laws, i.e. conservation of mass, momentum and energy (Losada and Revilla, 2009).

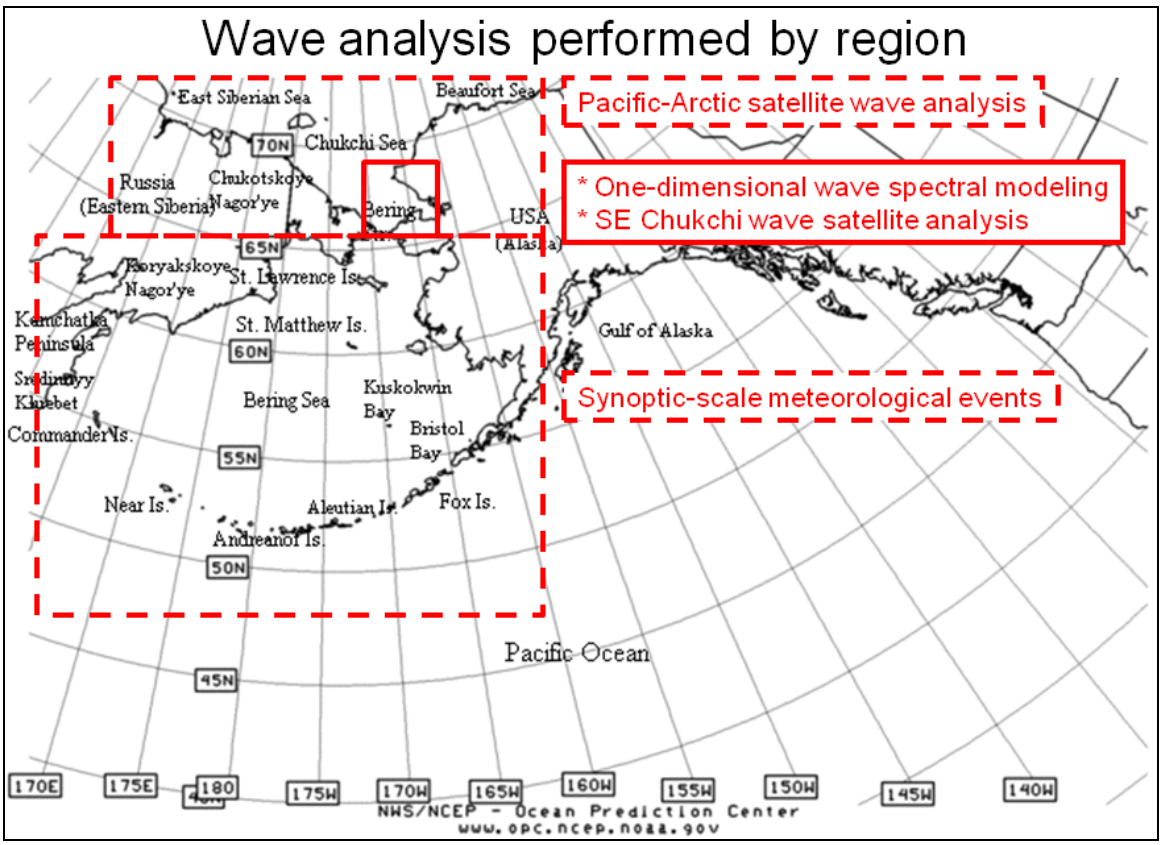

Figure 1.3 – Research analysis performed by region
The ocean wave synthesis performed by region: 1) Synoptic scale meteorological events in the Bering and Chukchi Seas/Pacific-Arctic Ocean (upper and lower dashed boxes), 2) One-dimensional wave spectral modeling and satellite wave analysis in the southeast Chukchi Sea (solid box), and 3) Satellite wave analysis in the Pacific-Arctic Ocean (upper dashed box).

The NCEP/NCAR Global Reanalysis, 1.0° resolution atmospheric dataset NCEP/National Center for Atmosphere Research Global Reanalysis data set (Kistler et al., 2001), and the NARR (North American Regional Reanalysis), 0.30° resolution reanalysis (Mesinger et al., 2006) provide wind forcing and atmospheric conditions for this study.

A secondary goal along technical/methodological lines concerned assessing the suitability of the various wave analysis approaches – *in situ*, satellite, modeling, and wind tools – for this difficult to access region. *In situ* wave measurements using RDCPs (see Appendix E for a technical summary) were placed in the southeast Chukchi Sea during July-December 2007 UTC and October 2009-September 2010 UTC (in water depths of 30-, 18-, 17-m). This data was used for two main purposes: to perform wave analysis and provide linkages to meteorological conditions. This data was also used for cross-validation with one-dimensional wave models and satellite altimetry data, the other two tools in this study. Wave data derived from satellite altimeter were also used to identify recent wave state trends.

The focus of these efforts can be addressed by the following research hypothesis of this dissertation: "Wave states in the Chukchi Sea, Bering Sea, and Pacific Arctic regions have displayed change throughout the last few decades, which can be attributed to environmental parameters such as sea-ice variability, and can be shown by the tools for analyzing waves used in this study, i.e. *in situ* and satellite measurements, and modeling." Therefore, three questions will be answered to address this hypothesis:

1. What is the best characterization of present wave states in the southern Chukchi Sea?
2. What are the atmospheric drivers responsible for the observed wave state in this region?

3. What has been the trend of the wave states in the Chukchi Sea over the last few decades, and what is the largest contributor to observed change: sea ice retreat or a change in the synoptic wind regime?

Following the Introduction chapter, the dissertation is divided up into four main scientific papers focusing on the three major questions identified above. This entails, Chapters 2 and 3 which focuses on the occurrence of waves from *in situ* observations and their synoptic drivers in the southeast Chukchi Sea for the offshore and nearshore regions, respectively, and classifies these storm events as wind-sea or swell. Chapter 4 classifies the wave state in the southeast Chukchi Sea using simple phase-resolving models, and uses two one-dimensional wave spectra models to distinguish wind-sea versus swell and validates these spectral models with *in situ* observations. Chapter 5 investigates satellite altimeter radar observations to determine the trend of significant wave heights in the southeast Chukchi Sea and Pacific-Arctic, and cross-validates these results using *in situ* observations for the southeast Chukchi Sea. Chapter 6 presents an overall Conclusion.

References

ACIA (2005). *Arctic Climate Impact Assessment*. Cambridge University Press, 1042 pp.

Airy, G.B. (1845). Tides and waves. *Encyc. Metrop.*, 192, 241–396.

Bouws, E., H. Gunther, W. Rosenthal, and C.L. Vincent (1985). Similarity of the Wind Wave Spectrum in Finite Depth Water 1. Spectral Form. *Journal of Geophysical Research*, Vol. 90, No. C1, pp. 975-986.

Caires, S., V.R. Swail, and X.L. Wang (2006). Projection and Analysis of Extreme Wave Climate. *Journal of Climate* 19:21, 5581-5605.

Comiso, J. C., C.L. Parkinson, R. Gersten, and L. Stock (2008). Accelerated decline in the Arctic sea ice cover. *Geophys. Res. Lett*. 35 doi:10.1029/2007GL031972.

Dean, R.G. and R.A. Dalrymple (1991). Water *wave mechanics for scientists and engineers*. Advanced Series on Ocean Engineering, 2. World Scientific. Publishing Company.

Ewing, J.A. (1980). Observations of Wind-waves and Swell at an Exposed Coastal Location. *Estuarine and Coastal Marine Science* 10, 543-554.

Goda, Y. (2000). *Random Seas and Design of Maritime Structures*. Advanced Series on Ocean Engineering. **15**. Singapore: World Scientific Publishing Company.

Grabemann, I. and R. Weisse (2008). Climate change impact on extreme wave conditions in the North Sea: an ensemble study. *Ocean Dynamics* 58:3-4, 199-212.

Hasselmann, K., T.P. Barnett, E. Bouws, H. Carlson, D.E. Cartwright, K. Enke, J.A. Ewing, H. Gienapp, D.E. Hasselmann, P. Kruseman, A. Meerburg, P. Müller, D.J. Olbers, K. Richter, W. Sell and H. Walden (1973). Measurements of wind-wave growth and swell decay during the Joint North Sea Wave Project (JONSWAP). *Deutsche Hydrographische Zeitschrift* A8 (12), 95pp.

Hasselmann, K., D.B. Ross, P. Müller and W. Sell, (1976). A parametric wave prediction model. *Journal of Physical Oceanography*, 6**,** pp. 200–228.

Janssen, P., S. Abdalla, H. Hersbach, J-R. Bidlot (2007) Error Estimation of Buoy, Satellite, and Model Wave Height Data. *J. Atmos. Oceanic Technol.*, 24, 1665–1677. doi:10.1175/JTECH2069.1

Jensen, R., N. Scheffner, S.J. Smith, D. Webb, and B. Ebersole. (2002). *Engineering Studies in Support of Delong Mountain Terminal Project ERDC/CHL TR-02-26*, September 2002, Vicksburg, MS.

Kistler, R., E. Kalnay, W. Collins, S. Saha, G. White, J. Woollen, M. Chelliah, W. Ebisuzaki, M. Kanamitsu, V. Kousky, H. van den Dool, R. Jenne, and M. Fiorino, (2001). The NCEP-NCAR 50-Year Reanalysis: Monthly Means CD-ROM and Documentation. *Bull. Amer. Meteor. Soc*., 82, 247-267.

Le Cozannet, G., S. Lecacheux, E. Delvallee, N. Desramaut, C. Oliveros, R. Pedreros (2011). Teleconnection Pattern Influence on Sea-Wave Climate in the Bay of Biscay. *J. Climate*, 24, 641–652.

Lewis, A.W. and R.N Allos (1990). JONSWAP's parameters: sorting out the inconsistencies. *Ocean Engineering*, 17, 409-415.

Li, J-G. and M. Holt (2007). Validation of a regional wave model with Envisat and Buoy observations. Proc. 'Envisat Symposium 2007', Montreux, Switzerland, 23–27 April 2007 (*ESA SP-636, July 2007)*.

Losada, I.J. and J.A. Revilla (2009). Applications to Fluid Mechanics: Water Wave Propagation, in Continuum Mechanics, (eds. Jose Merodio), in Encyclopedia of Life Support Systems (EOLSS), Developed under the Auspices of the UNESCO, Eolss Publishers, Oxford, UK, [http://www.eolss.net]

Lowe, J. A., Woodworth, P. L., Knutson, T., McDonald, R. E., McInnes, K. L., Woth, K., von Storch, H., Wolf, J., Swail, V., Bernier, N. B., Gulev, S., Horsburgh, K. J., Unnikrishnan, A. S., Hunter, J. R. and Weisse, R. (2010). *Past and Future Changes in Extreme Sea Levels and Waves, in Understanding Sea-Level Rise and Variability* (eds J. A. Church, P. L. Woodworth, T. Aarup and W. S. Wilson), Wiley-Blackwell, Oxford, UK. doi: 10.1002/9781444323276.ch11

Mesinger, F., G. DiMego, E. Kalnay, K. Mitchell, P.C. Shafran, W. Ebisuzaki, D. Jovic, J. Woollen, E. Rogers, E.H. Berbery, M.B. Ek, Y. Fan, R. Grumbine, W. Higgins, H. Li, Y. Lin, G. Manikin, D. Parrish, and W. Shi (2006). North American Regional Reanalysis. Boulder, CO NOAA.OAR/ESRL PSD:42.

Mesquita, M.D.S., D.E. Atkinson, and K.I. Hodges (2010). Characteristics and Variability of Storm Tracks in the North Pacific, Bering Sea, and Alaska. *Journal of Climate*, 23, 294-311. DOI: 10.1175/2009JCLI3019.1

Mitsuyasu, H., F. Tasai, T. Suhara, S. Mizuno, M. Ohkusu, T. Honda, and K. Rikiishi (1980). Observation of the Power Spectrum of Ocean waves Using a Cloverleaf Buoy. *Journal of Physical Oceanography*, 10, pp. 286-296.

Perovich D.K., J.A. Richter-Menge (2009). Loss of sea ice in the Arctic. *Annu Rev Mar Sci* 1:417–441.

Phillips, O. M. (1977). *The Dynamics of the Upper Ocean*, 336 pp., Cambridge Univ. Press, New York.

Pierson W.J. and L. Moskowitz (1964). A proposed spectral form for fully developed wind seas based on the similarity theory of S. A. Kitaigorodskii, *Journal of Geophysical Research* Vol. 69, No. 24, pp. 5181–5190.

Screen, J. A. and I. Simmonds (2010). The central role of diminishing sea ice in recent Arctic temperature amplification. *Nature* 464, 1334–1337, doi:10.1038/nature09051, 2010

Stokes G.G. (1847). On the theory of oscillatory waves. *Trans Cambridge Philos Soc*, 8, 441-473.

Vanem, E. (2010). Long-term time-dependent stochastic modelling of extreme waves. *Stochastic Environmental Research and Risk Assessment*. Volume 25, Number 2, 185-209, doi: 10.1007/s00477-010-0431-y

WAMDI Group (1988). The WAM model—A third generation ocean wave prediction model. *J. Phys. Oceanogr.,*18**,** 1775–1810.

Wang, D.W. and P.A. Hwang (2001). An Operation Method for Separating Wind Sea and Swell from Ocean Wave Spectra. *Journal of Atmospheric and Oceanic Technology*, 18, pp. 2052-2062.

Wang, X.L., F.W. Zwiers, V.R. Swail, (2004). North Atlantic Ocean Wave Climate Change Scenarios for the Twenty-First Century. *J. Climate*, 17, 2368–2383.

Wang, X.L. and V.R. Swail (2006). Climate change signal and uncertainty in projections of ocean wave heights. *Climate Dynamics* 26:2-3, 109-126.

Young, I.R. (1992). The determination of spectral parameters from significant wave ehight and peak period. *Ocean Engineering*, 19, 5, 497-508.

Young I.R. (1994). Global ocean wave statistics obtained from satellite observations. *Appl. Ocean Res.* 16*,* 235.

Young, I.R., S. Zieger, A.V. Babanin (2011). Global trends in wind speed and wave height. *Science* 332, pp. 451-455. DOI:10.1126/science.1197219.

Zhang, X. (2010). Sensitivity of Arctic summer sea ice coverage to global warming forcing: Toward reducing uncertainty in Arctic climate change projections. *Tellus* A. 62:220-227.

Zieger, S., J. Vinoth, I. R. Young (2009). Joint calibration of multiplatform altimeter measurements of wind speed and wave height over the past 20 years. *J. Atmos. Ocean. Technol.* 26*,* 2549.

Chapter 2 Synoptic forcing of wave states in the southeast Chukchi Sea, Alaska, at an offshore location[1]

Abstract

A bottom-mounted Recording Doppler Current Profiler (RDCP) was placed at an offshore location (depth of 34m) in the southeast Chukchi Sea, Alaska, from July through December, 2007 (UTC) with the objective of linking observed wave activity – wind-sea and swells – to their synoptic drivers. A total of 47 intervals of elevated wave state were recorded: 29 exceeding 1m significant wave height (SWH), 16 exceeding 2m SWH, and 3m exceeded on two occasions; during one of those a SWH of 4m was observed. Detailed analysis of the two large events, including comparison with high-resolution reanalysis wind data (North America Regional Reanalysis), showed wave direction from the east, varied about 15° to the north (counterclockwise) from the wind direction, and current flow in the opposite direction (from the west). This is thought to be the influence of a strong "wind-sea" presence. Regarding classic wave limitations, although the SE Chukchi Sea is a large embayment bordered by land to the east, fetch limitations from the northeast and southeast did not appear to be a constraint for the wind speeds indicated by reanalysis. These two events appeared to be driven by winds associated with cyclonic systems that moved into the eastern Bering Sea and stalled. Examination of smaller waves associated with these events suggested that waves of 1.5m SWH or less are likely

[1] Francis, O.P. and D.E. Atkinson (2012). Synoptic forcing of wave state in the southeast Chukchi Sea, Alaska, at an offshore location. *Natural Hazards,* **in press**, doi: 10.1007/s11069-012-0142-4.

part of another regime and can either be swell or wind-sea, moving in from the open Chukchi Sea to the northwest or through the Bering Strait to the south.

2.1. Introduction

Severe wind-generated sea states affects most users and inhabitants of coastal regions: shipping operations, coastal communities, engineering considerations and planners. Coastal western Alaska (Chukchi and Bering Seas – Figures 2.1, 2.2) is particularly vulnerable to severe wave states. Although the quantity of infrastructure in this area is limited, it is typically critical for the communities served. The coastal area is vulnerable to storm events because of the low elevation, and residents living in close proximity to the water. The remoteness of this region means damages to coastal infrastructure are difficult and costly to repair due to the expense of shipping materials and crews into the area, and the limited construction season. In the last 17 years, due to a decrease in sea ice cover (i.e. interannual variations of local shorefast ice and the multiyear ice pack) that has increased fetch and the duration of open water season (Francis et. al, 2011 in press). The decrease in ice cover combined with large synoptic-scale extreme storm events which pass through the area increases the potential for major damage. For example, there has been an increase in coastal erosion at communities in this region such as Kivalina where several meters of shoreline are usually lost from a single storm event (USACE 2003; USACE 2004). A major industrial stakeholder in this area is Teck Alaska Inc., who operates the Delong Mountain Terminal. This facility has experienced periods when waves have caused shutdowns due either to direct impact on the terminal infrastructure or to set up of dangerous conditions for handling the large freighters, which given their length (up to 300m), can be especially susceptible to wave

action. Finally, wave climatologies and their results impact engineers and planners who must design for the maximum anticipated loads on infrastructure; the highest magnitude impact on coastal infrastructure in terms of kinetic energy is often due to wave action. In each of these cases, the limited knowledge of wave state and its atmospheric linkages in this region impedes arriving at a balance between cost-effectiveness and safety for coastal engineering structures. Further, this area is presently experiencing increased activity associated with interest in oil development. Thus, to improve design and operational resilience, there is a longstanding need to improve our understanding of the specific linkages between atmospheric forcing and the resultant sea state. Therefore, there is a particular interest in the wave regime in the Chukchi Sea. Using an observational wave data set from Recording Doppler Current Profilers (RDCP), this paper focuses on the occurrence of waves and their associated synoptic drivers in the SE Chukchi Sea. Specifically, the focus is identifying drivers of "wind-sea" (i.e. waves under influence of wind) versus those causing "swell" (i.e. waves moved away from wind generating area, and not under influence of wind).

The focus in this study is significant wave height, as high magnitude winds are directly correlated to wave heights. Significant wave height is the highest 33% of wave heights in the wave record. The significant wave height depends primarily on fetch (the distance over which the wind blows), wind speed, (commonly measured at the 10m elevation), and the duration of the wind. Wind speed of greater magnitude results in greater wave height. The duration which is the time the wind blows in one direction,

results in greater wave height the longer the duration. The fetch which is the distance the wind blows in one direction, results in greater wave height the longer the fetch. In a fully developed sea, maximum fetch and maximum duration are reached, and significant wave height solely becomes the function of wind speed.

The primary objective of this study is to identify and characterize the synoptic and meso-scale patterns that drive observed occurrences of significant wave height (SWH) events in the southeast Chukchi Sea. A secondary objective is to distinguish between the occurrence of swells and wind-sea. A third objective is to assess the extent to which wind data extracted from a widely used, high-resolution reanalysis data set (NCEP North America Regional Reanalysis) is correlated to the observed wave conditions found in the RDCP wave data set, and thus its suitability for longer-term modeling of wave forecasting and hindcasting in this region. Although it is known that reanalysis winds tend to underestimate peak storm wind speeds (Swail and Cox, 2000), especially the large spatial scale global reanalyses, what this means specifically for reproducing waves in the southeast Chukchi is not precisely known. These tasks will utilize observational data acquired from Recording Doppler Current Profilers (RDCP) placed in the southeast Chukchi Sea in 2007. Estimates of observed SWH event occurrences will be generated using data from the 32-km resolution "North American Regional Reanalysis (NARR)" atmospheric dataset (Mesinger et al., 2006) and the NCEP/DOE Global Reanalysis 2 (Kistler et al., 2001). It is hypothesized that, in the SE Chukchi Sea study area, the primary wave direction is from the northwest because that is the direction of greatest

fetch and the land formation around the Bering Strait allows minimal Bering Sea swell to propagate through. These factors are elaborated upon below.

The organization of the paper consists of an overview of the regional atmospheric setting and instrumentation background, a results section describing major observed wave events with detailed analysis and intermediate conclusions. Broader conclusions and discussion are provided in the discussion section. It was felt that it would be more efficient to analyze the wave events as they were described, for clarity.

2.2. Background

2.2.1. Atmospheric circulation and synoptic conditions

The synoptic situation governing the Bering and Chukchi Seas in the July through December timeframe is dominated by transient low pressure systems – "storms" – moving into the region from the North Pacific. Mesquita et al. (2010) conducted a seasonal analysis of storm properties in this region, including frequency. Their work showed higher levels of various indicators of storm activity in the fall and winter seasons, including frequency, intensity, and track speed. Most storm systems do not form locally but move into the region when upper level winds are favorable. The more typical end point for these North Pacific systems is the Gulf of Alaska, a favored end location; however the Bering Sea is also a common end point. One aspect of the location of the Bering Sea with respect to the typical position of the jet stream, especially in fall/winter/early spring, is that storm systems can often stall in the eastern Bering Sea, where they linger until they infill and dissipate. In some cases storms moving into the Bering Sea transit the Bering Strait and move up into the Chukchi Sea area. A secondary storm pathway – "northern" storms – runs roughly east to west across the north Russian/Alaska coast.

Most of these storms are extra-tropical cyclones. These large weather systems (1000's of km in extent) in general depend on baroclinic atmospheric conditions, which explains their greater frequency in the non-summer period (Mesquita et al., 2010). The most powerful systems, which can attain central mean sea level pressures down into the

930hPa range with winds of +100 knots, form under less-common conditions when large quantities of water vapor are available in the mid-troposphere and dynamical support is available in the form of a suitably-situated upper-air trough.

Wave conditions generated by these systems may be categorized into several broad groups. Bering Sea storms, depending on their track and position, produce an easterly to southeasterly local wind flow across the SE Chukchi Sea region. If the storm center is situated farther to the west, the winds can be southerly. These prevailing wind directions generate corresponding wind-sea in the SE Chukchi, and there is the potential for swell to be transmitted northwards through the Bering Strait, which may be more readily observed if the storm is positioned farther south and the wind-sea regime is weaker. Northern storms generate southeast winds and wave directions over this region. All of this is mitigated by the yearly development of shore-fast ice. During the part of the year when most of the Chukchi Sea is open water, strong winds from northern storms can operate over considerable fetch (hundreds of km), driving waves to the southeast into the SE Chukchi region.

2.2.2. Site selection and RDCP instrument deployment

The observational location in southeast Chukchi Sea was chosen for several reasons: little work has been done north of the Bering Strait on the synoptic driving of sea states, the area has demonstrable strong wave forcing (Jensen et al., 2002) and possesses an interesting and complex regime that can include wind-sea and swell (Jensen et al., 2002), and there are various at-risk coastal inhabitants (several villages and an industrial operator).

The overall project entailed three data-gathering efforts using RDCP (Recording Doppler Current Profiler) deployments. One RDCP was deployed to an open-water location (34m depth) during the ice-free period, July through December 2007 UTC ("2007" in Figure 2.2), discussed in this paper, and two RDCPs were later deployed to coastal locations during ice-free and ice-covered periods October 2009 through September 2010 UTC ("2009S" and "2009N" in Figure 2.2, depth of 17m and 18m, respectively), discussed in a forthcoming paper.

2.3. Methods and data

For this study wind and wave direction are taken to be of the same convention. Wind direction is defined as the direction *from which* the wind is coming and is given in degrees true bearing. Current direction is defined as the direction *to which* the current flow is going toward in degrees true bearing. The *true bearing* to a point is the angle measured in degrees in a clockwise direction from the north line.

2.3.1. Atmospheric datasets

Atmospheric parameters were obtained from the "North American Regional Reanalysis (NARR)" dataset (Mesinger et al., 2006). This gridded data of 0.3° and 1° resolution is taken from model runs which are point-source and scatterometer data assimilated into atmospheric fluid-dynamic modeled fields. This system, a "reanalysis" data set, was developed and is maintained by the National Centers for Environmental Prediction (NCEP) of the US National Oceanic and Atmospheric Administration (NOAA). For this project three parameters were extracted from the NARR dataset - geopotential height at 925hPa, vector wind at 925hPa, and vector wind at 10 m. Storm center, position and tracking were evaluated using geopotential height at 925hPa and vector wind at 925hPa. Local winds were evaluated using vector wind at 10m and extracted as time series from the NARR grid point nearest to the RDCP instrument location (Figure 2.2 for NARR grid point locations). Mean sea level pressure data from the NCEP/National Center for Atmosphere Research Global Reanalysis data set (Kistler et al., 2001), were also used in this analysis.

2.3.2. RDCP wave parameters

The bottom-positioned RDCP (AADI, 2006), by analyzing Doppler shifts of acoustic returns, recorded a number of wave observations denoted here as N. The sampling frequency of the RDCP is 2Hz. A given N is a reduction of 15 minutes of individual wave observations i=1800 samples; this cycle occurs every time the RDCP awakens, which was once every two hours. Station 2007 conducted one set 15 minute measurements every 2.0h, resulting in 3816h and 6 minutes total recording time, so the number of wave observations was N = 1704. Each observation i includes wave height H_i, wave period T_i and wave direction D_i. From these parameters the RDCP estimates the following: significant wave height, H_{m0}, mean wave period, T_{m01}, mean zero crossing, T_{m02} *or* $\overline{T}_z$, Energy wave direction, D_E, Mean direction, D_m, and Peak direction, D_p. For this study, significant wave height, H_{m0}, mean zero crossing, T_{m02}, and mean wave direction, D_m were retained for analysis. The mean zero crossing parameter, T_{m02}, is the time obtained by dividing the record length by the number of downcrossings (or upcrossings) in the record (AADI, 2006), compared to the mean wave period, T_{m01}, which is the wave period corresponding to the mean frequency of the spectrum (WMO, 1998). Figure 2.3 shows a graphical representation of how the mean zero crossing parameter, T_{m02} is calculated – from the individual zero crossing wave period, T_i, where the individual wave height, H_i, performs a zero-upcrossing (red circles).

Wave spectra was estimated using the Maximum Likelihood Method (MLM). Upper cutoff frequency was 0.6Hz. Fast Fourier Transform (FFT) size was 128.

2.3.3. Wave event and atmospheric analysis

A "significant wave height" event (SWH) was defined along the lines of similar approaches used in Hudak and Young (2002) and Francis-Chythlook (2004); that is, the wave magnitude exceeds and remains over a given threshold for a period of 6h or more in duration. Three threshold set-points were established: 1m, 2m, 3m. The SWH event was considered to have ended when the wave magnitude dropped below the threshold for 6h or more.

Spatial plots of pressure and winds were manually examined to assess the atmospheric state at the time of identified SWH events. The atmospheric forcing typically was a "storm" as defined by the existence of a closed low feature on a 925hPa. However, persistent patterns consisting of strong pressure gradient that were not storms in transient short wave sense are not uncommon in this region. The 925hPa level was chosen to minimize interference from surface conditions yet provide a level low enough to adequately represent surface pressure conditions.

2.4. Station 2007 Results

2.4.1. Station 2007 overview

In the July-December 2007 recording period forty-seven (SWH) events were identified: twenty-nine 1m, sixteen 2m, and two 3m. The longest duration events occurred in two distinct periods: mid September to mid October and November to early December. The longest duration/large magnitude events (2m and 3m events) occurred in late November to early December. The SWH (Figure 2.4) for July-December 2007 encompasses the entire RDCP Station 2007 wave record. The NARR 10-m wind speed (Figure 2.5) also for July-December 2007, is shown to correlate well with the SWH (Figure 2.4), especially for wind speeds > 6m s^{-1}. This suggests that the waves are wind-driven.

The RDCP mean wave direction (Figure 2.6) for July-December 2007 is shown to arrive from all directions, with the largest number of *N* waves arriving from the westerly and northerly directions. These waves generally had SWHs <2m. During July to September, the wave direction was shown to be mainly westerly and northerly where most of the SWHs were less than 1m. During September to November, the wave direction was mostly northerly and some easterly where SWHs were generally between 1-2m. During December, westerly and northerly wave directions dominated, while SWHs were generally between 1-1.5m.

Sea surface temperature (SST), monitored by Station 2007, dropped and remained below 0ºC starting December 6, 2007. The water temperature can indicate the potential

for shore-fast-ice development. However, due to the wave activity where a northerly SWH >2m was generated from a northerly wind direction >6 m s^{-1} during mid-December (Figure 2.4), sea ice was thought to form right after this period.

The NARR 10-m wind direction (Figure 2.7) was not correlated to wave direction for SWHs <1.5m. However, for SWHs greater than 2m (Table 2.1), the wave and wind directions showed the strongest correlation. The results shown in Table 2.1 refer to the wave and wind conditions when the significant wave height $\geq$ 2m during a particular "event" – where an "event" is described in Section 2.3.3. The two largest SWH events, both 3m, are examined below in detail: event "SWH-3m-3" known as SWH Event 1 or "SE1" (Table 2.1), 18-27 September 2007, and event "SWH-3m-15", known as SWH Event 2 or "SE2" (Table 2.1), 22 November - 2 December 2 2007. For these two events the wave signal evolution is overviewed, followed by an examination of the lifecycle of the storm or atmospheric condition identified as the driving mechanism for the SWH event. Finally, a consideration of near-surface winds at the RDCP location in the context of fetch is presented.

2.4.2. SE1 (SWH-3m-3), September 18-21, 2007 UTC

SE1 (SWH-3m-3) commenced September 18 0800 UTC (all times are given in UTC) and ended September 21 0600, lasting for a total duration of 70h with SWH in excess of 1m. In brief, the event proceeded as follows (Figure 2.8): rapid initiation and SWH increase from approximately 0.5m to 3.5m in the first 10h, maintained the peak wave condition for 16h, followed by rapid wave height decay to 1.0-1.5m, and remained at that elevated state for the next 30h. The directional estimates for this event began with a westerly 1m SWH (Figure 2.9) that was maintained for 5h (September 18 0800 to September 18 1300). On September 18, 1500 a rapid change in wave direction to easterly occurred. After this change, SWH increased rapidly from 1m to 2m (also wave period increased rapidly from 4.3s to 5.0s). For the next 54h (September 18 1500 to September 20 2100), wave direction remained easterly. During this 54-hour period, a 3m SWH was sustained for 16h (September 18 1900 to September 19 1100). Following the 3m SWH period, the SWH decreased to 2m for 7h until September 19 1800. The final 36h saw a SWH of 1m ending on September 21 0600. In the final 9h (September 20 2100 to September 21 0600), wave direction changed again, back to westerly.

The primary feature of the synoptic situation (Figure 2.10) that evolved during the lifespan of SE1 was a storm that occurred over 15-18 September, which appeared to be the source of winds necessary to support the observed wave response. The storm entered the southwestern Bering Sea on September 15 0000, between Komandorskiye Ostrova (Commander Islands) (Russia) and Near Islands (US) (see Figure 2.1 for geographical

locations). The pressure gradient was enhanced by the juxtaposition of a high-pressure system to the southeast, over the Gulf of Alaska, resulting in the highest wind speeds in the southeast quadrant of the system. Throughout the day on September 15, the storm moved eastward, positioning itself between Near Islands and Andreanof Islands with wind speeds (925hPa) increasing to 16m s^{-1} by 1500. The storm then moved northward, positioning itself between the Andreanof Islands and St. Matthew Island by 16 September 0000 with geopotential height and wind magnitude and direction remaining constant. A drop in geopotential height and an increase in wind speed (925hPa) began on September 16 1800 as the storm entered a period of strong intensification. Over the next nine hours the geopotential height dropped rapidly from 650m to 450m and the wind speed (925hPa) increased from 16m s^{-1} to 35m s^{-1} as the storm entered its peak intensity phase. Low geopotential height (compared to other locations at the same latitude) indicates the presence of a storm, so the drop in geopotential height signifies the intensification of the storm.

The peak of the storm spanned the period 17 September 0900 to 19 September 0600 (45h). The 925hPa geopotential height remained consistently low during this period: 400-450m. Corresponding winds during this time affected the entire Bering Sea, with the strongest observed winds over the Andreanof Islands. By this point storm winds were also affecting southeast Chukchi Sea: easterly winds of approximately 25m s^{-1} were now in place over Station 2007 (925hPa). The Mean Sea Level Pressure (MSLP) for this storm event reached and remained at its minimum of 970hPa for a 36 hour period from

17 September 0900 to 18 September 2100. This time frame encompassed the beginning of SE1. The storm intensity began to wane on September 19 0600; the period of maximum SWH lasted only a few hours longer. By 19 September 1500, 925hPa winds over Kotzebue Sound had dropped to 10m s^{-1}, becoming SSE.

Figure 2.11 shows the wave spectrum at the highest SWH during 19 September 0400, which was at the end of the peak storm period over the Bering Sea (17 September 0900 to 19 September 0600). This was also a few hours before the highest wind speeds (+16m s^{-1}) over the SE Chukchi Sea (10m wind level). The color bar (top) and non-directional (bottom) gives the wave energy density, $E(f)$, in m^2Hz^{-1}. The Cartesian contour plot (Figure 2.11) shows that the energy is contained in a range of frequencies from 0.10Hz to 0.15Hz and a 80° direction range for $E(f)$ >2 m^2Hz^{-1}. The non-directional peak energy density was 14.0m^2Hz^{-1} (Figure 13 – bottom) at 0.14Hz while the directional (Figure 13 – top) was centered at 0.14Hz coming from 105° (East). The integral wave parameters of this particular spectrum were SWH=3.7m, T_{m02}=5.8sec, T_{m01}=6.0sec. The mean winds during the period of the spectrum had a wind speed of U_{10}=16.2m s^{-1} with wind direction of U_{dir}=97°. Wind and wave direction were both easterly, where wave direction (105°) was at an 8° clockwise difference from wind direction (97°). The wave phase speed is given by $g/2\pi f_p$ (Ewing, 1980), where f_p is the peak frequency or the inverse of the peak period. With the wind speed (16.2m s^{-1}) and the RDCP peak period, f_p (6.0s) the wind speed was greater than the wave phase speed (9.4m s^{-1}). When the wind speed is greater than the wave phase speed, this indicates

"wind-sea". When the wind speed is less than the wave phase speed, this indicates "swell". Since the wind speed is much greater than the wave phase speed, this strongly indicates an easterly "wind-sea" for the event of 19 September 0400.

At the beginning of SE1 the wind (at the 10m level) was ESE at 6m s^{-1} with its fetch from the vicinity of Cape Espenberg. However, the wave direction was westerly instead of easterly (Figure 2.9); that is, opposite to the local wind over the RDCP. By September 18 1500 this was changing rapidly as the wave direction switched almost 180º to easterly, closely matching the local wind direction. The wind magnitude also increased rapidly at this time to 9-12m s^{-1}. Over the next 9h surface wind magnitude increased to 16m s^{-1} at which point 3m SWHs were observed. Wind and wave directions both remained easterly, although directional consistency began to diverge for wind speeds below 10m s^{-1} on September 19 1300; and ultimately for winds less than 8m s^{-1} the wind direction bore almost no relationship to wave direction. On September 19 0900, the local wind speed dropped from 16m s^{-1} to 8m s^{-1} in 9h. The wave height also decreased in a manner proportional to the wind speed, lagging by about 5h. The wind and wave direction continued to coincide until September 20 2100, when the wave direction rotated to a westerly orientation with a wave height of 1m.

It was of interest to determine whether the NARR winds, as applied to a theoretical wave growth exercise, were able to reproduce the observed 3.7m SWH that was shown for the wave spectrum. The time of propagation, t, in deep water is $t = 4\pi X/(gT)$ where X is the fetch, and T is the wave period. The available fetch X to

the east of the RDCP was estimated at 175km. The wave period *T* was 6.0sec. This resulted in a time of propagation *t* for the wave at 10h. This would put the wave generation at September 18 1900. According the NARR 10m wind field estimates, the maximum sustained easterly wind speeds of 16m s^{-1} occurred around the beginning of this time at the RDCP location and throughout the Kotzebue Sound (see Figure 2.12).

To summarize this section, it appears that the Bering Sea low in progress over 17-19 September played a major role in wave development during event SE1, generating moderate-to-strong, local easterly winds that were of a magnitude not uncommon for this region. Driven by winds whose magnitude reached its highest state while wave height followed 2h later at its highest state, a well-defined local-wave state developed, with easterly SWH exceeding 3m for 16h which is classified as “wind-sea”.

2.4.3. SE2 (SWH-3m-15), November 22 - December 2, 2007 UTC

SE2 (SWH-3m-15) commenced on November 22 2100 and ended December 2 0800 (227h' duration). In brief, the event proceeded as follows (Figure 2.13): establishment of an approximate 5day period where SWH cycled between 1 and 2m, then about 2 days at 2.5m SWH, then an increase to a brief maximum 4m SWH over a ~2 day period before a rapid decay ensued. The event began with a 1m SWH with a westerly wave direction (Figure 2.14) in which the direction lasted for 72h (November 22 2100 to November 25 2100). After this a rapid change in wave direction to the east occurred; this direction persisted for the next one hundred and fifty hours (November 25 2100 to December 2 0300). However unlike SE1 (SWH-3m-3), a sudden increase in wave height and period was not observed; rather wave heights increased relatively gradually from 1m to 2m over a 45 hour period, and from 2m to 3m over an additional 108 hour period. A sustained 34 hour period of easterly 3m SWH was observed from November 30 0900 to December 1 1900; during this 3m event, significant wave heights exceeded 4m for 6h (December 1 0300 to 0900). After the 3m event, the SWH decreased to 2m and continued in the eastward direction for 8h (December 1 1900 to December 2 0300); then finally the SWH decreased further to 1m and wave direction changed around to southerly.

The synoptic situation during this period (Figure 2.15) featured most prominently a low pressure system that occurred over the Bering Sea from November 22-29, which was bordered to the east and northeast by an extensive, elongated high pressure system stretching from the Gulf of Alaska to the Beaufort Sea, resulting in the highest wind

speeds over the Eastern Bering and Southern Chukchi Seas. This storm, a classic stalled system, moved into the southwestern Bering Sea on November 22, north of the Andreanof Islands (US) and Near Islands (US) with an MSLP of 980hPa supporting maximum winds at 925hPa geopotential height of 18m s^{-1}. Throughout the day of November 23, the storm rapidly intensified, dropping to an MSLP of 960hPa, with the zone of maximum winds shifting around to a southeasterly direction blowing towards Kamchatka Peninsula (Russia) at 30m s^{-1}. The low pressure system moved slowly northwards over the Bering Sea before coming to rest north of Kamchatka Peninsula on December 1 1500, at which point the storm had weakened to an MSLP of 980hPa.

The "peak" of the storm occurred from November 27 1200 to November 29 1800 (54h). Corresponding winds (925hPa) during this time were southeasterly over the Aleutians, Seward Peninsula and southern Chukchi Sea, reaching speeds of 35m s^{-1}. MSLP reached a minimum of 960hPa for 42h from November 27 1500 to November 29 0900; the center of the low was positioned between the Near Islands and the Andreanof Islands, moving slowly northward towards Bering Strait. The drop in MSLP on November 27 immediately preceded the more active phase of SE2.

Figure 2.16 shows the wave spectrum at the highest SWH during 1 December 0300, which was three days after the peak storm period in the Bering Sea (November 28) and several hours after the peak wind of 20m s^{-1} in the SE Chukchi Sea (November 30). The color bar (top) and non-directional (bottom) gives the wave energy density, $E(f)$, in m^2Hz^{-1}. The Cartesian contour plot (Figure 2.16) shows that the spectra ranges from

0.10Hz to 0.15Hz and a 90° direction range for $E(f)$>2m^{2}Hz^{-1}, similar to SE1. The non-directional peak energy density was 21.0m^{2}Hz^{-1} (Figure 13 – bottom) at 0.12Hz while the directional (Figure 13 – top) was centered at 0.14Hz coming from 83° (East). The integral wave parameter estimates derived from the spectra result in a SWH=4.4m, T_{m02}=6.3sec, T_{m01}=6.5sec. The mean winds during the period of the spectrum included a wind speed of U_{10}=16.8m s^{-1} and a wind direction of U_{dir}=110°. Wind and wave direction were easterly, where wave direction (83°) was 27° counterclockwise from wind direction (110°). This was different compared to what was seen in SE1, where wave direction was clockwise to wind direction. The wind speed (16.8m s^{-1}) was again greater than the wave phase speed. Since the wind speed was much greater than the wave phase speed, this strongly indicates a locally generated easterly "wind-sea" for the event of 1 December 0300.

Similar to SE1, the largest SWH represented wind-seas with some of the 1m SWH clearly uncorrelated to the wind direction and presumably representing swell energy derived from a distant source. During the first part of SE2 winds were predominantly northwesterly and then change to easterly as the stronger southeast winds from the storm build into the Seward Peninsula area. Beginning November 22 2100, a northwesterly wave of 1m SWH commenced. Although the wave direction was coincident to the local wind direction, the wind magnitude – 3m s^{-1} – was not strong enough to develop the observed 1+m sea, indicating swell propagating in from the broader Chukchi Sea. The wind direction changed to easterly on November 24 1800 while the wave direction did not change to easterly until 27h later on November 25 2100.

At this time wave height and period increased from 1m to 2m SWH and 4s to 5s, respectively. Wind speed also increased from 8m s^{-1} to 10m s^{-1}. During the 27 hour period while wind and wave direction were not similar, wind speed increased from 5m s^{-1} to 10m s^{-1}.

SE2 wave heights are shown to be affected by prior wind events. On December 1 0300 the local wind speed dropped from 20m s^{-1} to 17m s^{-1} in 3h, during the start of the 4m SWHs. The 4m SWHs lasted 6.75h and the 3m SWH continued on for 9h after the end of the 4m SWH. Prior to the 4m SWH event, the local wind speed was approximately 20m s^{-1} for 20h. The wind speed dropped to 16m s^{-1} during the 17h while the 4m and 3m SWH events were happening. This was also assessed by using the wave parameters that occurred in the wave spectra (Figure 2.16). The exercise whereby NARR winds are used to reproduce the event peak was repeated for SE2 for the observed 4.4m SWH that was shown for the wave spectrum. Using time of propagation $t = 4\pi X/(gT)$ where X is the fetch at 180km, and T is the wave period at 6.5 sec, this resulted in a t=10h. This would put the wave generation at November 30 1700. According the NARR 10m wind field estimates, the highest wind speeds values (+19m s^{-1}) at the RDCP location and in the Kotzebue Sound (see Figure 2.17) occurred during this time for SE2. This in turn yielded the highest wave height, recorded by the RDCP for SE2.

It appears that synoptic-scale low pressure and a neighboring high pressure system lasting for several days caused high wind speeds over the eastern Bering Sea and southern Chukchi Sea that drove the wave conditions observed during SE2. Unlike SE1

which saw a well-defined local-wave state develop within 9h, SE2 developed after 117h where easterly SWH exceeding 3m for 34h, and reached over 4m for 6h. Similar to SE1, SE2 was also classified as “wind-sea”.

2.5. Conclusion

Significant wave heights exceeding 2m observed by the RDCP in the SE Chukchi Sea in the fall of 2007 appeared to be locally generated wind-sea and not derived from distant energy sources typically suggesting swell. The primary support for this is the observation that, for the two 3m SWH events, wind and wave directions during the event peak were easterly, with wind/wave direction exhibiting strong phase locking.

Wave direction was opposite of the current flow direction, however. There is a strong current prominent in the southeast Chukchi Sea region, traveling eastward (Coachman and Tripp, 1970; Overland and Roach, 1987; Woodgate et al., 2005; Panteleev et al., 2010) over the Station 2007 area. This was thought to be due to the influence of a strong "wind-sea" seen for the higher significant wave heights (<2m). The lower significant wave heights (<1m) showed a westerly wave direction, the same direction that the current over Station 2007 also flows. Therefore, current flow from the west that is present at Station 2007 was overcome by the strong easterly winds, which caused the wave state to become easterly, creating an easterly "wind-sea".

It is apparent that the available fetch from the Kotzebue Sound was sufficient to generate large waves over Station 2007. It is suggested that observed wave states are dependent on fetch and not just wind magnitude, since the NARR reanalysis data set showed that the boundary of the generating wind field lay in the proximity of what was estimated in this study when using variables known such as wave period and time of

propagation. Winds from the NARR reanalysis data set were also shown to adequately provide the wind forcing needed for the observed wind-sea states.

Given the orientation of the Sound, it is not clear that northeast and southeast fetch directions, which are more constrained than fetches aligned more due east as well as to most westerly directions, would be able to sustain similar SWH under similar wind speeds. However, a key point for the offshore southeast Chukchi Sea region (i.e. region around Station 2007) is that, unlike farther more southern regions, storms often stall and when they do they are often positioned over the eastern Bering Sea. A stalled weather pattern allows wind duration to be maximized, which allows a given wind magnitude to reach fully developed sea state for the given fetch. This is important because, for this fetch limited region, if a storm does not stall, a fully-developed sea-state is unlikely to be attained and, with maximum wind speeds rarely exceeding 40m s^{-1}, waves exceeding 2m are unlikely to occur otherwise.

The wave state potential for this region has been demonstrated to be capable of supporting a SWH of 4m and extended storm durations of +3m SWH. An easterly wind and thus wave direction would impact the main shipping route through the Bering Strait, and could hamper operations, resulting in delays. Examples of operations in the Bering Strait include Coast Guard vessels, oil lease support vessels and drilling activity, the bulk carriers that travel to and from the Teck Alaska Inc. Delong Mountain Terminal, along with local small craft from various coastal communities. It is anticipated with the reduction in the Arctic ice pack, an increasing quantity of traffic moving through the area

will increase. Any developers of off-shore structures, such as jack-up rigs or artificial production islands, must factor sea-states of at least this magnitude into design considerations and must assume that they will occur annually given the frequency of storms and of stalled storms that occur in the Bering Sea region.

Acknowledgements

This publication is the result in part of research sponsored by the Cooperative Institute for Arctic Research (CIFAR) with funds from the National Oceanic and Atmospheric Administration (NOAA) under cooperative agreement NA17RJ1224 with the University of Alaska. Funding also provided by NOAA projects, NA06OAR4600179 and NA08OAR4600856. Generous logistical support from Teck Alaska Incorporated and Foss Maritime Company has been provided to this project from its beginning.

References

AADI (Aanderaa Data Instruments) (2006). *RDCP Primer TD 220c*, 70 pp.

Coachman, L. K. and R. B. Tripp (1970). Currents North of Bering Strait in Winter. *Limnology and Oceanography*, Vol. 15, No. 4, 625-632

Ewing, J.A. (1980). Observations of Wind-waves and Swell at an Exposed Coastal Location. *Estuarine and Coastal Marine Science* 10, 543-554.

Francis-Chythlook, O. (2004) Coastal Processes in Elson Lagoon, Barrow, Alaska. MS Thesis, University of Alaska Anchorage, Anchorage, Alaska.

Hudak DR and JMC Young (2002) Storm climatology of the southern Beaufort Sea. *Atmosphere Ocean,* 40, 145–158.

Jensen, R., N. Scheffner, S.J. Smith, D. Webb, and B. Ebersole. (2002). *Engineering Studies in Support of Delong Mountain Terminal Project ERDC/CHL TR-02-26*, September 2002, Vicksburg, MS.

Kistler, R., E. Kalnay, W. Collins, S. Saha, G. White, J. Woollen, M. Chelliah, W. Ebisuzaki, M. Kanamitsu, V. Kousky, H. van den Dool, R. Jenne, and M. Fiorino, (2001). The NCEP-NCAR 50-Year Reanalysis: Monthly Means CD-ROM and Documentation. *Bull. Amer. Meteor. Soc*., 82, 247-267.

Mesinger, F., G. DiMego, E. Kalnay, K. Mitchell, P.C. Shafran, W. Ebisuzaki, D. Jovic, J. Woollen, E. Rogers, E.H. Berbery, M.B. Ek, Y. Fan, R. Grumbine, W. Higgins, H. Li, Y. Lin, G. Manikin, D. Parrish, and W. Shi (2006). North American Regional Reanalysis. Boulder, CO NOAA.OAR/ESRL PSD:42.

Mesquita, M.D.S., D.E. Atkinson, and K.I. Hodges (2010). Characteristics and Variability of Storm Tracks in the North Pacific, Bering Sea, and Alaska. *Journal of Climate*, 23, 294-311. DOI: 10.1175/2009JCLI3019.1

Overland, J.E. and A.T. Roach (1987). Northward flow in the Bering and Chukchi Seas. *Journal of Geophysical Research*, Vol.92, No.C7, 7097-7105.

Panteleev, G., D.A. Nechaev, A. Proshutinsky, R. Woodgate, and J. Zhang (2010). Reconstruction and analysis of the Chukchi Sea circulation in 1990-1991. *Journal of Geophysical Research*, 115, C08023, doi:10.1029/2009JC005453.

Swail, Val R., Andrew T. Cox, 2000: On the Use of NCEP–NCAR Reanalysis Surface Marine Wind Fields for a Long-Term North Atlantic Wave Hindcast. *J. Atmos. Oceanic Technol.*, **17**, 532–545.

USACE (2003). *Kivalina Relocation Planning Project Inventory and Village Requirements, Kivalina, Alaska*. Prepared by Tryck Nyman Hayes, Inc. for US Army Corps of Engineers, Alaska District.

USACE (2004). *Kivalina Relocation Master Plan, Kivalina, Alaska*. Prepared by Tryck Nyman Hayes, Inc. for US Army Corps of Engineers, Alaska District.

WMO (World Meteorological Organization) (1998). *Guide to Wave Analysis and Forecasting, Second Edition*. WMO-No. 702, Secretariat of the World Meteorological Organization – Geneva Switzerland. ISBN 92-63-12702-6. 159 pp.

Woodgate, R.A., K. Aagaard, and T. Weingartner (2005). A year in the physical oceanography of the Chukchi Sea: Moored measurements from autumn 1990-91, *Deep-Sea Research, Pt. II*, 52 (24-26): 3116-3149.

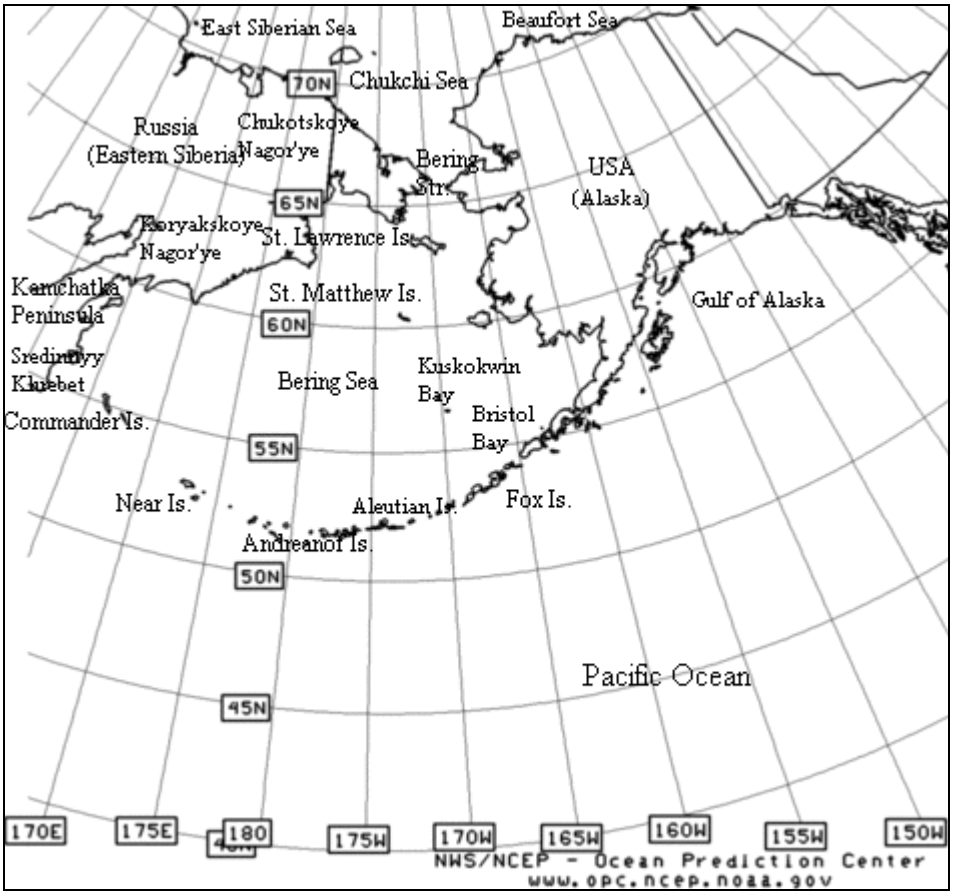

Figure 2.1 - Geographical map of East Siberia/Alaska

Geographical map of Northern Hemisphere – East Siberia/Alaska region. Map taken NWS/NCEP (www.opc.ncep.noaa.gov) and modified by O. Francis, April 2011.

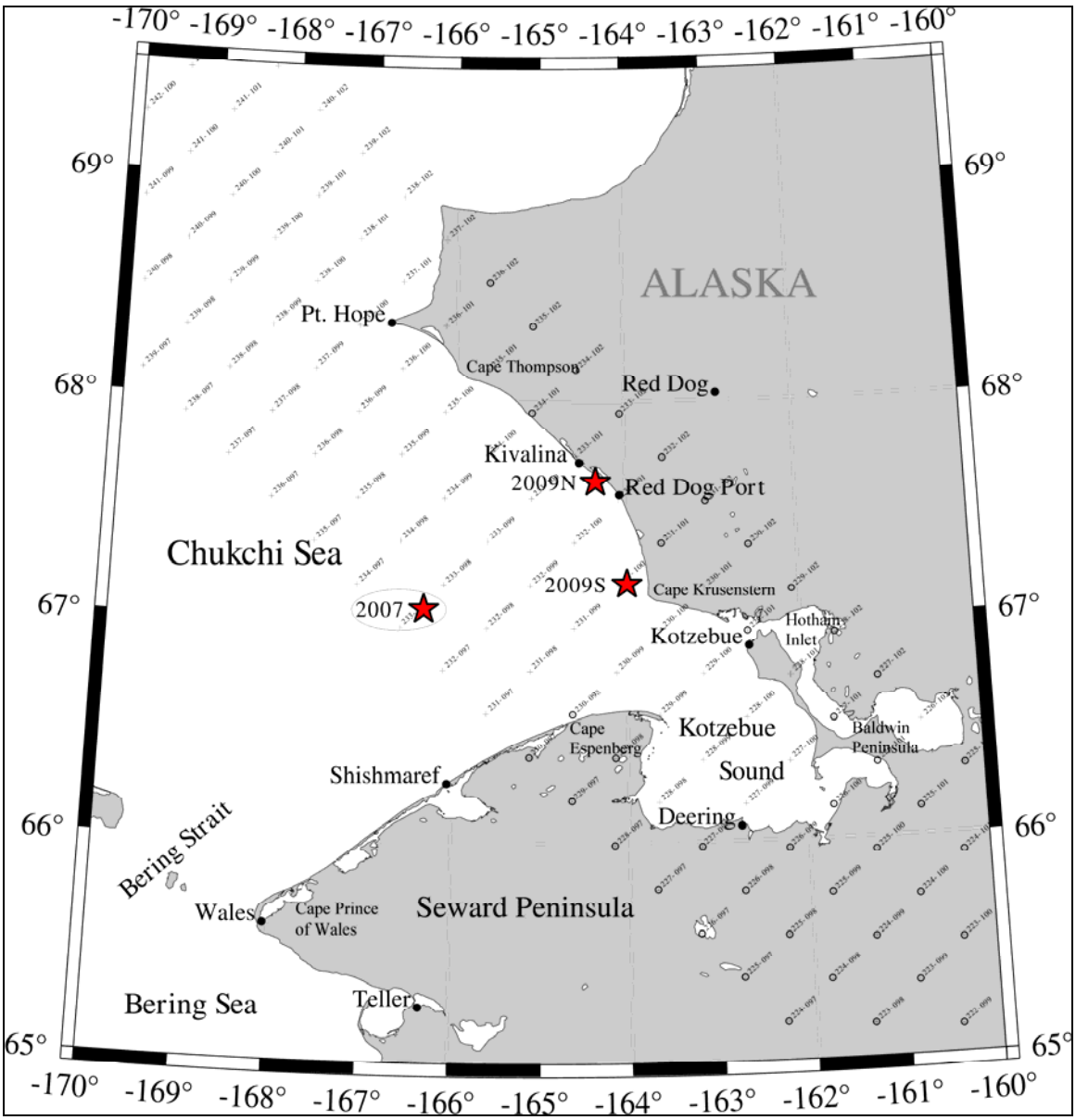

Figure 2.2 – *In situ* measurement locations in the Chukchi Sea
Geographical map of south-eastern Chukchi Sea showing location of North American Regional Reanalysis (NARR) 10m winds (small print – for location purposes only) and the three Recording Doppler Current Profiler (RDCP) Stations 2007 (mentioned in Chapter 2, offshore – "circled star"), 2009N, and 2009S (stars) (mentioned in a Chapter 3 for the nearshore).

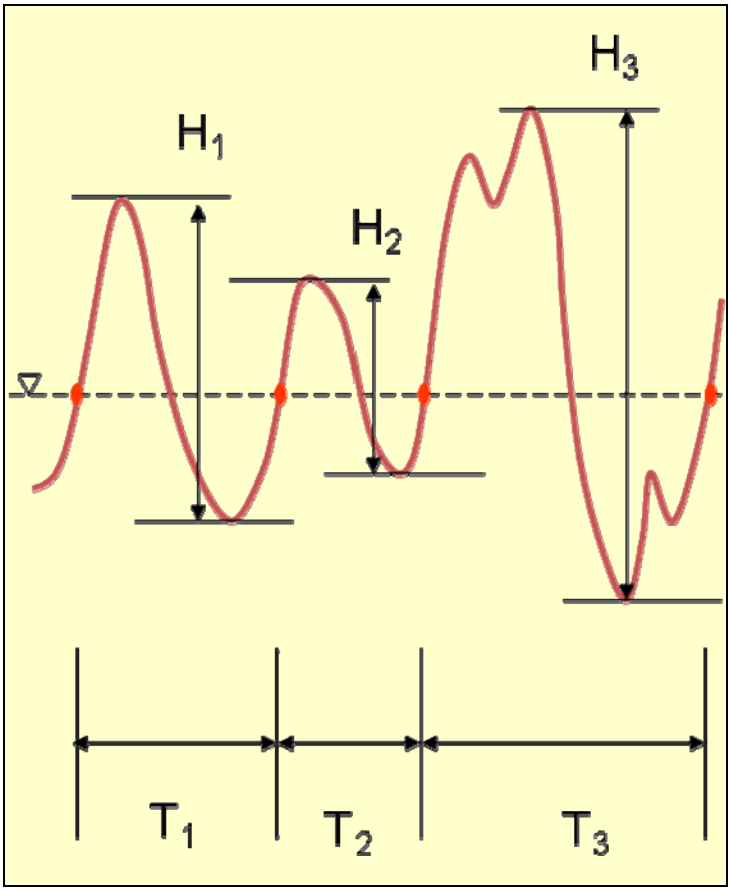

Figure 2.3 – Representation of wave height and zero crossing period

Graphical representation of individual wave height, H_i, and the corresponding individual zero crossing wave period, T_i. Mean zero crossing parameter, T_{m02} is calculated from the individual zero crossing wave period, T_i, where the individual wave height, H_i, performs a zero-upcrossing (red circles).

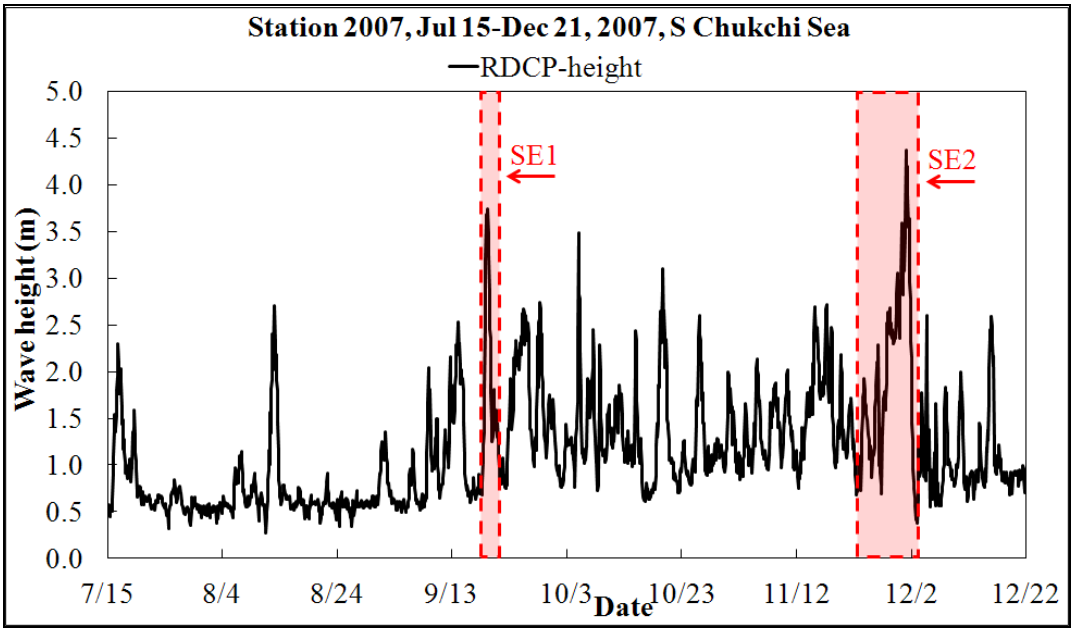

Figure 2.4 – Station 2007 significant wave height
Recording Doppler Current Profiler (RDCP) significant wave height (SWH) at Station 2007 for entire RDCP wave record 15 July - 21 December 2007. Station location and depth are 67º3'29.94"N, 166º20'43.02"W, and 34m, respectively.

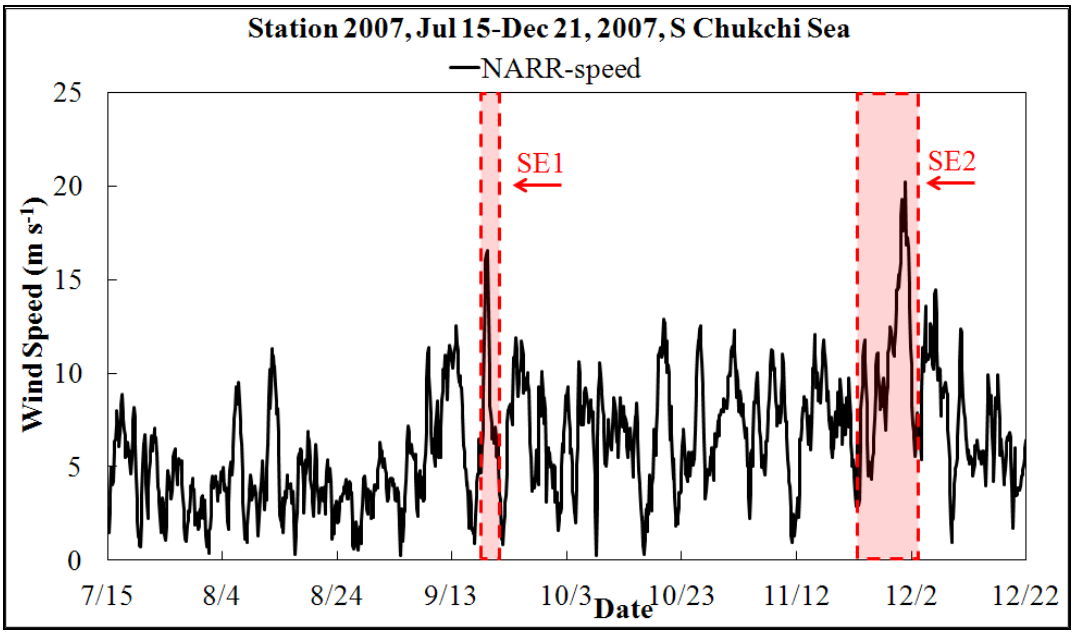

Figure 2.5 – Station 2007 wind speed
North American Regional Reanalysis (NARR) 10m wind speed at Station 2007 for entire Recording Doppler Current Profiler (RDCP) wave record 15 July - 21 December 2007. Station location and depth are 67º3'29.94"N, 166º20'43.02"W, and 34m, respectively.

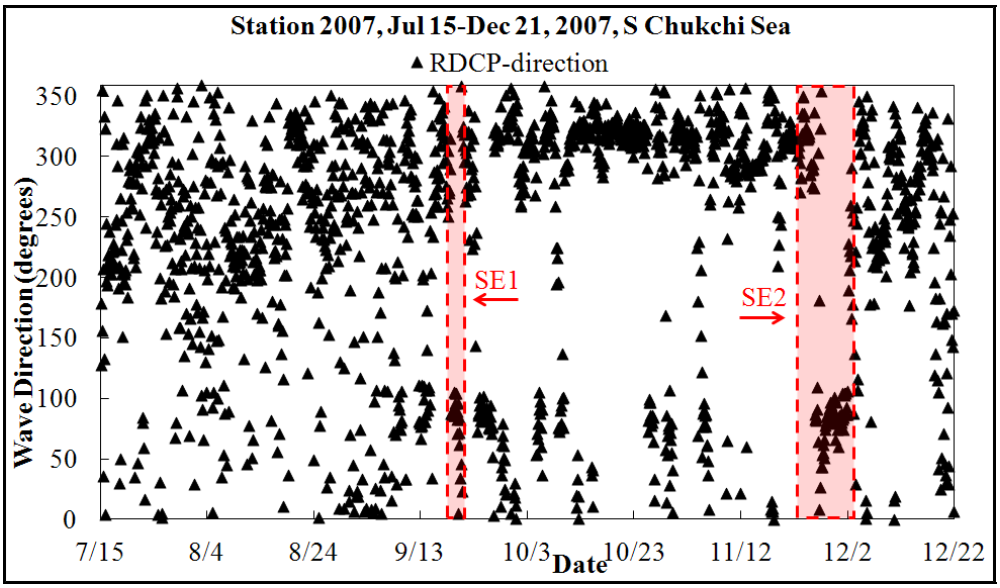

Figure 2.6 – Station 2007 wave direction

Recording Doppler Current Profiler (RDCP) wave direction at Station 2007 for entire RDCP wave record 15 July - 21 December 2007. Station location and depth are 67º3'29.94"N, 166º20'43.02"W, and 34m, respectively.

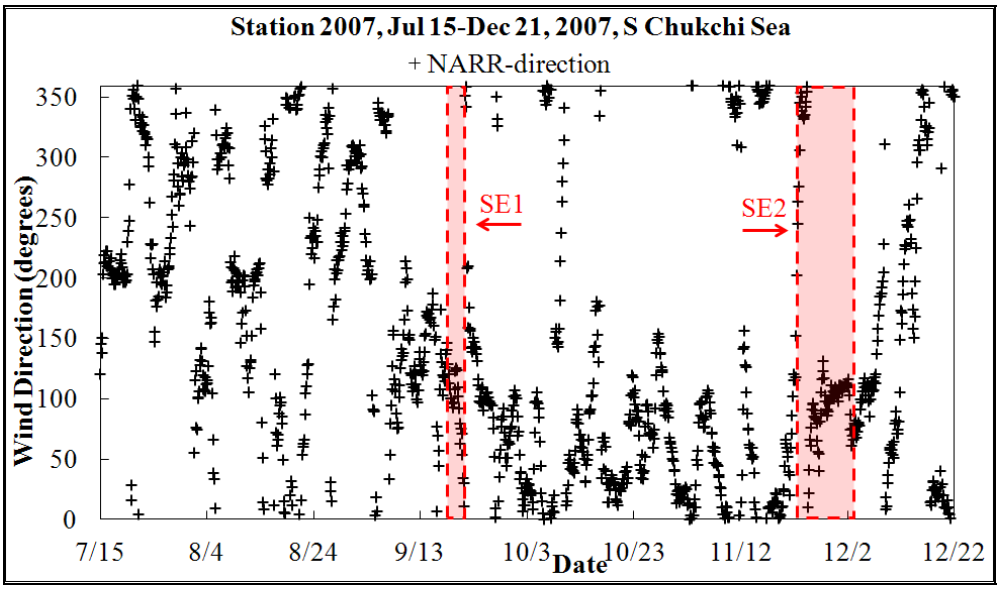

Figure 2.7 – Station 2007 wind direction

North American Regional Reanalysis (NARR) 10m wind direction at Station 2007 for entire Recording Doppler Current Profiler (RDCP) wave record 15 July - 21 December 2007. Station location and depth are 67º3'29.94"N, 166º20'43.02"W, and 34m, respectively.

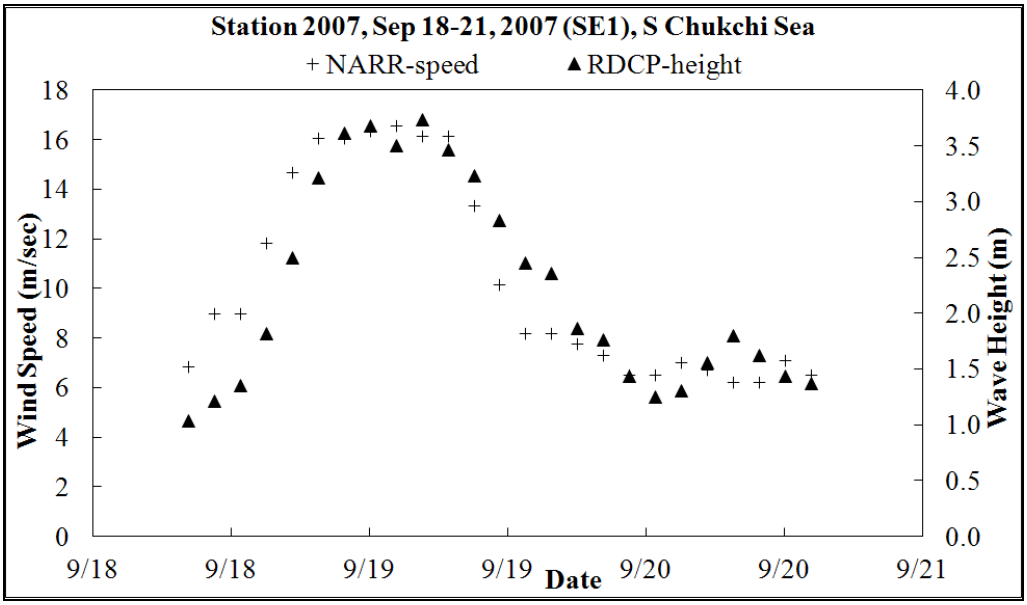

Figure 2.8 – SE1 wave height versus wind speed
Comparison of Recording Doppler Current Profiler (RDCP) significant wave height and North American Regional Reanalysis (NARR) 10m wind speed at Station 2007 for wave record 18-21 September 2007 (SE1) at 67º3'29.94"N, 166º20'43.02"W and a water depth of 34m.

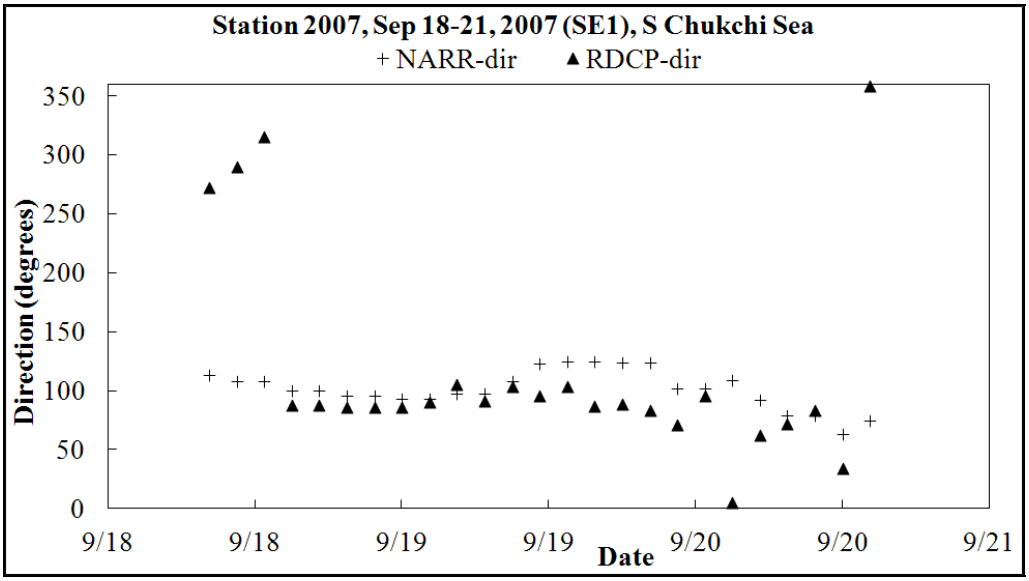

Figure 2.9 – SE1 wave direction versus wind direction
Comparison of Recording Doppler Current Profiler (RDCP) mean wave direction and North American Regional Reanalysis (NARR) 10m wind direction at Station 2007 for wave record 18-21 September 2007 (SE1) at 67º3'29.94"N, 166º20'43.02"W and a water depth of 34m.

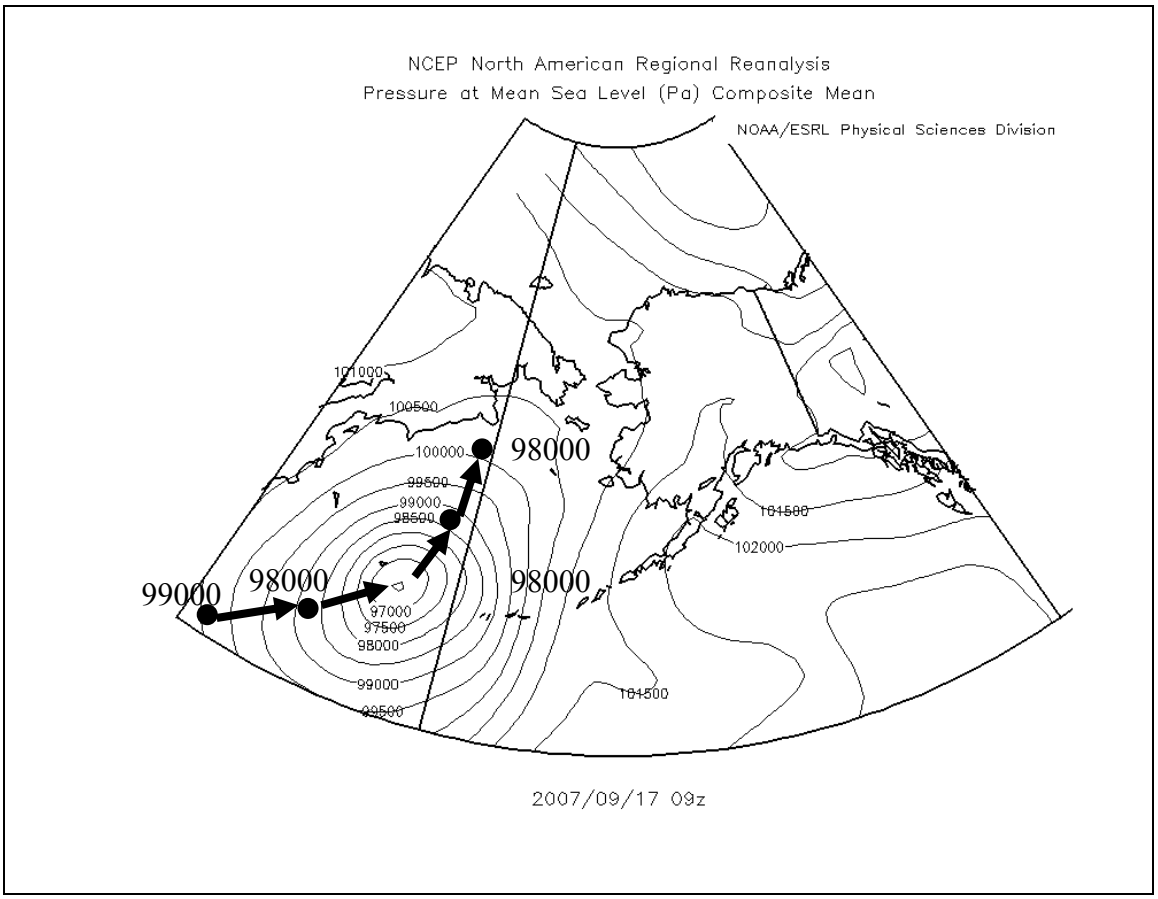

Figure 2.10 – SE 1 storm maxima
Storm maxima during SE1 on 17 September 2007 0900 UTC shown on North American Regional Reanalysis (NARR) Mean Sea Level Pressure (MSLP) map. Image provided by the NOAA-ESRL Physical Sciences Division, Boulder Colorado at http://www.esrl.noaa.gov/psd. Modified by O. Francis, January 2011.

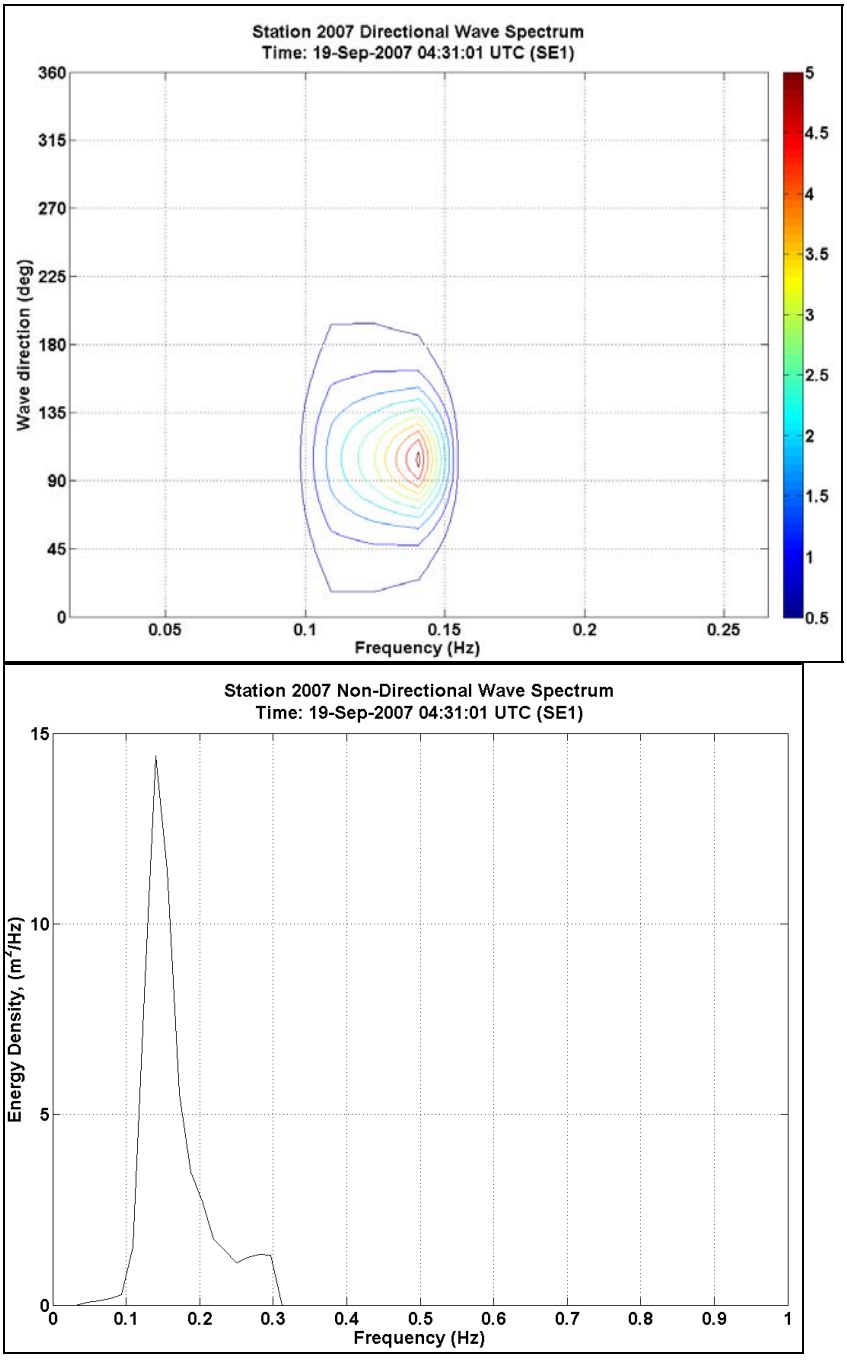

Figure 2.11 – SE1 wave spectrum

Directional (top) and non-directional (bottom) wave spectra Cartesian projection of highest SWH in SE1 on 19 September 2007 0431 UTC during SE1, SWH=3.7m recorded by the Recording Doppler Current Profiler (RDCP) at Station 2007 at 67º3'29.94"N, 166º20'43.02"W and with a water depth of 34m. The color bar (top) and non-directional (bottom) gives the wave energy density, $E(f)$, in m^2Hz^{-1}.

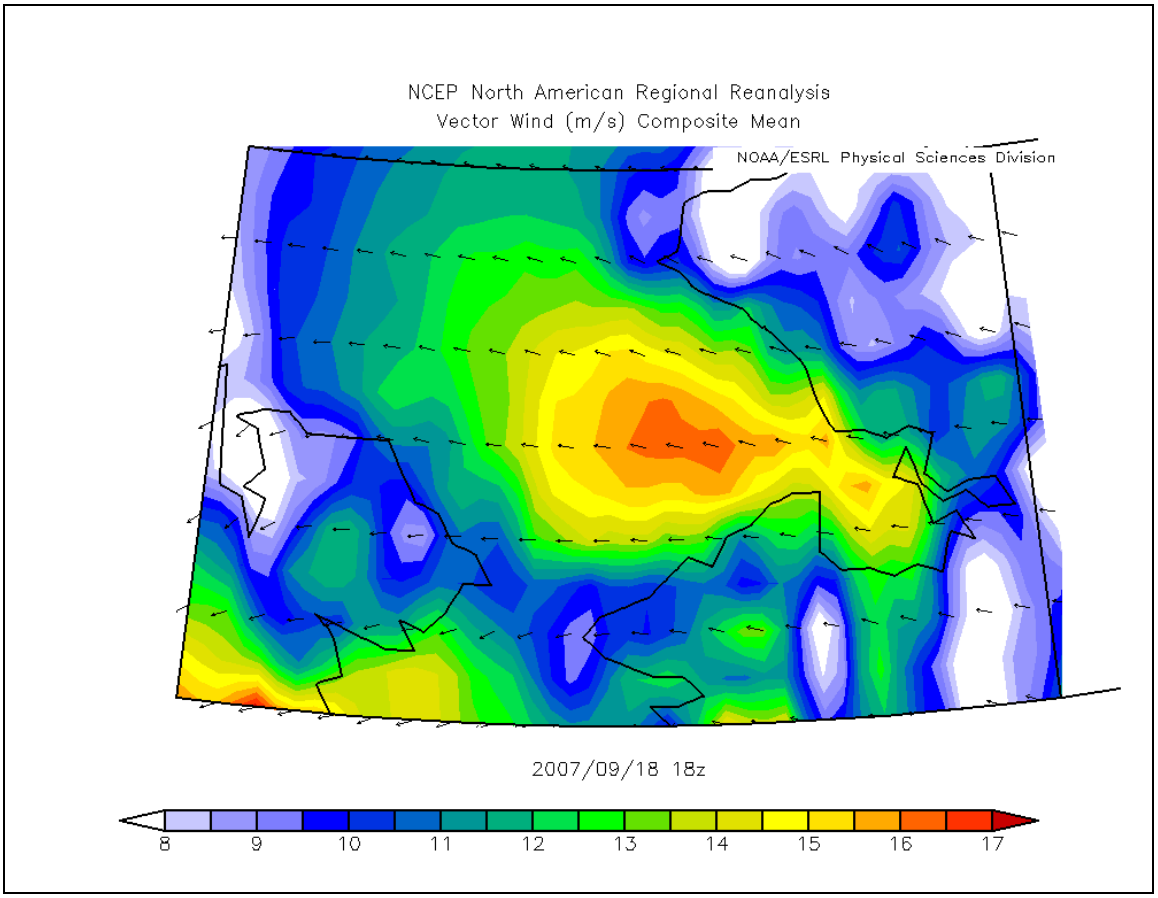

Figure 2.12 – SE1 vector wind composite
North American Regional Reanalysis (NARR) 0.3° resolution 10m wind showing magnitude and direction at September 18, 2007 1800 UTC, 1 hour before wave generation of highest SWH in SE1.

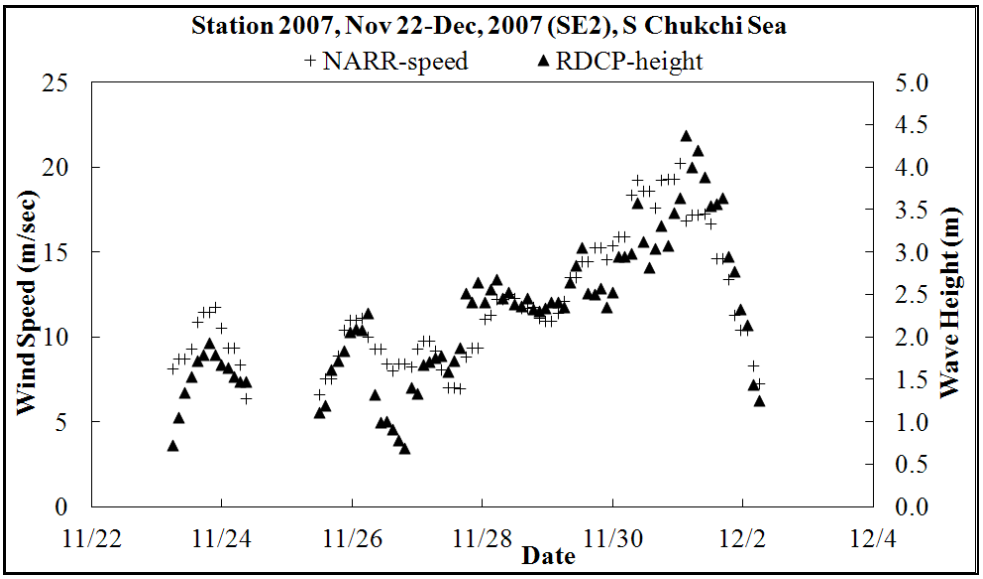

Figure 2.13 – SE2 wave height versus wind speed
Comparison of Recording Doppler Current Profiler (RDCP) significant wave height and North American Regional Reanalysis (NARR) 10m wind speed at Station 2007 for wave record 22 November – 2 December 2007 (SE2) at 67º3'29.94"N, 166º20'43.02"W and with a water depth of 34m.

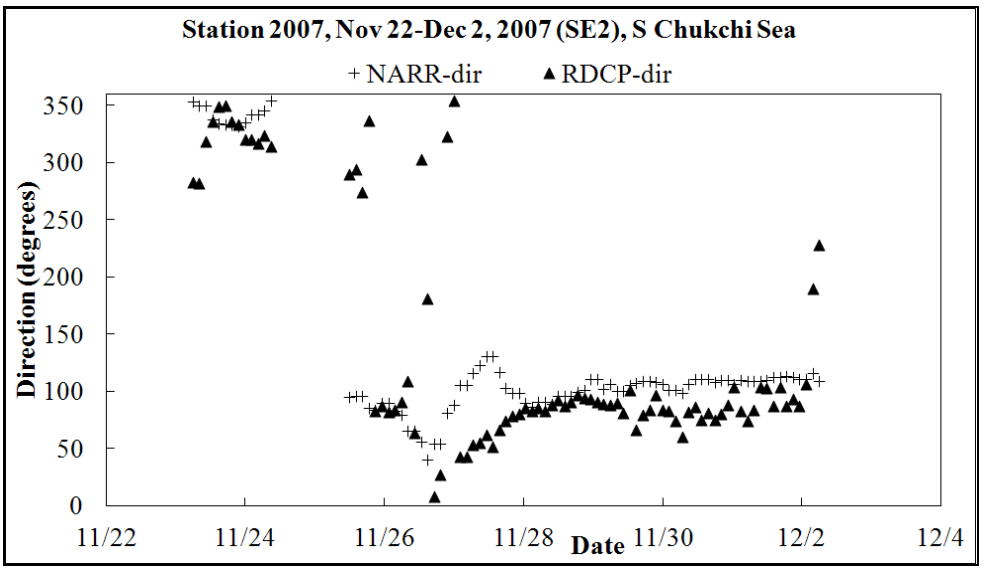

Figure 2.14 – SE2 wave direction versus wind direction
Comparison of Recording Doppler Current Profiler (RDCP) mean wave direction and North American Regional Reanalysis (NARR) 10m wind direction at Station 2007 for wave record 22 November – 2 December 2007 (SE2) at 67º3'29.94"N, 166º20'43.02"W and with a water depth of 34m.

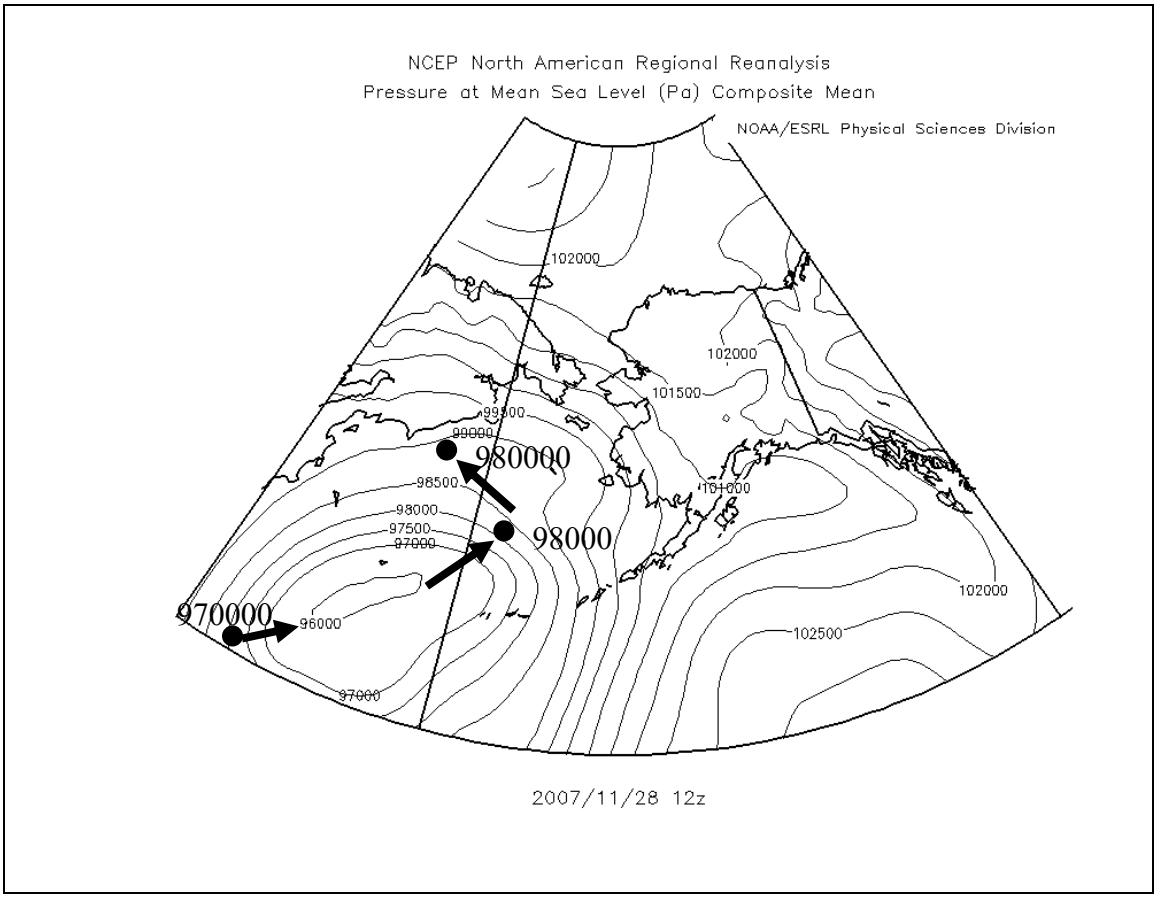

Figure 2.15 – SE 2 storm maxima
Storm maxima during SE2 on 28 November 2007 1200 UTC shown on North American Regional Reanalysis (NARR) Mean Sea Level Pressure (MSLP) map. Image provided by the NOAA-ESRL Physical Sciences Division, Boulder Colorado at http://www.esrl.noaa.gov/psd. Modified by O. Francis, January 2011.

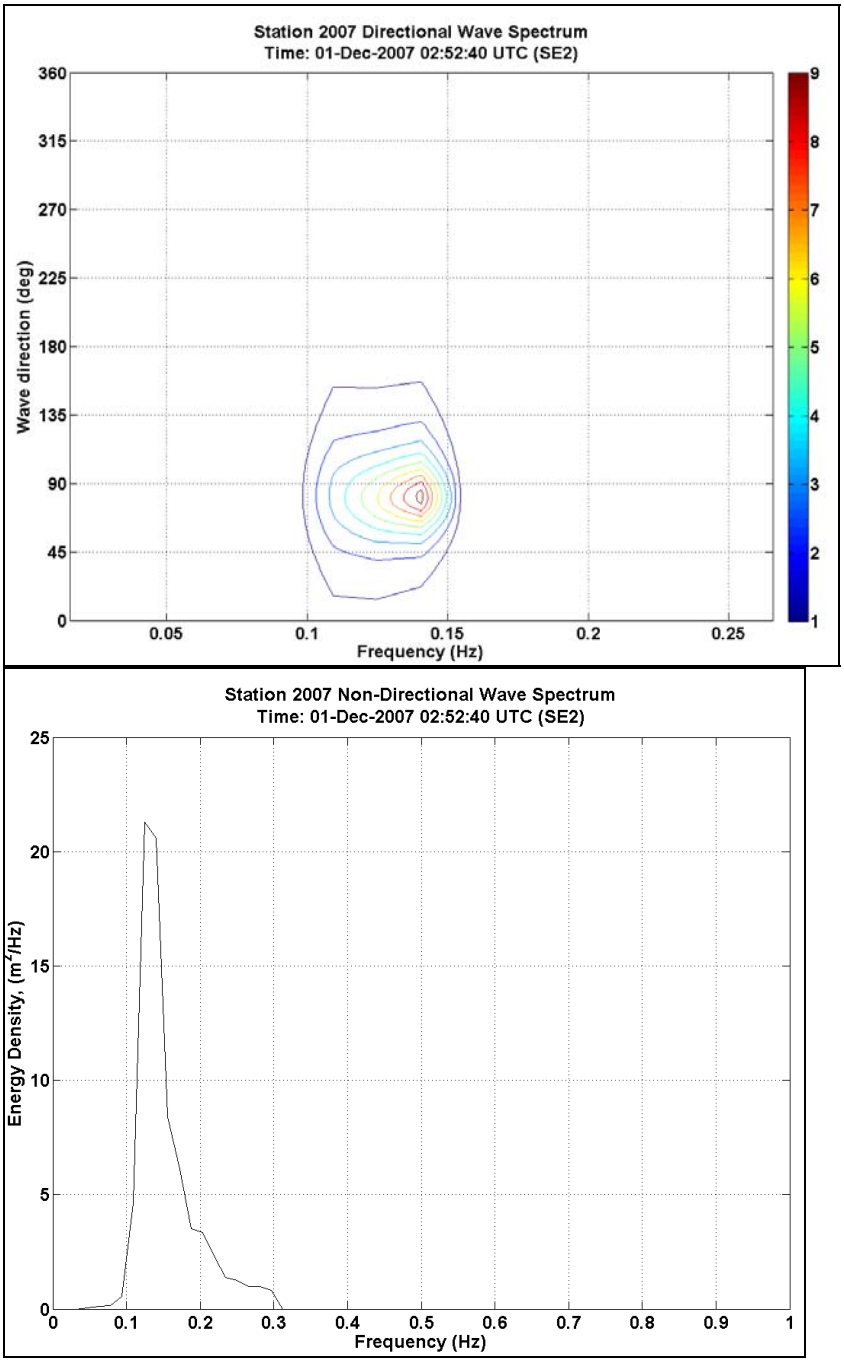

Figure 2.16 – SE2 wave spectrum

Directional (top) and non-directional (bottom) wave spectra Cartesian projection of highest SWH in SE2 on 1 December 2007 0252 UTC during SE2, SWH=4.4m recorded by the Recording Doppler Current Profiler (RDCP) at Station 2007 at 67º3'29.94"N, 166º20'43.02"W with a water depth of 34m. The color bar (top) and non-directional (bottom) gives the wave energy density, $E(f)$, in m^2Hz^{-1}.

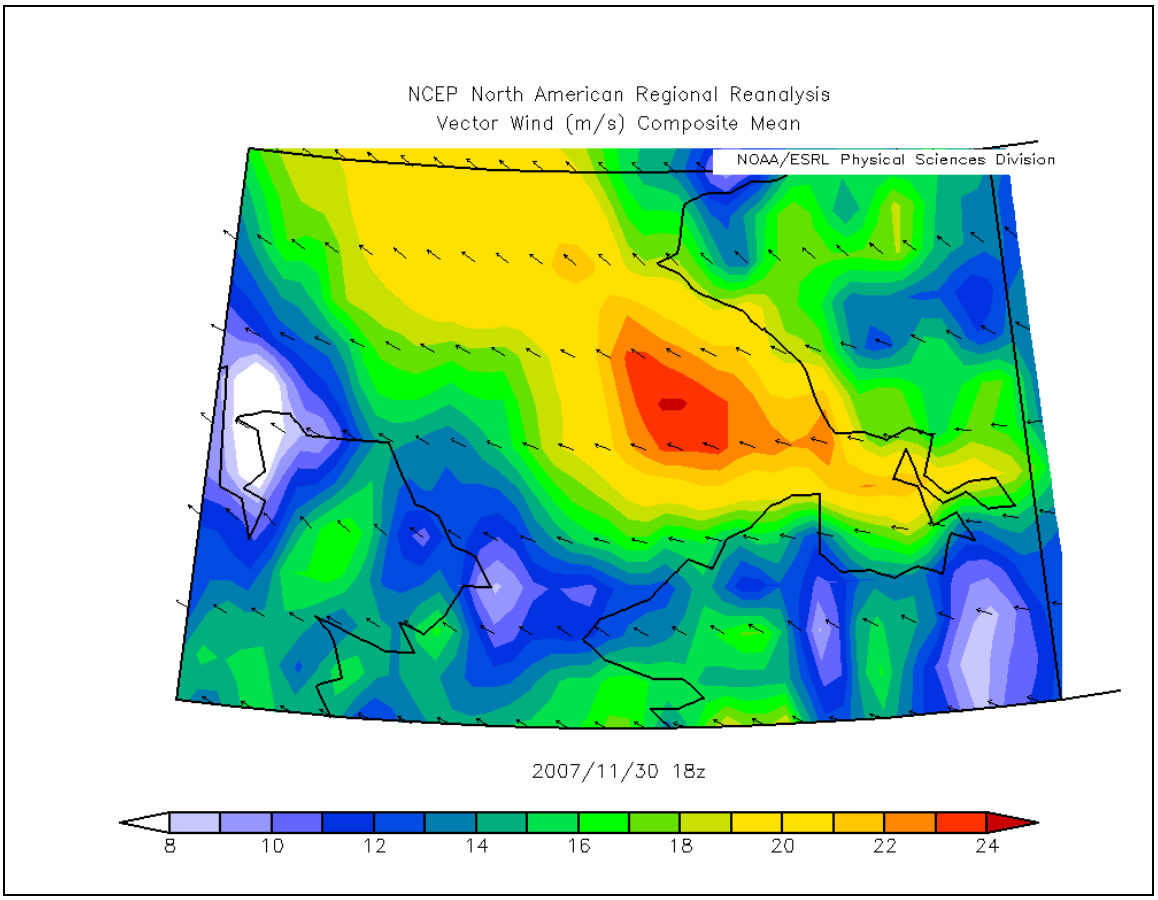

Figure 2.17 – SE2 vector wind composite
North American Regional Reanalysis (NARR) 0.3° resolution 10m wind showing magnitude and direction at November 30, 2007 1700 UTC, 1 hour after wave generation of highest SWH in SE2.

Table 2.1 – Station 2007 significant wave height events ≥ 2m

Station 2007 significant wave height (SWH) events (2m-"minor" and 3m-"major" in *italics* to designate "SE"), (l to r) SWH duration, SWH, wave period, wave direction, fetch, wind speed, wind direction for wave record 15 July 2007 – 21 December 2007 UTC at 67º3'29.94"N, 166º20'43.02"W, water depth 34m.

SWH Event	Date	SWH Duration (hrs)	Hm0 (m)	Tm02 (sec)	Wave Dir (deg)	Wind Spd (m/s)	Wind Dir (deg)
2007-2m-1	8/12-8/13/2007	18	2.3	4.7	207	10.2	201
2007-2m-2	9/13-9/14/2007	22.5	2.2	4.8	108	10.4	161
[1] 2007-3m-3	*9/18-9/19/2007*	*24.75*	*3.1*	*5.5*	*93*	*13.1*	*106*
2007-2m-4	9/23-9/26/2007	58.5	2.3	5.1	87	10.2	100
2007-2m-5	9/28-9/28/2007	15.75	2.5	5.2	57	7.9	80
2007-2m-6	10/4-10/5/2007	11.25	2.7	5.4	86	8.6	87
2007-2m-7	10/7-10/7/2007	6.75	2.2	5.0	330	6.8	7
2007-2m-8	10/14-10/15/2007	6.75	2.3	5.0	19	7.7	99
2007-2m-9	10/19-10/20/2007	31.5	2.4	5.4	326	11.6	22
2007-2m-10	10/25-10/26/2007	15.75	2.3	5.1	87	11.7	71
2007-2m-11	11/15-11/15/2007	22.5	2.4	5.3	294	10.0	351
2007-2m-12	11/16-11/17/2007	13.5	2.5	5.2	1	9.8	4
2007-2m-13	11/17-11/18/2007	9	2.3	5.1	91	6.5	12
2007-2m-14	11/25-11/26/2007	9	2.1	5.0	86	10.6	84
[2] 2007-3m-15	*11/27-12/2/2007*	*105.75*	*2.9*	*5.5*	*86*	*14.1*	*104*
2007-2m-16	12/15-12/16/2007	20.25	2.3	5.4	310	7.5	338

[1] 2007-3m-3 (also known as SE1)

[2] 2007-3m-15 (also known as SE2)

Chapter 3 Synoptic forcing of wave states in the southeast Chukchi Sea, Alaska, at nearshore locations[1]

Abstract

Two bottom-mounted Recording Doppler Current Profilers (RDCP) were deployed at nearshore locations (approximately 3 and 8km offshore, in about 18m water depth) in the southeast Chukchi Sea, Alaska, from October 2009 through September 2010 (UTC) with the goal of linking observed wave activity – wind-sea and swells – to their synoptic drivers. The northerly RDCP recorded a total of 16 events of elevated wave states: 15 exceeding 1m significant wave height (SWH), and 1 exceeding 2m SWH. The southerly RDCP recorded a total of 25 events of elevated wave states: 23 exceeding 1m SWH, 2m exceeded on two occasions and a SWH of 3m was observed. Detailed analysis of the three large events (i.e. SWH events $\geq$ 2m), including comparison with high-resolution reanalysis wind data (North America Regional Reanalysis), strongly suggested the wave energy evolved from a distant storm, and would be defined as swell. Due to the close proximity of the shoreline to the east of the instruments, windspeeds based on reanalysis were constrained so fetch was westerly. Wave direction was also westerly, varying about 25° to the north (clockwise) or the south (counterclockwise) from the wind direction which is believed to be influenced by fetch and the strong current flow located where the nearshore RDCPs were deployed. Shore-fast sea ice is also believed to play a role but shown to only dampen wave activity for 3 months (January to April 2010), thus implying

[1] Francis, O.P. and D.E. Atkinson (2012). Synoptic forcing of wave state in the southeast Chukchi Sea, Alaska, at nearshore locations. *Natural Hazards*, **in press**, doi: 10.1007/s11069-012-0148-y.

early ice break-up in this nearshore region. Two events appeared to be driven by southwesterly winds associated with cyclonic systems that moved into the eastern Chukchi Sea and then stalled. However, the second storm event appeared to be driven by northwesterly winds associated with a cyclonic system over the Brooks Range; a less common occurrence. Given that the typical storm activity in the region occurs as storms move into the Bering Sea in fall, this represents another potential source for wave conditions posing danger to people on the water or to coastal infrastructure.

3.1. Introduction

Francis and Atkinson (2012) presented an analysis of the highest significant wave height (SWH) events of duration $\geq$ 6h for the period July - December 2007 at an *offshore* location. Their analyses placed the recorded wave data in the context of the evolving meteorological condition at the synoptic and mesoscale levels. The synoptic-scale included evaluating large cyclonic systems in the Bering Sea. The mesoscale involved evaluating high winds events at the edge of these cyclones, or bordering high and low pressures.

This companion paper also analyzes waves within a meteorological context, but does so for 2010 and at two *nearshore* locations. In particular, proximity to the coast is expected to dampen both wind and wave activity compared to an offshore location, as will be shown in this paper. For a complete background, the reader should refer to the *Introduction*, and *Background* sections in Francis and Atkinson (2012).

As mentioned in Francis and Atkinson (2012), a major industrial stakeholder in this area is Teck Alaska Inc., who operates the Delong Mountain Terminal. This facility has experienced periods when waves have caused shutdowns due either to direct impact on the terminal infrastructure or to set up of dangerous conditions for handling the large freighters, which given their length (up to 300m), can be especially susceptible to long-period swell energy at or near the resonance of the vessel. In particular, these nearshore gauge deployments have specific relevance for the Teck operations. Freighters do not berth at a dock but are positioned for loading 3-6km offshore, where the newly deployed

Recording Doppler Current Profilers were positioned. Therefore, using an observational wave data set from Recording Doppler Current Profilers (RDCP), this paper focuses on the occurrence of waves and their synoptic drivers in the SE Chukchi Sea. Of particular interest is the identification of atmospheric forcing functions defining wind-seas and swell wave conditions.

The primary objective of this study is to identify and characterize the synoptic patterns that drive observed occurrences of SWH events in the southeast Chukchi Sea. A secondary objective is to distinguish between the occurrence of swell and wind-sea in a nearshore region. A third objective is to assess the extent to which wind data extracted from a widely used, high-resolution reanalysis data set (NCEP North America Regional Reanalysis) is correlated to the observed RDCP wave data set, and thus examine its suitability for longer-term modeling of wave forecasting and hindcasting in this region. This is performed evaluating how wind speed and direction vary with wave height and direction on time series and spectral plots. Although it is known that reanalysis winds tend to underestimate peak storm wind speeds, especially the coarse resolution global reanalyses, what this means specifically for reproducing waves in the southeast Chukchi is not precisely known. These tasks will utilize observational data acquired from Recording Doppler Current Profilers (RDCP) placed in the southeast Chukchi Sea in 2009-2010. Estimates of observed SWH event occurrences will be generated using data from the 32-km resolution “North American Regional Reanalysis (NARR)” atmospheric dataset (Mesinger et al., 2006) and the NCEP/DOE Global Reanalysis 2 (Kistler et al.,

2001). It is hypothesized that, in the SE Chukchi Sea study area, the primary wave direction nearshore is from the northwest because that is the direction of greatest fetch that allows waves to propagate across the Chukchi Sea. These factors are elaborated upon below.

The present paper has one additional goal: to compare data from two RDCPs deployed concurrently in 2009-2010 and separated by 53km. Francis and Atkinson (2012) examined RDCP data collected in 34m water depth approximately 82km north of the nearest coastline (Seward Peninsula, Alaska) in the offshore Chukchi Sea in 2007. In this paper, the two RDCPs were within 3.5km and 10.8km off the western Alaskan coast, and in water depths of 17m and 18m, respectively. The results provide the opportunity to compare similarities and differences in wave conditions for the deployment in the SE Chukchi Sea.

The organization of the paper consists of an overview of the regional atmospheric setting and instrumentation background, a results section containing description of major observed wave events with detailed analysis and intermediate conclusions. Broader conclusions and discussion are reserved for the conclusions section. Wave events were analyzed as they were described, for a more efficient presentation.

3.2. Methods and data

For this paper, wind and wave direction use the same convention. Wind direction is defined as the direction *from which* the wind is coming and is given in degrees true bearing. Current direction is defined as the direction *to which* the current flow is going toward in degrees true bearing. The *true bearing* to a point is the angle measured in degrees in a clockwise direction from the north line.

3.2.1. Atmospheric datasets

Atmospheric parameters were obtained from the "North American Regional Reanalysis (NARR)" dataset (Mesinger et al., 2006). This gridded data of 0.3° and 1° resolution is taken from model runs which assimilate point-source and scatterometer data into a weather forecast model. This system, a "reanalysis" data set, was developed and is maintained by the National Centers for Environmental Prediction (NCEP) of the US National Oceanic and Atmospheric Administration (NOAA). For this project three parameters were extracted from the NARR dataset - geopotential height at 925hPa, vector wind at 925hPa, and vector wind at 10 m. Storm center, position and tracking were evaluated using geopotential height at 925hPa and vector wind at 925hPa. Local winds were evaluated using vector wind at 10m and extracted as time series from the NARR grid point nearest to the RDCP instrument location (see Figure 3.1 for NARR grid point locations). Mean sea level pressure data, drawn from the NCEP/National Center for Atmosphere Research Global Reanalysis data set (Kistler et al., 2001), were also used for this analysis.

3.2.2. RDCP instrument deployment and wave parameters

The overall project entailed three data-gathering efforts using RDCP (Recording Doppler Current Profiler) deployments. One RDCP was deployed to an open-water location during the ice-free period, July through December 2007 UTC ("2007" in Figure 3.1), discussed in Francis and Atkinson (2012), and two RDCPs were later deployed to coastal locations during ice-free and ice-covered periods October 2009 through September 2010 UTC ("2009N" and "2009S" in Figure 3.1), discussed in this paper. Station 2007 was located 82km north of the Seward Peninsula, Alaska in a water depth of 34m. Station 2009N was located 3.5km off the western Alaskan coast in a water depth of 17m. Station 2009S was located 10.8km off the western Alaskan coast in a water depth of 18m.

The bottom-positioned RDCP (AADI, 2006), by analyzing Doppler shifts of acoustic returns, recorded a number of wave observations denoted here as *N*. The frequency of the RDCP is 2Hz. Each N observation lasts 15 minutes where the RDCP awakens every 1.5h (for 2007 it was every 2h) and records for 15 minutes sampling at 2Hz which provides i=1800 samples for each N observation.

Station 2009N recorded every 1.5h for 8041h and 15 minutes, for N = 4596. Station 2009S recorded every 1.5h for 8204h, for N = 4689. Each observation i includes wave height H_i, wave period T_i and wave direction D_i. From these parameters the RDCP estimates the following: significant wave height (SWH), H_{m0}, mean wave period, T_{m01}, mean zero crossing, T_{m02} *or* $\overline{T}_z$, Energy wave direction, D_E, Mean direction, D_m,

and Peak direction, D_p . For this study, significant wave height, H_{m0} , mean zero crossing, T_{m02} , and mean wave direction, D_m were retained for analysis. The mean zero crossing parameter, T_{m02} , is the time obtained by dividing the record length by the number of downcrossings (or upcrossings) in the record (AADI, 2006), compared to the mean wave period, T_{m01} , which is the wave period corresponding to the mean frequency of the spectrum (WMO, 1998).

Wave spectra was estimated using the Maximum Likelihood Method (MLM). The wave direction was also based on all cells. Upper cutoff frequency was 0.6Hz. Fast Fourier Transform (FFT) size was 128.

3.2.3. Wave event and atmospheric analysis

A “significant wave height” event (SWH) was defined using approaches outlined in Hudak and Young (2002) and Francis-Chythlook (2004); that is, the wave magnitude exceeds and remains over a given threshold for a period of 6h or more in duration. Two threshold set-points were established: 1m, 2m (for 2007 - three threshold set-points were established: 1m, 2m, 3m). The SWH event was considered to have ended when the wave magnitude dropped below the threshold for 6h or more.

Spatial plots of pressure and winds were manually examined to assess the atmospheric state at the time of identified SWH events. The atmospheric progenitor typically was a “storm” as defined by the presentation of a closed low feature on a 925hPa. However, persistent patterns characterized by strong pressure gradients that were not storms in motion are not uncommon in this region. The 925hPa level was chosen to minimize interference from surface conditions yet provide a level low enough to adequately represent surface pressure conditions.

3.3. Station 2009N and 2009S Analysis and Results

3.3.1. Station 2009N and 2009S overview

At Station 2009N, during the October 2009 through September 2010 UTC recording period, seventeen significant wave height (SWH) events were identified: sixteen 1m, and one 2m. The longest duration events (1m) occurred during mid July to mid August. The large magnitude events (2m event) of longest duration occurred in mid July. At Station 2009S, during the October 2009 through September 2010 UTC recording period, twenty-seven (SWH) events were identified: twenty-five 1m and two 2m. The longest duration events (1m) occurred during mid July to mid August, and also in mid October. The longest duration/large magnitude events (2m events) occurred in mid July and mid August.

Sea surface temperature (SST), monitored by Station 2009N, dropped and remained below 0ºC starting November 9, 2009 to July 2, 2010. Sea surface temperature (SST), monitored by Station 2009S, dropped and remained below 0ºC starting November 11, 2009 to July 1, 2010. SST is important since wave action is dampened by first-year sea ice that forms when freeze-up occurs, so being able to identify when SST remains below 0ºC (i.e. freeze-up) helps to identify variability of SWH events throughout the 11-month wave record. Therefore, these freeze-up periods indicate the generation of ice coverage (shore-fast ice) at the free surface, and a substantial reduction in the wave climate. For the 11-month wave record of Stations 2009N and 2009S, the main events (SE3, SE4, SE5) occurred during a 1-month time frame (i.e. mid-July through mid-

August). This was shortly after SST warmed to above 0ºC, and not later in the year as seen in the offshore region in 2007 (Francis and Atkinson, 2012).

The SWH (H_{m0}) (Figure 3.2) for October 2009 to September 2010 encompasses the entire RDCP Station 2009N wave record. SST monitored by Station 2009N, dropped and remained below 0ºC starting November 9, 2009 to July 2, 2010. However, SWHs between 1.0m-2.0m was seen during November 2009 to January 2010, and also during June to July 2010. The highest SWHs during November 2009 to July 2010 between 1.5m to 2.0m were observed during December 2009, and April to June 2010. The period of minimal wave activity (i.e. SWHs < 0.5m) occurred during January to April 2010. This wave activity (i.e. SWH>1.5m) that began in mid April 2010 implies break up of sea ice began very early in the season at Station 2009N. Therefore breakup for shore-fast sea ice began at an earlier period (mid April 2010), than what the RDCP SST implies (early July 2010).

The NARR 10-m wind speed (Figure 3.3) also for October 2009 to September 2010, does not correlate with the SWHs <1m (Figure 3.2). Only with wind speeds > $6\,\mathrm{m\,s^{-1}}$ was there some correlation with wave activity (Figure 3.2, 3.3), although the wind and wave directions differed by 10°-25° (Figures 3.4 and 3.5). Although the waves may have been somewhat wind-driven, there was probably an external factor act work such as current flow and shoreline bathymetry.

The RDCP mean wave direction (D_m) (Figure 3.4) at Station 2009N for October 2009 to September 2010, is shown. From November 2009 to June 2010, the wave

direction is shown to arrive from all directions. However, this was during a freeze-up period, so sea ice cover would dominate the region during this time (i.e. November 2009 to June 2010). The sea ice cover would dampen wind-wave interaction, so waves would be more affected by currents and swell. These ice-covered waves generally had SWHs $\leq$ 0.5m, with the exception of SWHs between 1-2m (Figure 3.2) during the months of December, January, April and June. Francis and Atkinson (2012) found that December cyclones coincided with considerable SWH (i.e. 1.5-2.5m) at an offshore location (Station 2007). This also agrees with the fact that the strongest extra-tropical cyclones are most likely to form in December and January (Sienkiewicz et al., 2005). During October to November 2009 (before freeze-up), and July to September 2010 (after freeze-up), the wave direction was shown to be mainly westerly where most of the highest SWH (i.e. 1-2.5m) activity occurred.

The NARR 10-m wind direction (Figure 3.5) was not correlated with the wave direction (Figure 3.4). The wind direction displayed mainly northerly and easterly directions during October 2009 to September 2010 (Figure 3.5). For the highest SWHs (i.e. SWHs occurring before and after freeze-up), the wind direction was southerly, westerly, and northerly. This is consistent with the notion that easterly wind directions do not affect wave states since the shoreline is only several kilometers to the east, limiting available fetch needed to generate easterly waves.

The SWH (Figure 3.6) for October 2009 to September 2010 encompasses the entire RDCP Station 2009S wave record. SST monitored by Station 2009S, dropped and

remained below 0ºC starting November 11, 2009 to July 1, 2010. However, SWH activity of 1.0m-2.0m was seen during November 2009 to January 2010, and also during June to July 2010. Also, uncharacteristically high SWHs > 2.5m were observed during April to May 2010, which followed a long period (January – April 2010) of virtually no wave activity (i.e. SWHs < 0.5m). This wave activity implies break up of sea ice began very early in the season (i.e. mid April 2010) at Station 2009S implying earlier periods for breakup of shore-fast sea ice.

The NARR 10-m wind speed (Figure 3.7) for October 2009 to September 2010, also shows similar characteristics of wave-wind relationships as shown for Station 2009N (Figures 3.2, 3.3) where wind and wave directions differed by 10°-25° (Figures 3.8 and 3.9). Similar to Station 2009N, it is also thought that waves may have been somewhat wind-driven, but that there was an external factor at work such as current flow and shoreline bathymetry.

The RDCP mean wave direction (Figure 3.8) and the NARR 10-m wind direction (Figure 3.9) at Station 2009S for October 2009 to September 2010 are shown. Again, the wind and wave directions for Station 2009S (Figures 3.8, 3.9) are very similar to Station 2009N (Figures 3.4, 3.5) where wind direction (Figure 3.9) is uncorrelated with wave direction (Figure 3.8). It was concluded that wave states were affected by sea ice cover during almost the same period as Station 2009N, and were additionally affected by shoreline and the current flow.

The results shown in Tables 3.1 and 3.2 refer to the wave and wind conditions when the significant wave height $\geq$ 1m during a particular "event" – where an "event" is described in Section 3.2.3. The three largest SWH events, i.e. $\geq$ 2m, are examined below in detail: event "2009N-2m-12" known as SWH Event 3 or "SE3" (from Table 3.1), July 22-23, 2010, event "2009S-2m-15" known as SWH Event 4 or "SE4" (from Table 3.2), July 16-18, 2010, and event "2009S-2m-20" known as SWH Event 5 or "SE5" (from Table 3.2), August 17-20, 2010. For these three events the wave signal evolution is reviewed, followed by an examination of the lifecycle of the storm, and atmospheric forcing identified as the cause for that SWH event. Also, consideration of near-surface winds at the RDCP location in the context of fetch is presented. Finally, for Stations 2009N and 2009S, the SWH (H_{m0}), and mean wave direction (D_m) were compared for all three SWH events.

3.3.2. SE3 (2009N-2m-12), July 22-23, 2010 UTC

The event identified as SE3 (2009N-2m-12) commenced July 22 0800 UTC (all times are given in UTC) and ended July 23 2100, for a total duration of 37h with SWH in excess of 1m (Figure 3.10). In brief, the storm took the form of a cyclonic pattern, with a low pressure centered over the Chukchi Sea/Arctic Ocean, between Wrangel Island and Alaska. Winds were southerly and highest over the eastern Chukchi Sea coast to the north of Bering Strait. On the western flank of the storm, northerly winds extended from the Arctic Ocean to the northern Siberian coast. The SWH event proceeded as follows (Figure 3.10): the SWH increased rapidly from ~0.96m to 2.42m over a 9 hour period after which this "peak" wave state persisted for 7h, before SWH decreased gradually to 0.92m over the next 26h. Figure 3.11 shows that the event began with waves from the west at 1m SWHs, which then became southwesterly as SWH reached 2m, and then returned to a westerly direction as SWH tapered down to 1m.

The primary feature of the synoptic situation (Figure 3.12) that gave rise to these events observed through SE3 were the winds associated with the low pressure system in the northeast Chukchi Sea that began on July 21 2100. A high pressure system bordered the low pressure system along the southeast Chukchi Sea; the resulting pressure gradient favored strong southwesterly winds in the southeast Chukchi Sea region. As the low moved south-southeast, towards the northern Alaska coast the high pressure system did not move. This caused the pressure gradient to strengthen with a concomitant increase in

the wind speed (925hPa) over Station 2009N from 10m s^{-1} to 14m s^{-1} in 6h. By the start of SE3, wind speeds were at 15m s^{-1} over Station 2009N.

The peak of the "storm" was from July 22 1500 to July 22 2200 (7h). The 925hPa geopotential height remained moderately low (650-660m) during this period and the storm domain extended southward to Bering Strait. The juxtaposition with the high pressure system farther south resulted in strong southwesterly winds (18m s^{-1}) over the Bering Strait, Seward Peninsula and SE Chukchi Sea regions. The Mean Sea Level Pressure (MSLP) for this storm event reached and remained at its minimum of 975hPa for a 24 hour period from July 21 2100 to July 22 2100. This time frame encompassed the beginning of SE3 starting when SWH exceeded 1m through the period during which SWH was >2m. The storm intensity began to wane on July 23 1200; the duration of 1m SWH's lasted only a few hours longer. By July 23 0300, 925hPa winds over Station2009N had decreased to and 8m/s and became westerly.

Figure 3.13 shows the wave spectrum at the highest SWH during 22 July 1400, which was at the beginning of the peak storm period over the Bering Strait (22 July 1500 to 22 July 2200). Although, the peak storm event began at 22 July 1500, highest wind speeds (10m s^{-1}) began 4h earlier which continued throughout the peak storm event. The color bar (top) and non-directional (bottom) gives the wave energy density, $E(f)$, in m^2Hz^{-1}. The Cartesian contour plot (Figure 3.13) shows that the spectra ranges from 0.14Hz to 0.23Hz and an 80° direction range for $E(f)$>0.15m^2Hz^{-1}. This was a much smaller wave energy density than what was seen in Francis and Atkinson (2012) for the

offshore. The non-directional peak energy density was 3.3m^{2}Hz^{-1} (Figure 13 – bottom) at 0.17Hz while the directional (Figure 13 – top) was centered at 0.22Hz coming from 217° (southwest). The corresponding wave parameters were SWH=2.4m, T_{m02}=4.4sec, T_{m01}=4.7sec. The mean winds during the period of the spectrum included a wind speed of U_{10}=10.5m s^{-1} and a wind direction of U_{dir}=185°. Although wind and wave direction were southwesterly, wave direction (217°) was at a 32° difference clockwise from wind direction (185°). The wave phase speed is given by $g/2\pi f_p$ (Ewing, 1980), where f_p is the peak frequency or the inverse of the peak period. With the wind speed (10.5m s^{-1}) and the RDCP peak period, f_p (4.7sec) the wind speed was greater than the wave phase speed (7.3m s^{-1}). When the wind speed is greater than the wave phase speed, this indicates "wind-sea". When the wind speed is less than the wave phase speed, this indicates "swell". Since the wind speed was greater than the wave phase speed, this indicates a southwesterly "wind-sea" for the event of 22 July 1400.

At the beginning of SE3 the 10-m surface wind over Station 2009N was southerly at 7.5m s^{-1} from the vicinity of the Seward Peninsula and Bering Strait. The wave direction was southwesterly to south-southwesterly, therefore took on a more western direction than the wind direction. During the first 3h, the wind magnitude increased rapidly from 7m s^{-1} to 10m s^{-1}. By July 23 0300 both surface wind and wave direction over Station 2009N became westerly, corresponding almost perfectly. After remaining at a peak of 10m s^{-1} for 9h, the wind magnitude decreased to 6.4m s^{-1} within 7h.

It was of interest to determine whether the NARR winds, as applied to a theoretical wave growth exercise, were able to reproduce the observed 2.4m SWH that was shown for the wave spectrum. The time of propagation, t, in deep water is $t = 4\pi X/(gT)$ where X is the fetch, and T is the wave period. The fetch (X) was estimated to be 129km to the SSW of the RDCP. The wave period (T) was 4.7sec. This resulted in a time of propagation (t) for the wave at 9.7h. This would identify the timing of the wave generation to begin at July 22 0500. According the NARR dataset, southerly wind speeds averaging 8m/s started and continued for 9h throughout this time.

In summary, it appears that the Chukchi Sea low present on July 22 played a major role in wave development during SE3, generating moderate southwesterly winds. These winds, which were of a magnitude typical in this region, drove a wave state with southwesterly SWH exceeding 2m.

3.3.3. SE4 (2009S-2m-15), July 16-18, 2010 UTC

SE4 (2009S-2m-15) commenced July 16 0500 and ended July 18 0900 (52h duration). In brief, the event proceeded as follows (Figure 3.14): the SWH cycled between 1 and 2m for a 23hr period, then averaged 2.2m SWH for 12h, and finally a decreased to between 1 and 2m for 17.5h before termination. More specifically, the event began with a 1m SWH with a southwesterly wave direction for 3.5h, then west-southwesterly direction for the next 17.5h, then southwesterly for the next 21h, then westerly for the last 10.5h (Figure 3.15). The "peak" wave states (i.e. SWH$\geq$2m) were from the southwest.

The synoptic situation during this period (Figure 3.16) prominently featured a low pressure system that began over the Western Chukchi Sea and Wrangel Island from July 15-17. The low was bordered to the southeast by a strong high pressure ridge extending northeast to east over the eastern to northern Bering Sea region. This resulted in the highest wind speeds over the Chukchi Sea, Kotzebue Sound, and Bering Strait region. This storm moved southeast over the Chukchi Sea towards northern Alaska with maximum winds of 16-18m s^{-1} at 925hPa. By July 17 1800 the low had stalled, and then weakened to a central pressure of 1007hPa. This low pressure system remained in this state through the end of the SWH event at 0900 on July 18.

The peak of the "storm" occurred from July 16 1200 to July 17 0900 (21h). MSLP reached a minimum of 1002hPa for 36h from July 15 2100 to July 17 0900; the center of the low moved eastward from Wrangel Island to the eastern Chukchi Sea on the Alaskan

coast. The slight drop in MSLP on July 17 immediately preceded the more active phase of SE4.

Figure 3.17 shows the wave spectrum during one of the higher SWH during 17 July 0800, which was near the end of the peak storm period over the Chukchi Sea (16 July 1200 to 17 July 0900). This was also at the end of the highest wind speeds (8-9m s^{-1}) which lasted about the same amount of time as the peak storm event, and lasted 20h over the SE Chukchi Sea. The color bar (top) and non-directional (bottom) gives the wave energy density ($E(f)$) in m^2Hz^{-1}. Figure 3.17 indicates that the spectra ranges from 0.14Hz to 0.21Hz and a 90° direction range for $E(f)$>0.10m^2Hz^{-1}. The non-directional peak energy density was 2.6m^2Hz^{-1} (Figure 13 – bottom) at 0.15Hz while the directional (Figure 13 – top) was centered at 0.2Hz coming from 225° (southwest). The wave parameters for this particular spectrum were SWH=2.1m, T_{m02}=4.5sec, T_{m01}=4.7sec. The mean winds during the period of the spectrum included a wind speed of U_{10}=7.0m s^{-1} and a wind direction of U_{dir}=200°. Although wind and wave direction were southwesterly, wave direction (225°) was at a 25° difference clockwise from wind direction (200°). With the wind speed (7.0m s^{-1}) and the RDCP peak period, f_p (4.7sec) the wind speed was less than the wave phase speed (7.3m s^{-1}). Since the wind speed is less than the wave phase speed, this indicates a southwesterly "swell" for the event of 17 July 0800.

Similar to SE3, the SWHs represented surface winds (10m) as indicated by their directions. During the first part of SE4 winds were predominantly south-southwesterly while waves were southwesterly to west-southwesterly. Beginning July 16 1400, surface

wind direction changed to southerly while wave direction remained west-southwesterly. As the "peak" wave state (i.e. SWH≥2m) began to occur, the surface wind direction became south-southwesterly while the wave direction became southwesterly. During the final stages of SE4, the surface wind direction was southerly while the wave direction was westerly. Therefore, wave direction always remained more westerly than the wind direction, similar to what happened in the case of SE3.

It was again of interest to determine whether the variation in NARR winds were compatible to the observed 2.1m SWH that was shown for the wave spectrum. The time of propagation, t, in deep water is $t = 4\pi X/(gT)$ where X is the fetch, and T is the wave period. The fetch X to the SSW of the RDCP was estimated at 97km. The wave period T was 4.7sec. This resulted in a time of propagation t for the wave at 7.3h. This would put the wave generation beginning at July 17 0100. According the NARR dataset, SSW wind speeds of 8m s^{-1} occurred around the beginning of this time and continued until July 17 0800. Therefore, the winds are consistent with the wave propagation.

In summary, the Chukchi Sea low present during July 15-17 played a major role in wave development during SE4, generating moderate southwesterly winds. This was similar to what occurred for SE3 but with a less pronounced cyclonic storm system.

3.3.4. SE5 (2009S-2m-20), August 17-20, 2010 UTC

SE5 (2009S-2m-20) commenced August 17 1700 and ended August 20 0600 (61h duration). In brief, the event proceeded as follows (Figure 3.18): SWH started at 1.2m and rose to 2.2m during the first 7hr period, then were between 2m to 4m for 33h, and finally decreased from 1.8m to 1.0m during the last 20.5h before terminating. More specifically, for the first 31h the wave direction was westerly which included part of the "peak" wave state (Figure 3.19). Then the wave direction became west-northwesterly for the next 26h during the remaining "peak" wave state, before becoming westerly in the final 3.5h.

The synoptic situation during this period (Figure 3.20) featured most prominently a large low pressure system over the Brooks Range in northern Alaska during August 17-18, which was bordered to the west by a high pressure system over Chukotskoye Nagor'ye. This resulted in the highest wind speeds over the eastern Chukchi Sea and Kotzebue Sound. The MSLP was 1000hPa supporting maximum winds of 16m s^{-1} at 925hPa. This storm migrated north from the Brooks Range to the northeastern Chukchi Sea during August 17-19 as the low pressure system weakened to an MSLP of 1005hPa. The final stage of this low pressure system was marked by its further weakening to a central MSLP of 1015hPa on August 20 0300, as it left the Chukchi Sea and moved north over the Arctic Ocean.

The peak of the "storm" occurred from August 18 0000 to August 19 0600 (30h). Corresponding winds (925hPa) during this time were northwesterly over the eastern

Chukchi Sea, and Kotzebue Sound reaching speeds of 16m s^{-1}. MSLP reached a minimum of 1000hPa for 24h from August 17 1500 to August 18 1500; the center of the low remained over the Brooks Range.

Unlike SE3 and SE4 where wind direction was at a more southerly direction with respect to wave direction, SE5 wave direction was more northerly with respect to wind direction throughout the wave record. Winds were predominantly west-northwesterly while waves were westerly, during the first part of SE5. Starting at August 19 0100, the wave direction changed to west-northwesterly while wind direction remained west-northwesterly. On August 19 1100, the surface wind direction changed to northwesterly to north-northwesterly while wave direction remained the same (i.e. west-northwesterly).

Figure 3.21 shows the wave spectrum at one of the higher SWH during 18 August 1700, which was in the middle of the peak storm period over the eastern Chukchi Sea and Kotzebue Sound (18 Aug 0000 to 19 Aug 0600). The peak storm event began at 18 August 0000, and the highest wind speeds (10m s^{-1}) began 2h after continuing throughout the peak storm event. The Cartesian contour plot (Figure 3.21) shows that the spectra ranges from 0.13Hz to 0.22Hz and a 110° direction range for $E(f)$>0.20m^2Hz^{-1}, a higher energy density than for SE3 and SE4. The non-directional peak energy density was 7.0m^2Hz^{-1} (Figure 13 – bottom) at 0.14Hz while the directional (Figure 13 – top) was centered at 0.2Hz coming from 280° (west). The wave characteristics for this particular spectrum were SWH=3.0m, T_{m02}=5.2sec, T_{m01}=5.5sec. The mean winds during the period of the spectrum included a wind speed of U_{10}=8.3m s^{-1} and a wind direction of U_{dir}=293°.

Although wind and wave direction were northwesterly, wave direction (280°) was at a 13° difference counterclockwise from wind direction (293°). This was different compared to what was seen in SE3 and SE4, where wave direction was clockwise of wind direction. The wind speed (8.3m s^{-1}) was again slightly less than the wave phase speed (8.5m s^{-1}). Since the wind speed is less than the wave phase speed, this indicates a westerly "swell" for the event of 18 August 1700.

In determining if the NARR winds provide accurate forcing for the observed 3.0m SWH that was shown for the wave spectrum, the results were consistent and similar to SE4. Given a fetch of 109km WNW of the RDCP and a wave period T was 5.5sec, then the time of propagation ($t = 4\pi X/(gT)$) was 7h. This would put the wave generation start at August 18 1000. Based on analysis of NARR winds, WNW wind speeds averaged 8.8m s^{-1} over these 7h.

In summary, it appears that the Brooks Range low during August 17-18 played a major role in wave development during SE5, generating moderate northwesterly winds from a cyclonic storm system.

3.3.5. Comparison of Station 2009N and 2009S for SE3, SE4, and SE5

For SE3, Station 2009N had a SWH "event" ≥2m. For SE3 significant wave height (SWH) H_{m0}, comparison between Station 2009N and 2009S generally showed a higher SWH for Station 2009S, with the exception of Station 2009N which had a higher SWH during the "peak" wave state of SE3 (Figure 3.22). Also, although Station 2009S did not have a SWH "event" ≥2m during this period, Station 2009S SWH did peak over the 2m threshold twice during this wave record. In addition, Station 2009S had a SWH "event" ≥1m, 2009S-1m-16 (Table 3.2).

For SE3 mean wave direction (D_m) Station 2009S generally experienced a more westerly wave direction than Station 2009N (Figure 3.23), which instead exhibited southwesterly (Table 3.1) waves. An exception occurred when Station 2009N wave direction was briefly more westerly than Station 2009S; this took place during a period of higher SWH for Station 2009S.

For SE4, Station 2009S was the main focus with a SWH "event" ≥2m. For SE4 significant wave height (SWH) H_{m0}, the comparison between Station 2009N and 2009S showed a much higher SWH for Station 2009S for half of the wave record (Figure 3.24). For the other half of the wave record, Station 2009N SWH was seen to be at or slightly higher than Station 2009S SWH. Also, although Station 2009S did not have a SWH "event" ≥2m during this period, Station 2009N SWH peaked over the 2m threshold once briefly during this wave record. In addition, Station 2009N had a SWH "event" ≥1m, 2009N-1m-11 (Table 3.1) for the entire wave record.

For SE4 mean wave direction D_m, Station 2009S was at a more westerly wave direction than Station 2009N (Figure 3.25), which was west-southwesterly (Table 3.2). This more westerly direction for Station 2009S was similar to what the wave record for SE3 showed.

For SE5, Station 2009S was the main focus with a SWH "event" $\geq$2m. For SE5 significant wave height (SWH) H_{m0}, the comparison between Station 2009N and 2009S showed a much higher SWH for Station 2009S for the entire wave record (Figure 3.26). Station 2009S's SWH was between 0.5m-1.2m higher than Station 2009N's SWH, a notable difference. However, Station 2009N had a SWH "event" $\geq$1m, 2009N-1m-15 (Table 3.1) for part of the wave record, and peaked over the 2m threshold once briefly during the wave record (Figure 3.26).

For SE5 mean wave direction D_m, Station 2009S was situated west-northwesterly and Station 2009N was situated west-southwesterly (Figure 3.27). Again, Station 2009S experienced waves coming from a less southerly direction.

3.4. Discussion and Conclusion

From this study, significant wave heights at their highest (i.e. ≥2m) were chosen to determine whether these waves were swell or wind-sea. The results showed that the location of the RDCP Station determined the type of incoming waves. Wave direction was westerly, generally being 25° to the north (clockwise) of the predominant southwest wind direction during two storm events, and 25° to the south (counterclockwise) of the predominant northwest wind direction during another storm event. The highest waves collected at the north Station (Station 2009N) were southerly "wind-sea". The highest waves collected at the south Station (Station 2009S) were westerly "swell".

Station 2009N displayed more south winds/waves compared to Station 2009S which had southwest to west-northwest winds/waves. A possible explanation for this would be wave refraction. There is a strong current prominent in the southeast Chukchi Sea region, traveling eastward and northward (Coachman and Tripp, 1970; Overland and Roach, 1987; Woodgate et al., 2005; Panteleev et al., 2010). At Station 2009S, this current is found to travel eastward and northward, which corresponds with the westerly and southwesterly wave direction. At Station 2009S, this current is found to travel northward, which corresponds with the southerly wave direction. Therefore, westerly waves that would have been present at Station 2009N may have been refracted due to the strong current traveling northward.

The southerly wave direction at Station 2009N may also be possible due to fetch. Station 2009N was positioned further north than Station 2009S and the greater fetch

allowed south winds to propagate longer over the water creating south wind-sea as the highest SWHs. Wave direction for Station 2009S had more open westerly fetch for waves to propagate.

Station 2009N also exhibited SWHs that were smaller in magnitude and fewer in number than those recorded at Station 2009S (Tables 3.1, 3.2). This was due to its proximity to an enclosed embayment north of Station 2009N, formed by the Point Hope promontory, sheltering it from northwesterly waves (Figure 3.1). In addition, Station 2009N documented wind-sea compared to Station 2009S which experienced swell, due to the direction and magnitude of the winds. The Delong Mountain Terminal is positioned between Station 2009N and 2009S, so it should expect to encounter both swell and wind-sea of greater than 2m heights in the early open water season, with greater than 3m swell heights.

Besides current flow and fetch, shore-fast sea ice was also shown to play a role in wave activity. Although SST< 0° from November 2009 to July 2010 (7-8 months), wave activity was dampened only during January to April 2010 (3 months) implying early ice break-up in this nearshore region. This early ice breakup is thought to be caused by extra-tropical cyclonic activity later and earlier in the seasons (Sienkiewicz et al., 2005), and less available sea ice (Comiso et al., 2008).

Low pressure systems and neighboring high pressure systems that last for several days are the primary cause of high wind speeds over the southern Chukchi Sea that force the wave states observed during the three SWH events selected for this study. Low

pressure systems converging over the eastern Chukchi Sea for SE3 and SE4 produced strong southwesterly winds over the southeast Chukchi Sea. A low pressure system over the Brooks Range in northern Alaska for SE5 produced strong northwesterly winds over the southeast Chukchi Sea. For SE3 and SE5, these storms took the form of a strong cyclonic pattern. For SE4, the cyclonic pattern was weaker.

The wave state potential for this region has been demonstrated to be capable of supporting a SWH of 3m and extended periods of greater than 2m SWH. A westerly wave direction implies that the main shipping route through the Bering Strait is susceptible to a direct influence from these waves. Users of this area currently affected include Coast Guard vessels, oil lease support vessels and drilling activity, the bulk carriers that connect with the Teck Alaska Inc. Delong Mountain Terminal, small craft from coastal communities, and the ever-increasing traffic around the Arctic that is spurred on by sea ice decline. Any developers of off-shore structures, such as jack-up rigs or artificial production islands, must factor sea-states of at least this magnitude into design considerations and must assume that they will occur annually given the frequency of storms that occur in the Chukchi Sea region.

This study also demonstrates that early-season westerly winds are able to cause the highest wave events for the study period in this region. These are caused by northern storms during the non-stormy period of the summertime (July-August) in contrast to southeasterlies/southerlies from Bering Sea lows in the later fall. Although these wave heights may not hamper heavy shipping traffic, these types of waves/winds could affect

small craft and contribute to coastal erosion and sediment transport. In addition, this study suggests that the Delong Mountain Terminal port site may experience the need for continuous dredging, due to these types of south and west wave events.

Acknowledgements

This publication is the result in part of research sponsored by the Cooperative Institute for Arctic Research (CIFAR) with funds from the National Oceanic and Atmospheric Administration (NOAA) under cooperative agreement NA17RJ1224 with the University of Alaska. Funding also provided by NOAA projects, NA06OAR4600179 and NA08OAR4600856. Generous logistical support from Teck Alaska Incorporated and Foss Maritime Company has been provided to this project from its beginning.

References

AADI (Aanderaa Data Instruments) (2006). *RDCP Primer TD 220c*, 70 pp.

Coachman, L. K. and R. B. Tripp (1970). Currents North of Bering Strait in Winter. *Limnology and Oceanography*, Vol. 15, No. 4, 625-632

Comiso, J. C., C.L. Parkinson, R. Gersten, and L. Stock (2008). Accelerated decline in the Arctic sea ice cover. *Geophys. Res. Lett*. 35 doi:10.1029/2007GL031972.

Ewing, J.A. (1980). Observations of Wind-waves and Swell at an Exposed Coastal Location. *Estuarine and Coastal Marine Science* 10, 543-554.

Francis, O.P. and D.E. Atkinson (2012). Synoptic forcing of wave state in the southeast Chukchi Sea, Alaska, at an offshore location. *Natural Hazards,* in press, doi: 10.1007/s11069-012-0142-4.

Francis-Chythlook, O. (2004) Coastal Processes in Elson Lagoon, Barrow, Alaska. MS Thesis, University of Alaska Anchorage, Anchorage, Alaska.

Hudak DR and JMC Young (2002) Storm climatology of the southern Beaufort Sea. *Atmosphere Ocean,* 40, 145–158.

Kistler, R., E. Kalnay, W. Collins, S. Saha, G. White, J. Woollen, M. Chelliah, W. Ebisuzaki, M. Kanamitsu, V. Kousky, H. van den Dool, R. Jenne, and M. Fiorino, (2001). The NCEP-NCAR 50-Year Reanalysis: Monthly Means CD-ROM and Documentation. *Bull. Amer. Meteor. Soc*., 82, 247-267.

Mesinger, F., G. DiMego, E. Kalnay, K. Mitchell, P.C. Shafran, W. Ebisuzaki, D. Jovic, J. Woollen, E. Rogers, E.H. Berbery, M.B. Ek, Y. Fan, R. Grumbine, W. Higgins, H. Li, Y. Lin, G. Manikin, D. Parrish, and W. Shi (2006). North American Regional Reanalysis. Boulder, CO NOAA.OAR/ESRL PSD:42.

Overland, J.E. and A.T. Roach (1987). Northward flow in the Bering and Chukchi Seas. *Journal of Geophysical Research*, Vol.92, No.C7, 7097-7105.

Panteleev, G., D.A. Nechaev, A. Proshutinsky, R. Woodgate, and J. Zhang (2010). Reconstruction and analysis of the Chukchi Sea circulation in 1990-1991. *Journal of Geophysical Research*, 115, C08023, doi:10.1029/2009JC005453.

Sienkiewicz, J.M, J.M. Von Ahn, and G. M. McFadden (2005). Hurricane Force Extratropical Cyclones. *American Meteorology Society* (2005-07-18).

WMO (World Meteorological Organization) (1998). *Guide to Wave Analysis and Forecasting, Second Edition*. WMO-No. 702, Secretariat of the World Meteorological Organization – Geneva Switzerland. ISBN 92-63-12702-6. 159 pp.

Woodgate, R.A., K. Aagaard, and T. Weingartner (2005). A year in the physical oceanography of the Chukchi Sea: Moored measurements from autumn 1990-91, *Deep-Sea Research, Pt. II*, 52 (24-26): 3116-3149.

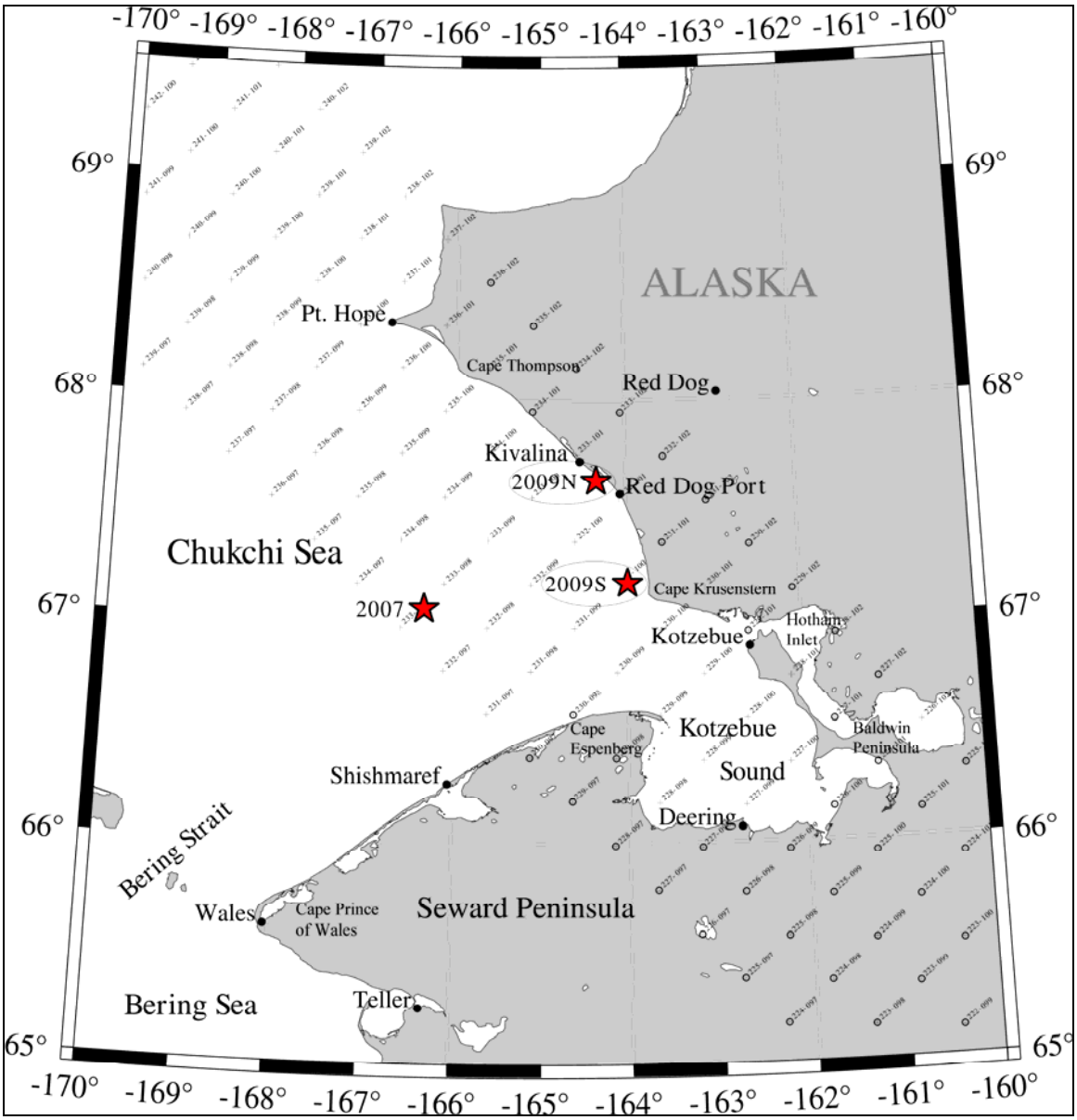

Figure 3.1 – *In situ* measurement locations in the Chukchi Sea
Geographical map of south-eastern Chukchi Sea showing location of North American Regional Reanalysis (NARR) 10m winds (small print – for location purposes only) and the three Recording Doppler Current Profiler (RDCP) Stations 2009N and 2009S (mentioned in Chapter 3 for the nearshore - "circled stars") and Station 2007 (mentioned in Chapter 2, offshore – star).

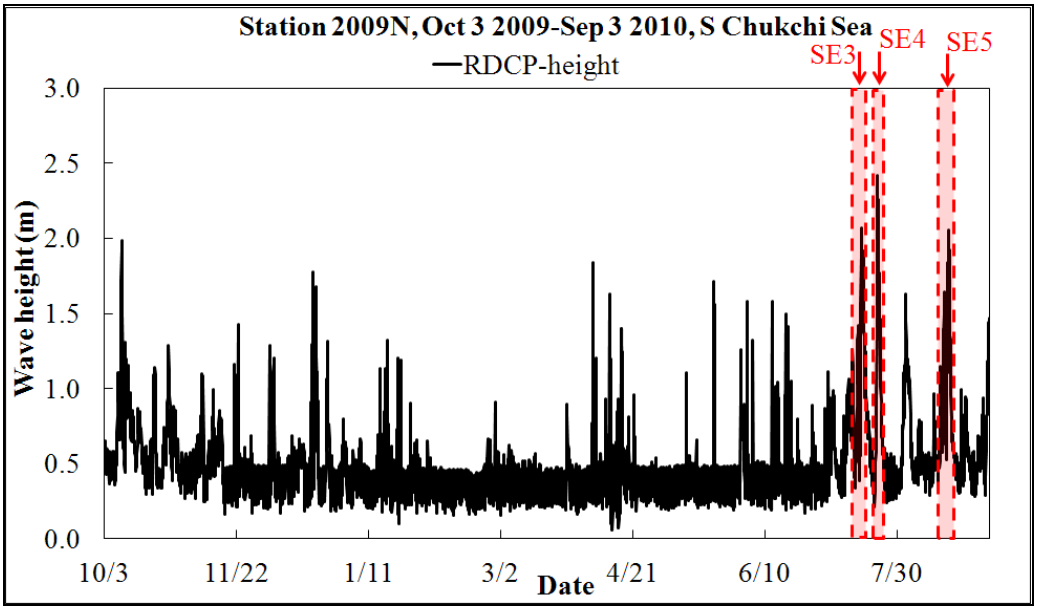

Figure 3.2 – Station 2009N significant wave height
Recording Doppler Current Profiler (RDCP) significant wave height (SWH) at Station 2009N for entire RDCP wave record 3 Oct 2009 – 3 Sep 2010. Station location and depth are 67º38'17.76"N, 164º20'46.26"W (near Kivalina, AK), and 17m, respectively.

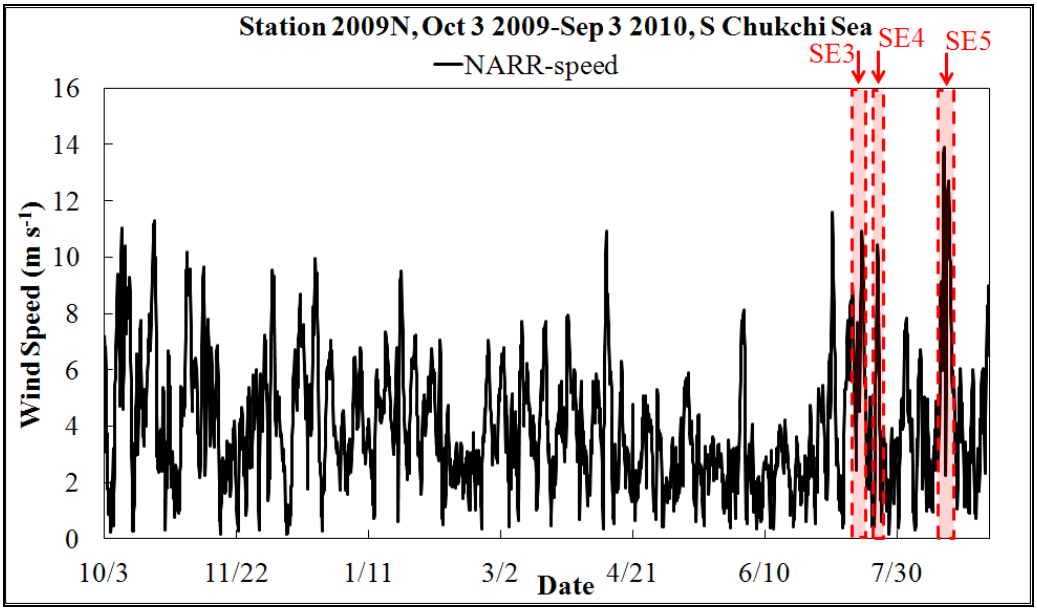

Figure 3.3 – Station 2009N wind speed
North American Regional Reanalysis (NARR) 10m wind speed at Station 2009N for entire Recording Doppler Current Profiler (RDCP) wave record 3 Oct 2009 – 3 Sep 2010. Station location and depth are 67º38'17.76"N, 164º20'46.26"W (near Kivalina, AK), and 17m, respectively.

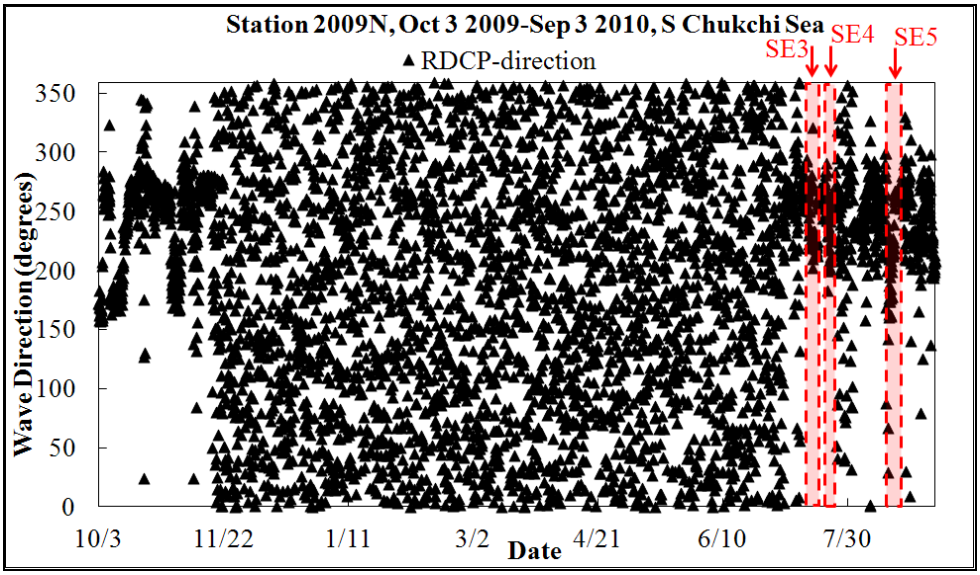

Figure 3.4 – Station 2009N wave direction

Recording Doppler Current Profiler (RDCP) wave direction at Station 2009N for entire RDCP wave record 3 Oct 2009 – 3 Sep 2010. Station location and depth are 67º38'17.76"N, 164º20'46.26"W (near Kivalina, AK), and 17m, respectively.

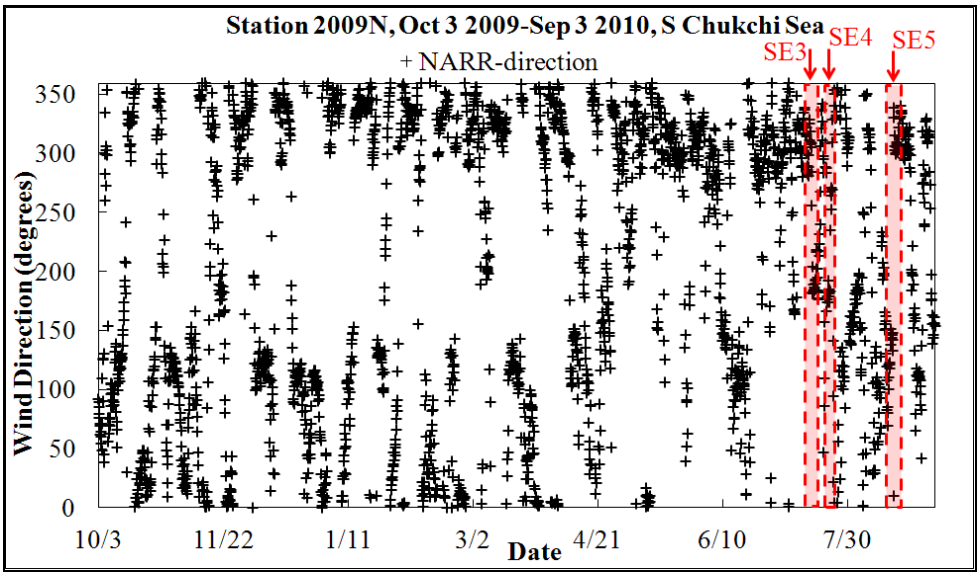

Figure 3.5 – Station 2009N wind direction

North American Regional Reanalysis (NARR) 10m wind direction at Station 2009N for entire Recording Doppler Current Profiler (RDCP) wave record 3 Oct 2009 – 3 Sep 2010. Station location and depth are 67º38'17.76"N, 164º20'46.26"W (near Kivalina, AK), and 17m, respectively.

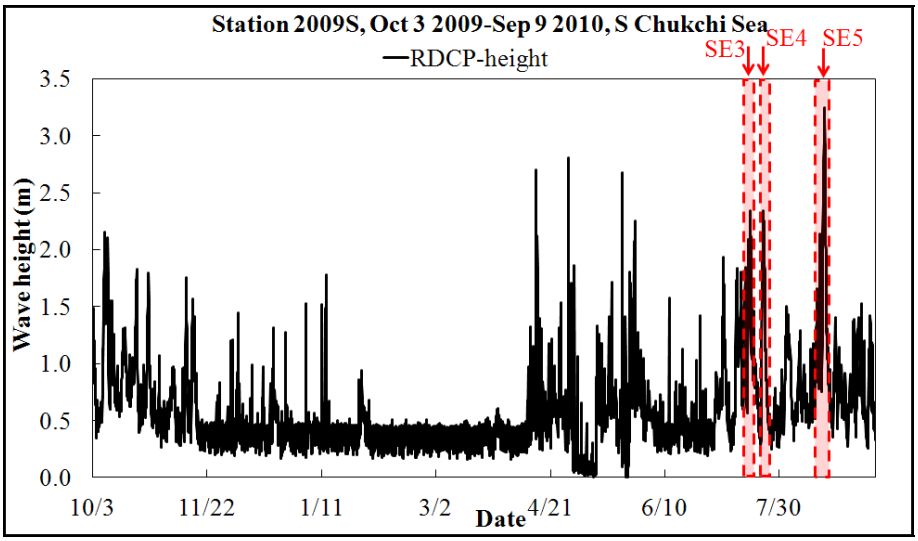

Figure 3.6 – Station 2009S significant wave height

Recording Doppler Current Profiler (RDCP) significant wave height (SWH) at Station 2009N for entire RDCP wave record 3 Oct 2009 – 9 Sep 2010. Station location and depth are 67º10'33.30"N, 163º59'23.94"W (near Cape Krusenstern, AK), and 18m, respectively.

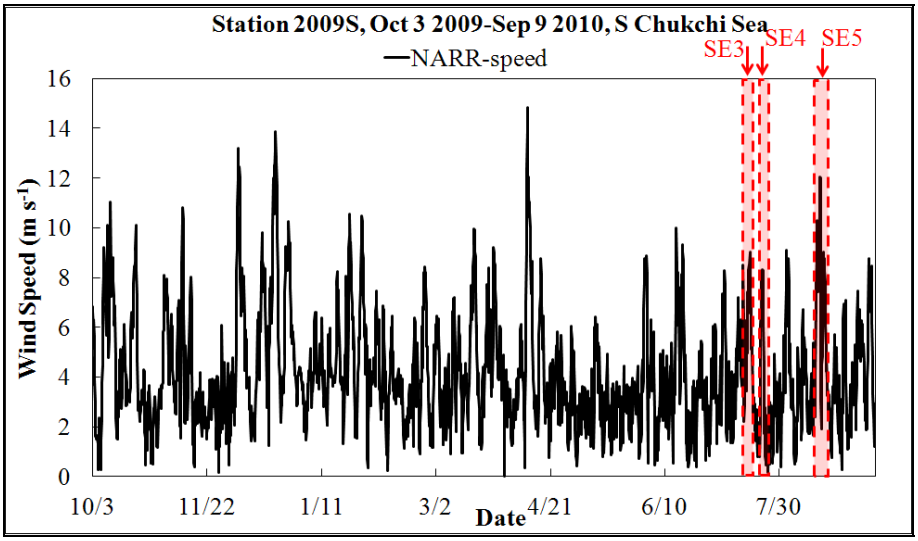

Figure 3.7 – Station 2009S wind speed

North American Regional Reanalysis (NARR) 10m wind speed at Station 2009S for entire Recording Doppler Current Profiler (RDCP) wave record 3 Oct 2009 – 9 Sep 2010. Station location and depth are 67º10'33.30"N, 163º59'23.94"W (near Cape Krusenstern, AK), and 18m, respectively.

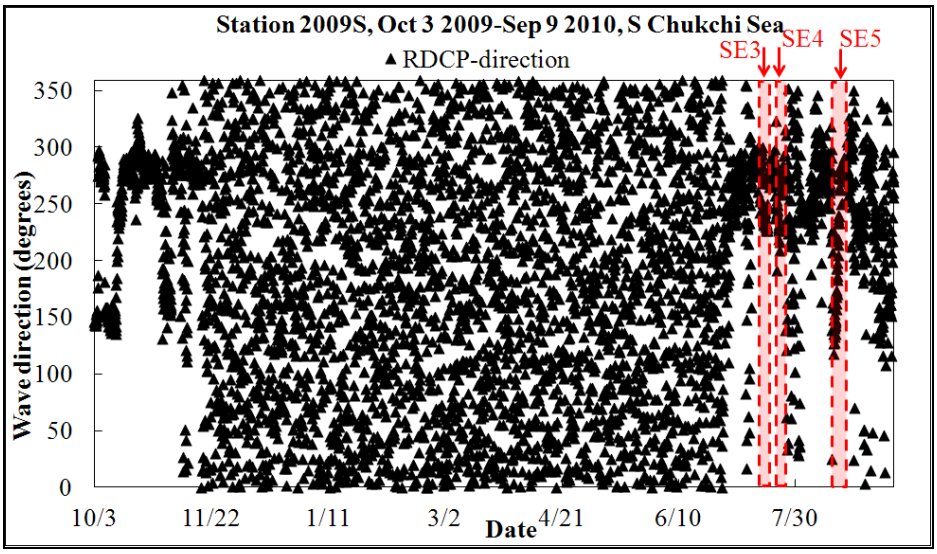

Figure 3.8 – Station 2009S wave direction
Recording Doppler Current Profiler (RDCP) wave direction at Station 2009N for entire RDCP wave record 3 Oct 2009 – 9 Sep 2010. Station location and depth are 67º10'33.30"N, 163º59'23.94"W (near Cape Krusenstern, AK), and 18m, respectively.

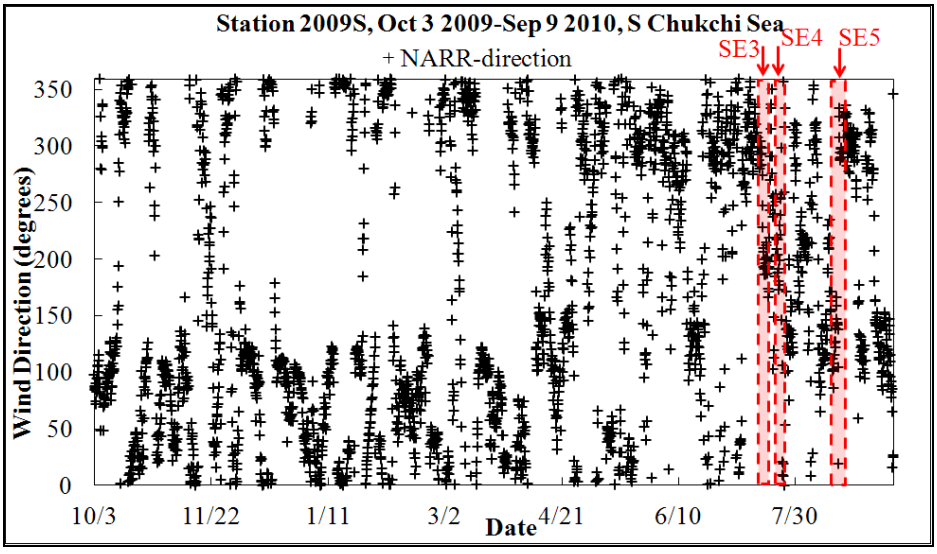

Figure 3.9 – Station 2009S wind direction
North American Regional Reanalysis (NARR) 10m wind direction at Station 2009N for entire Recording Doppler Current Profiler (RDCP) wave record 3 Oct 2009 – 9 Sep 2010. Station location and depth are 67º10'33.30"N, 163º59'23.94"W (near Cape Krusenstern, AK), and 18m, respectively.

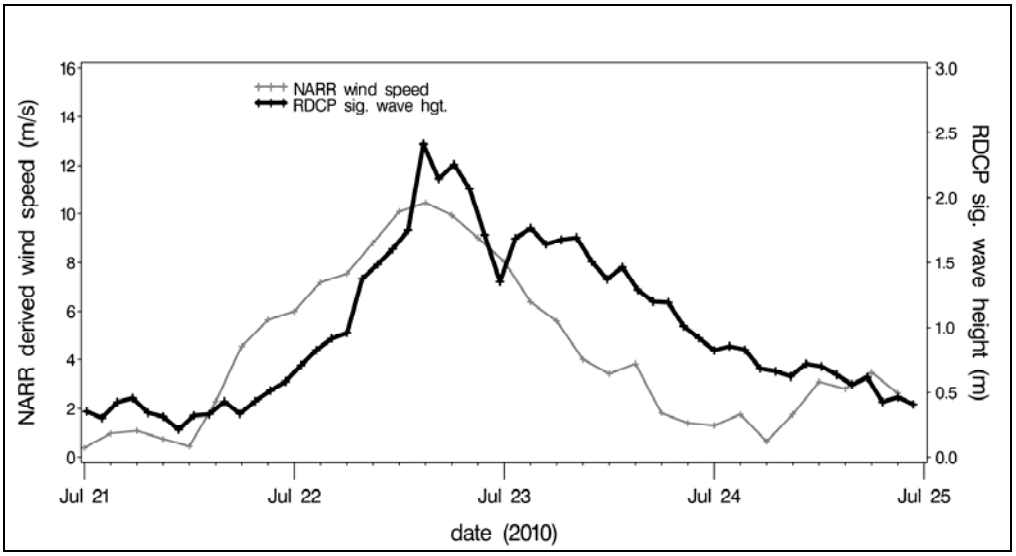

Figure 3.10 – SE3 wave height versus wind speed

Comparison of Recording Doppler Current Profiler (RDCP) significant wave height (SWH) and North American Regional Reanalysis (NARR) 10m wind speed at Station 2009N for wave record 22 – 23 Jul 2010 (SE3). Station location and depth are 67º38'17.76"N, 164º20'46.26"W (near Kivalina, AK), and 17m, respectively.

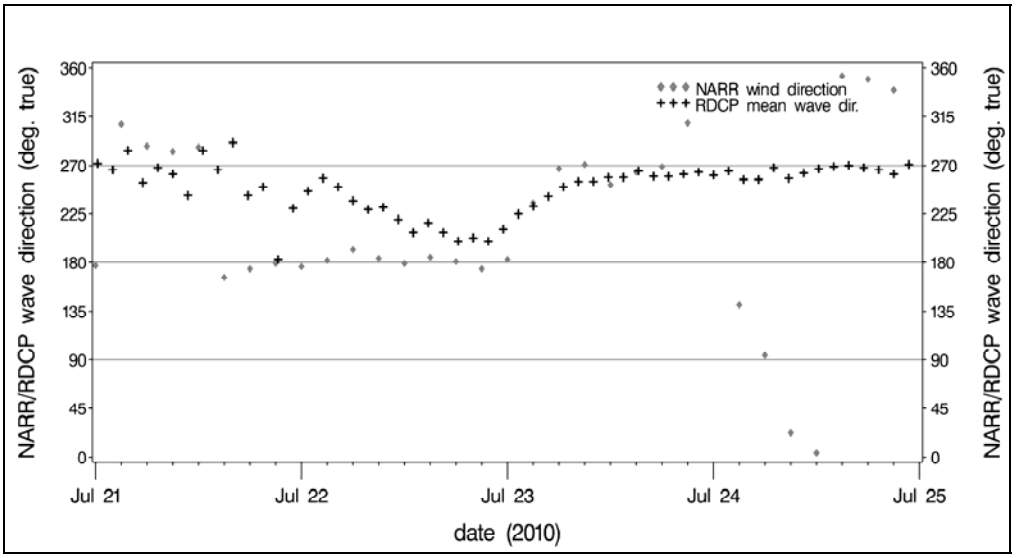

Figure 3.11 – SE3 wave direction versus wind direction

Comparison of Recording Doppler Current Profiler (RDCP) mean wave direction and North American Regional Reanalysis (NARR) 10m wind direction at Station 2009N for wave record 22 – 23 Jul 2010 (SE3). Station location and depth are 67º38'17.76"N, 164º20'46.26"W (near Kivalina, AK), and 17m, respectively.

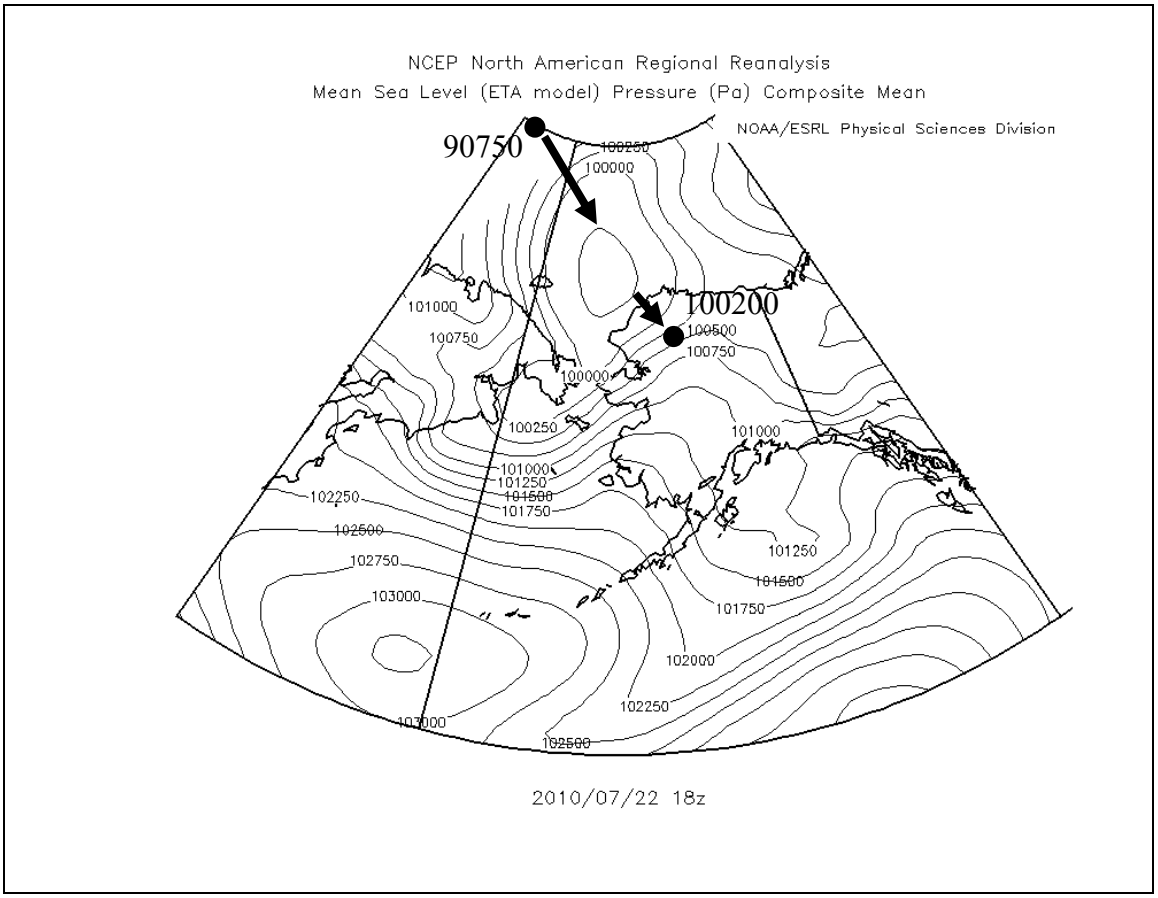

Figure 3.12 – SE3 storm maxima
Storm maxima during SE3 on 22 Jul 2010 1800 UTC shown on North American Regional Reanalysis (NARR) Mean Sea Level Pressure (MSLP) map. Image provided by the NOAA-ESRL Physical Sciences Division, Boulder Colorado at http://www.esrl.noaa.gov/psd. Modified by O. Francis, Jan 2011.

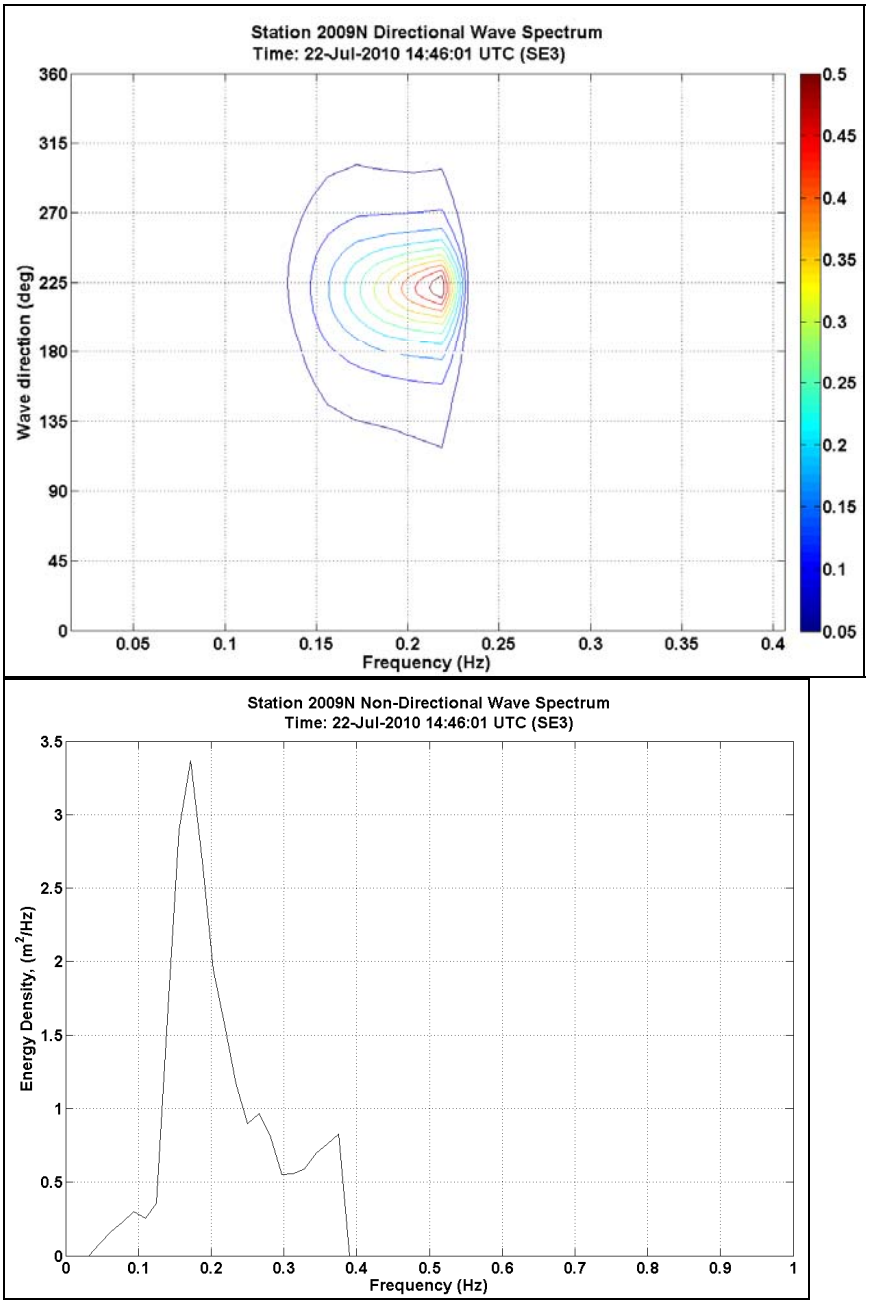

Figure 3.13 – SE3 wave spectrum

Directional (top) and non-directional (bottom) wave spectra Cartesian projection of highest SWH in SE3 on 22 Jul 2010 1446 UTC, SWH=2.4m recorded by the Recording Doppler Current Profiler (RDCP) at Station 2009N at 67º38'17.76"N, 164º20'46.26"W (near Kivalina, AK), and with a water depth of 17m. The color bar (top) and non-directional (bottom) gives the wave energy density, $E(f)$, in m^2Hz^{-1}.

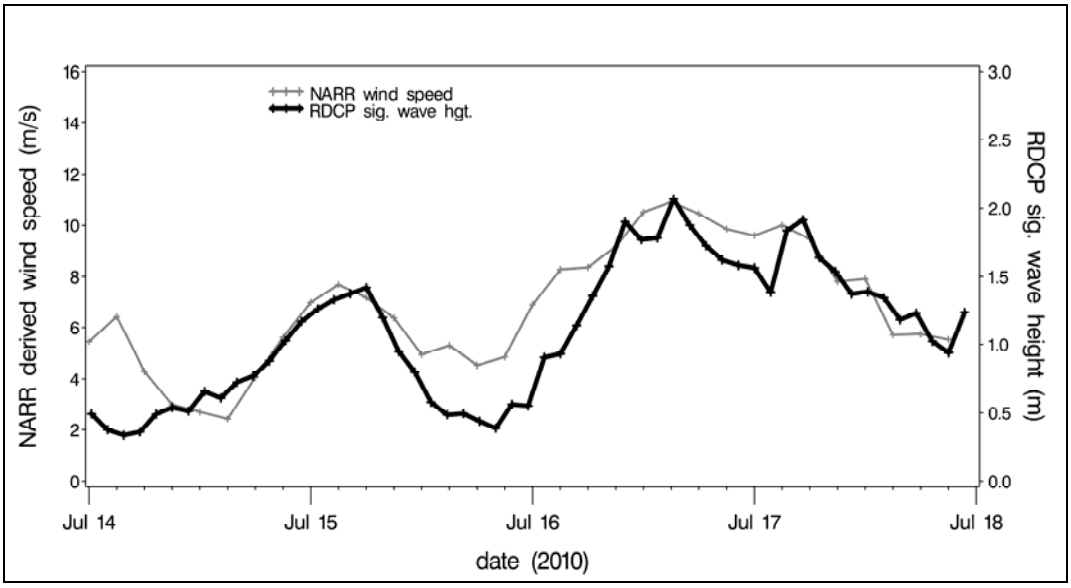

Figure 3.14 – SE4 wave height versus wind speed
Comparison of Recording Doppler Current Profiler (RDCP) significant wave height (SWH) and North American Regional Reanalysis (NARR) 10m wind speed at Station 2009S for wave record 16 – 18 Jul 2010 (SE4). Station location and depth are 67º10'33.30"N, 163º59'23.94"W (near Cape Krusenstern, AK), and 18m, respectively.

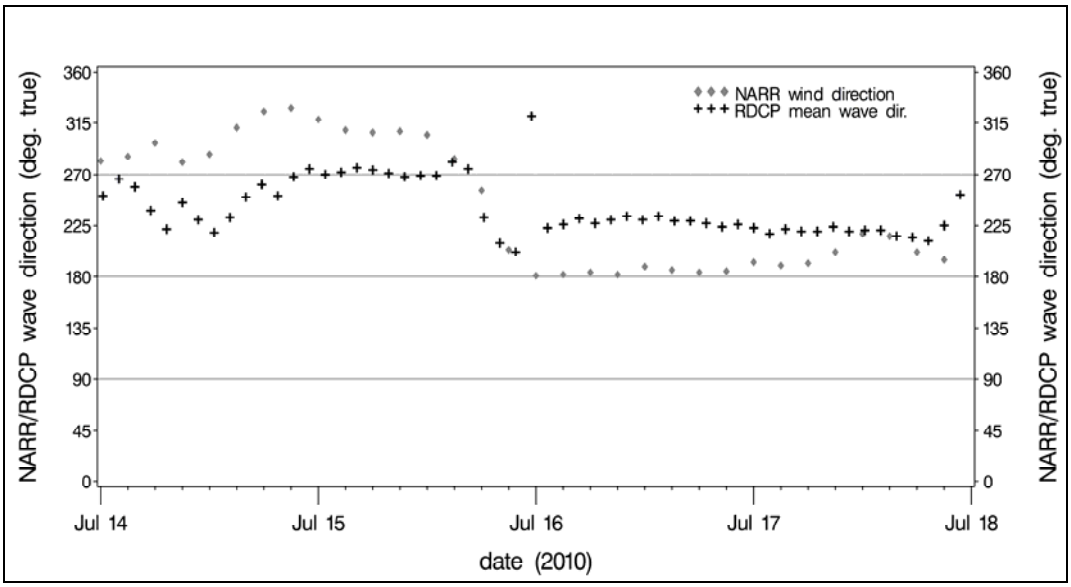

Figure 3.15 – SE 4 wave direction versus wind direction
Comparison of Recording Doppler Current Profiler (RDCP) mean wave direction and North American Regional Reanalysis (NARR) 10m wind direction at Station 2009S for wave record 16 – 18 Jul 2010 (SE4). Station location and depth are 67º10'33.30"N, 163º59'23.94"W (near Cape Krusenstern, AK), and 18m, respectively.

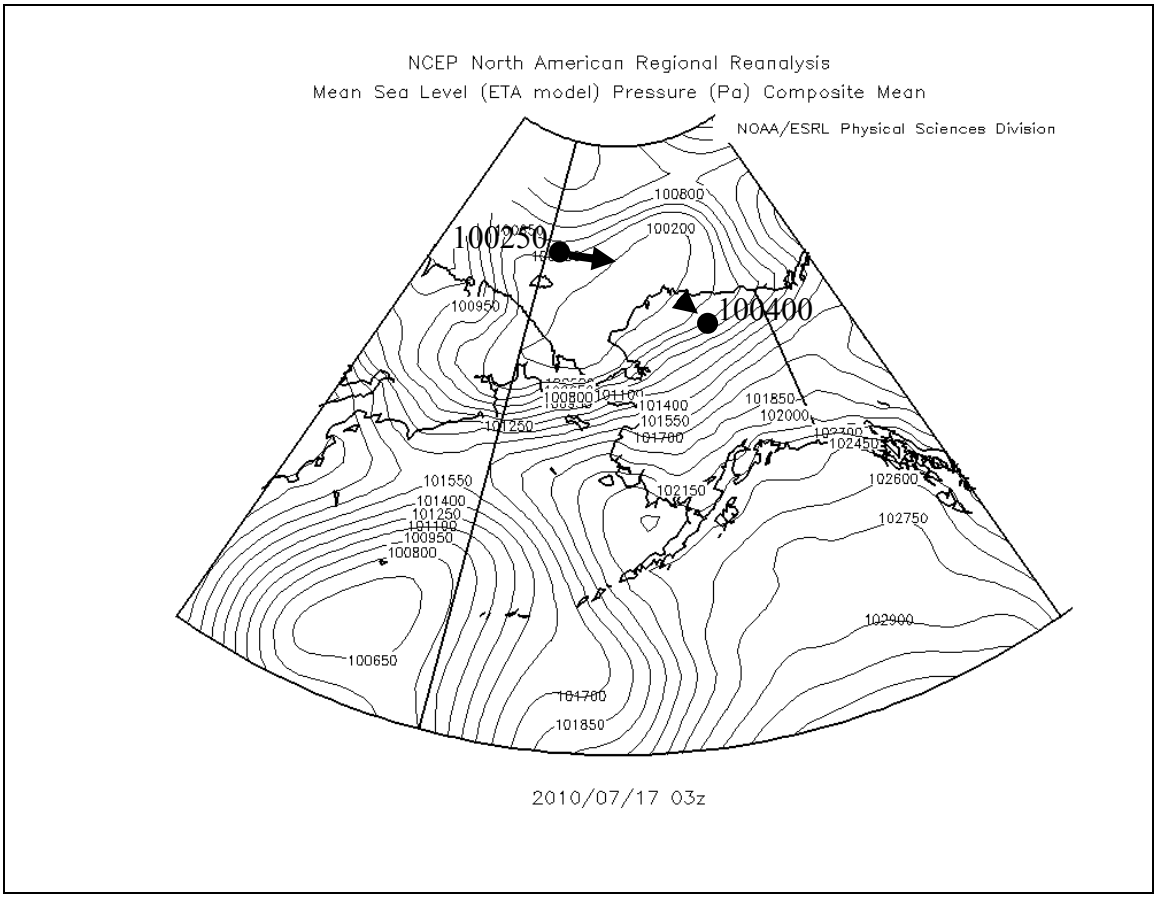

Figure 3.16 – SE4 storm maxima
Storm maxima during SE4 on 17 Jul 2010 0300 UTC shown on North American Regional Reanalysis (NARR) Mean Sea Level Pressure (MSLP) map. Image provided by the NOAA-ESRL Physical Sciences Division, Boulder Colorado at http://www.esrl.noaa.gov/psd. Modified by O. Francis, Jan 2011.

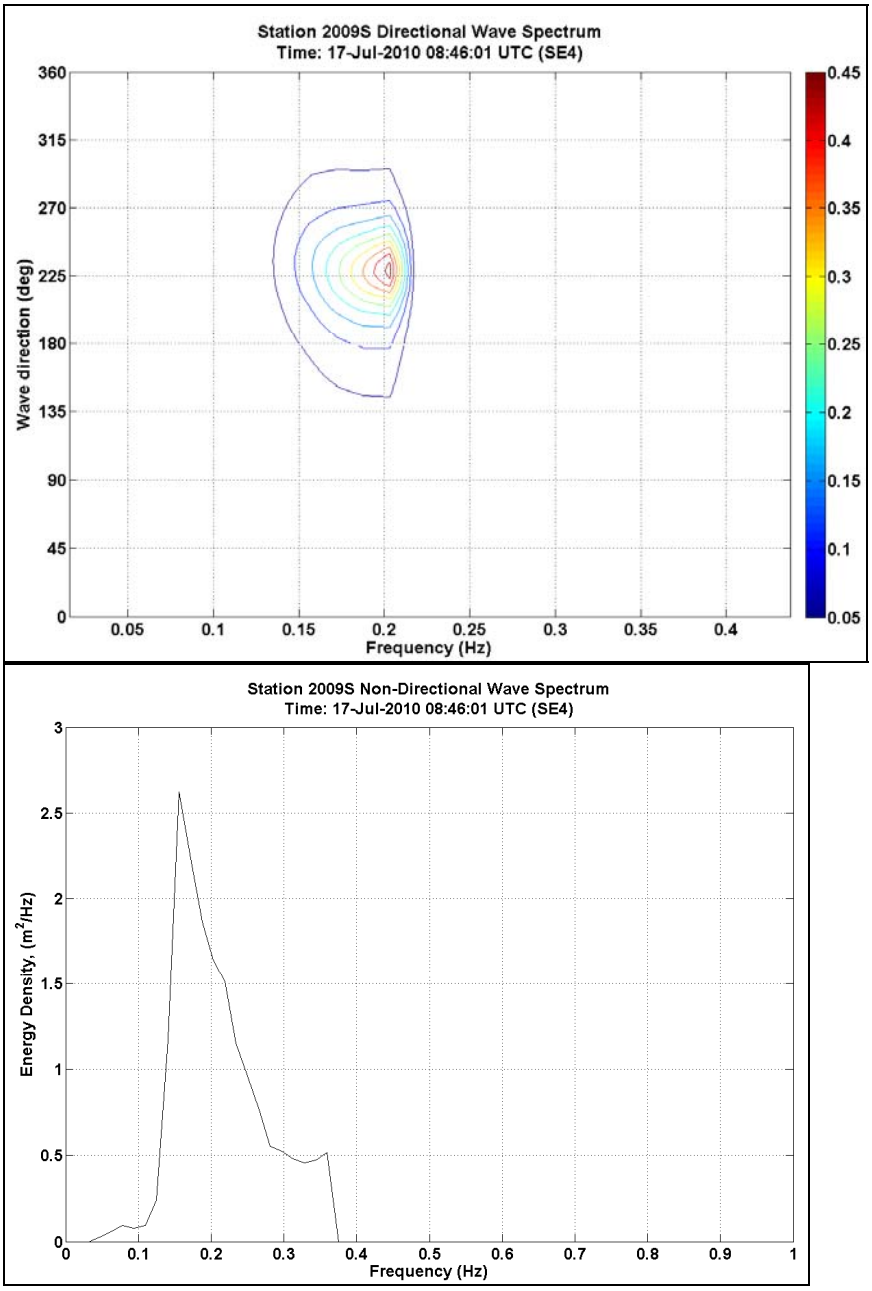

Figure 3.17 – SE4 wave spectrum

Directional (top) and non-directional (bottom) wave spectra Cartesian projection of highest SWH in SE4 on 17 Jul 2010 0846 UTC, SWH=2.1m recorded by the Recording Doppler Current Profiler (RDCP) at Station 2009S at 67º10'33.30"N, 163º59'23.94"W (near Cape Krusenstern, AK), and with a water depth of 18m. The color bar (top) and non-directional (bottom) gives the wave energy density, $E(f)$, in m^2Hz^{-1}.

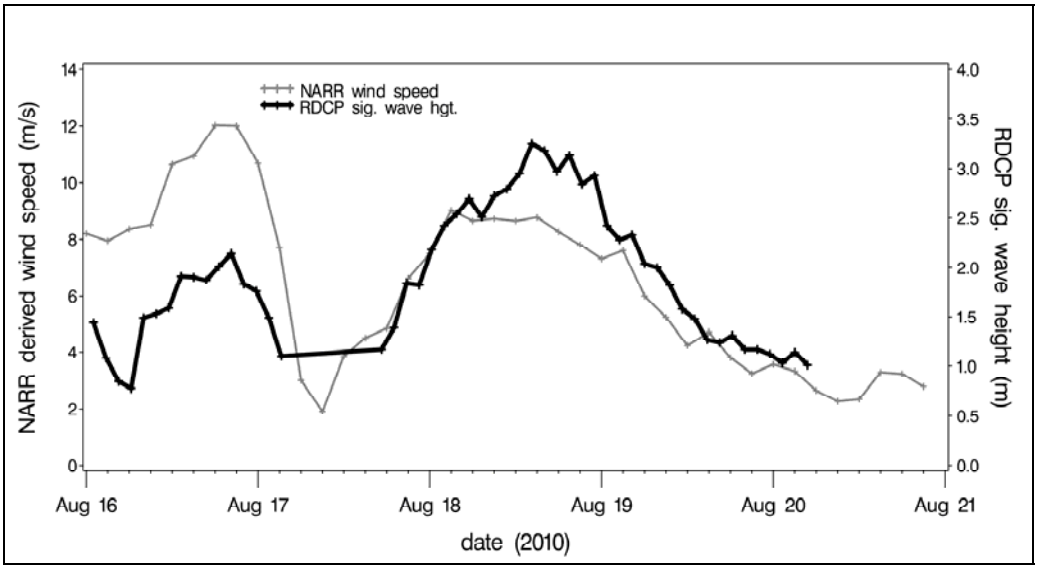

Figure 3.18 – SE5 wave height versus wind speed
Comparison of Recording Doppler Current Profiler (RDCP) significant wave height (SWH) and North American Regional Reanalysis (NARR) 10m wind speed at Station 2009S for wave record 17 – 20 Aug 2010 (SE5). Station location and depth are 67º10'33.30"N, 163º59'23.94"W (near Cape Krusenstern, AK), and 18m, respectively.

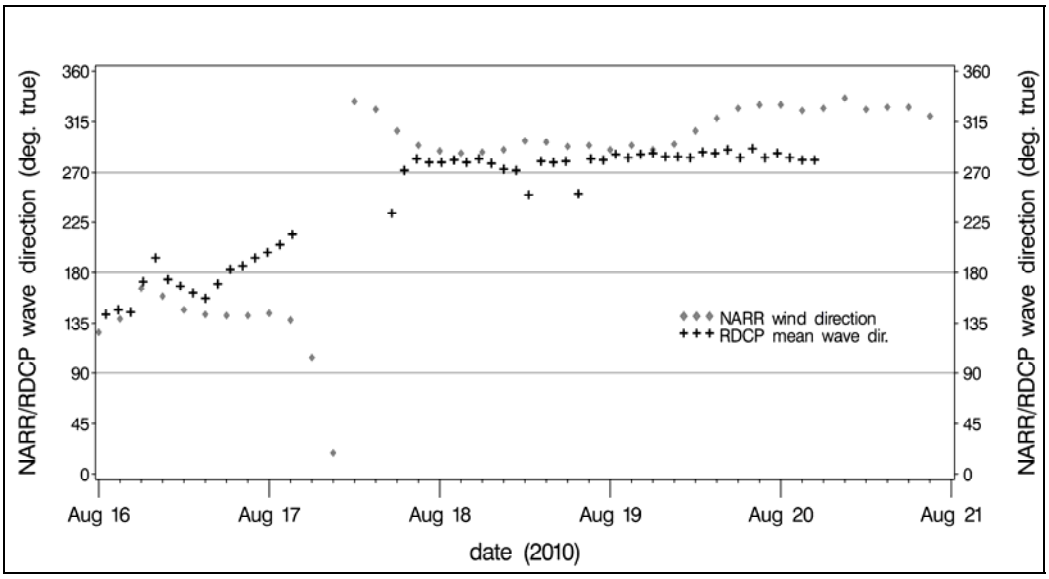

Figure 3.19 – SE5 wave direction versus wind direction
Comparison of Recording Doppler Current Profiler (RDCP) mean wave direction and North American Regional Reanalysis (NARR) 10m wind direction at Station 2009S for wave record 17 – 20 Aug 2010 (SE5). Station location and depth are 67º10'33.30"N, 163º59'23.94"W (near Cape Krusenstern, AK), and 18m, respectively.

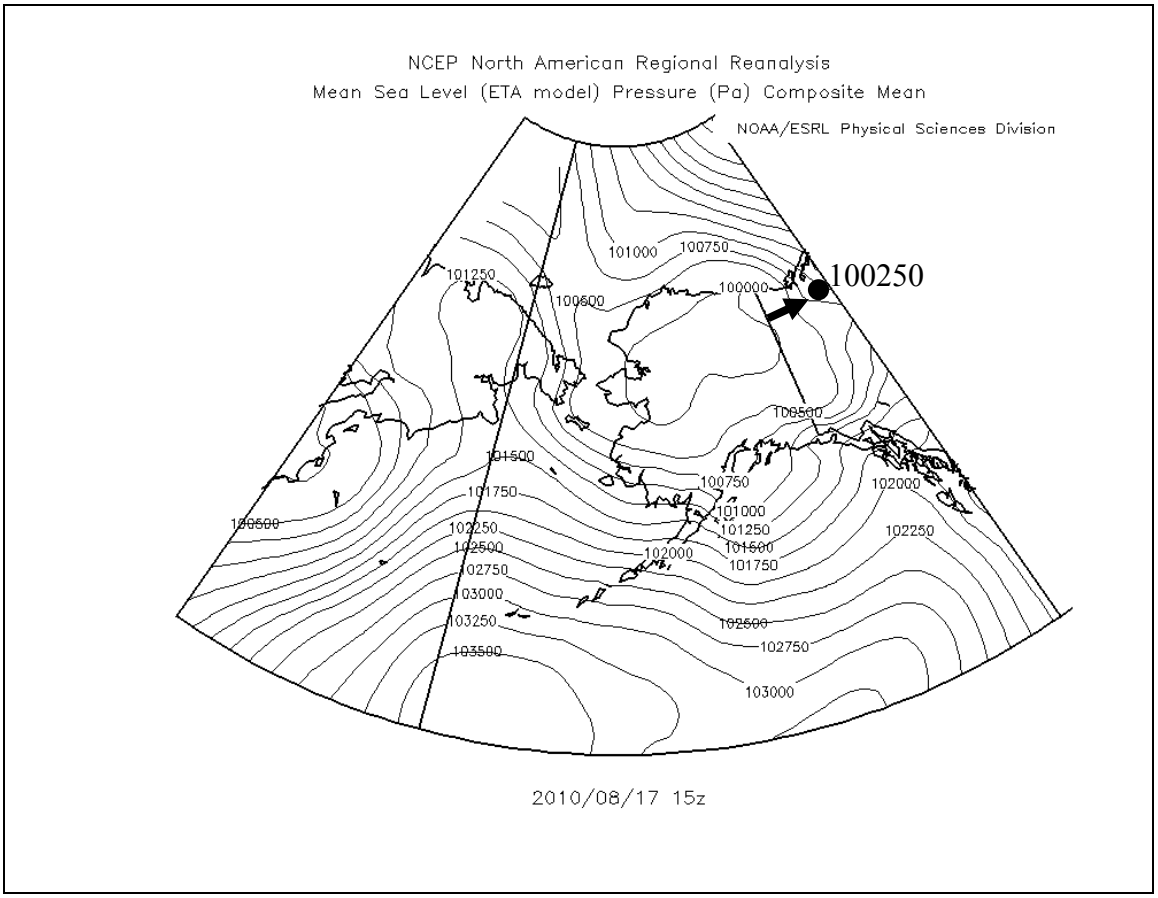

Figure 3.20 – SE5 storm maxima
Storm maxima during SE5 on 17 Aug 2010 1500 UTC shown on North American Regional Reanalysis (NARR) Mean Sea Level Pressure (MSLP) map. Image provided by the NOAA-ESRL Physical Sciences Division, Boulder Colorado at http://www.esrl.noaa.gov/psd. Modified by O. Francis, Jan 2011.

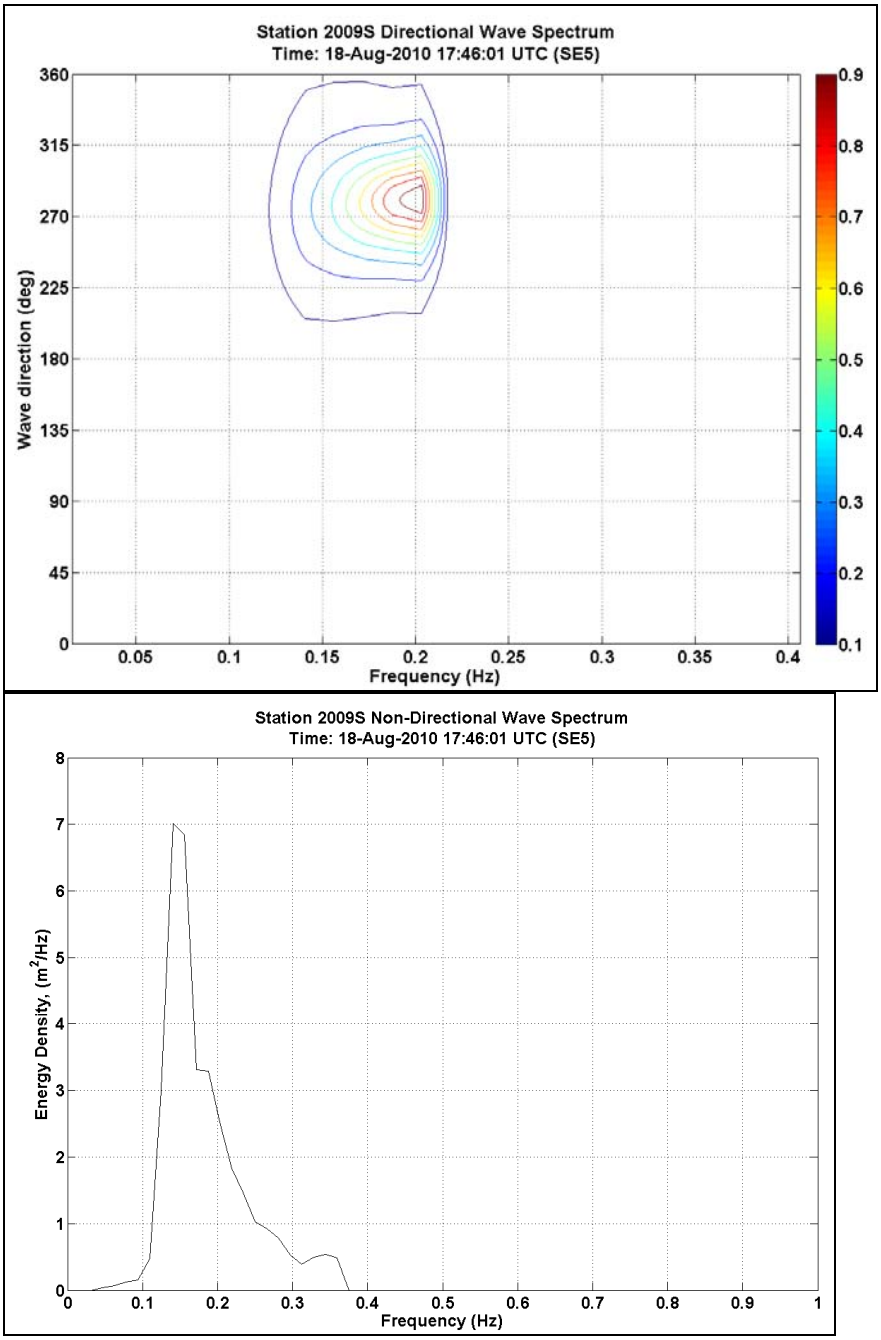

Figure 3.21 – SE5 wave spectrum

Directional (top) and non-directional (bottom) wave spectra Cartesian projection of highest SWH in SE5 on 18 Jul 2010 1416 UTC, SWH=3.3m recorded by the Recording Doppler Current Profiler (RDCP) at Station 2009S at 67º10'33.30"N, 163º59'23.94"W (near Cape Krusenstern, AK), and with a water depth of 18m. The color bar (top) and non-directional (bottom) gives the wave energy density, $E(f)$, in m^2Hz^{-1}.

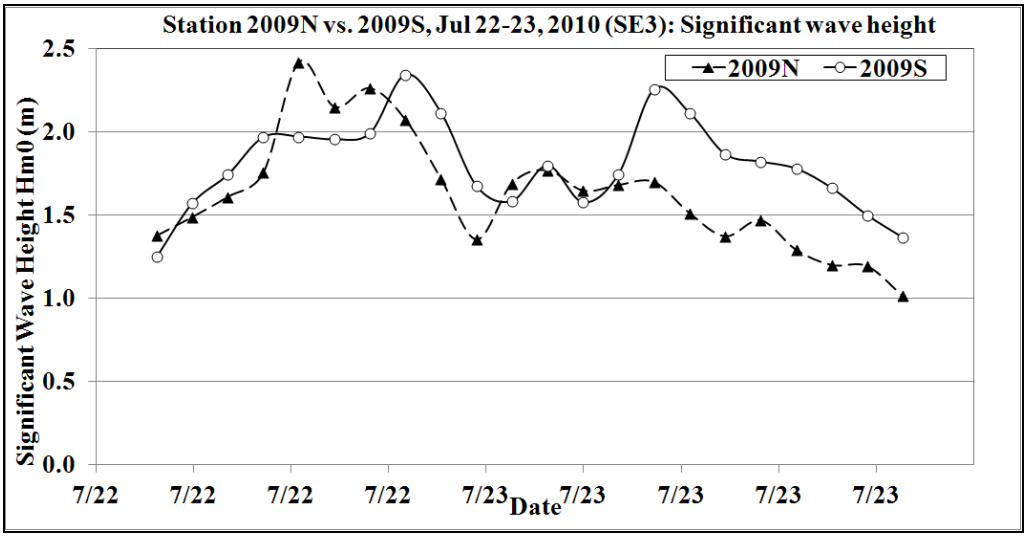

Figure 3.22 – SE3 significant wave height comparison
Comparison of Recording Doppler Current Profiler (RDCP) significant wave height (SWH) during wave record 22 – 23 Jul 2010 (SE3) for two different Stations: 1) Station 2009N, 67º38'17.76"N, 164º20'46.26"W, north location near Kivalina, AK, water depth 17m, and 2) Station 2009S, 67º10'33.30"N, 163º59'23.94"W, south location near Cape Krusenstern, AK, water depth 18m.

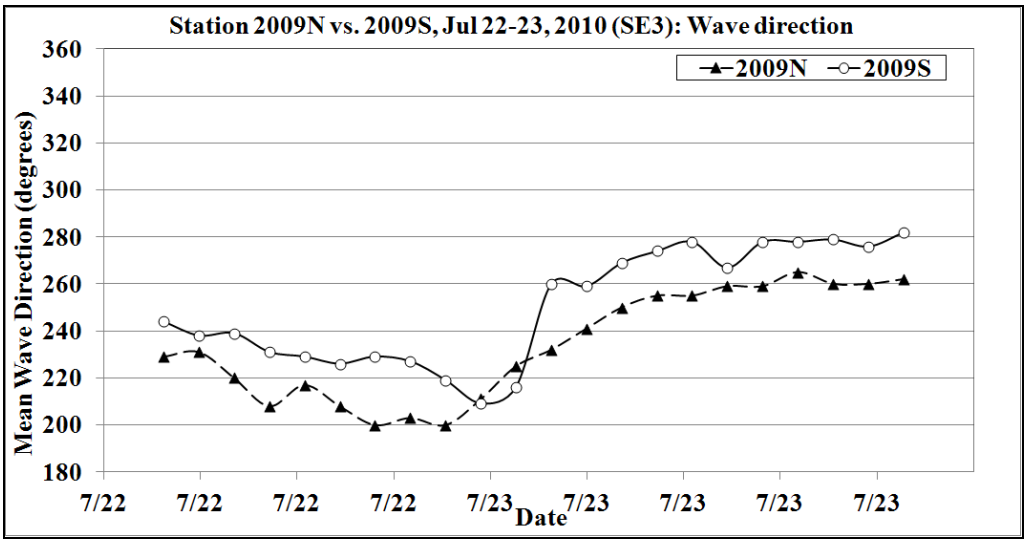

Figure 3.23 – SE3 wave direction comparison
Comparison of Recording Doppler Current Profiler (RDCP) mean wave direction during wave record 22 – 23 Jul 2010 (SE3) for two different Stations: 1) Station 2009N, 67º38'17.76"N, 164º20'46.26"W, north location near Kivalina, AK, water depth 17m, and 2) Station 2009S, 67º10'33.30"N, 163º59'23.94"W, south location near Cape Krusenstern, AK, water depth 18m.

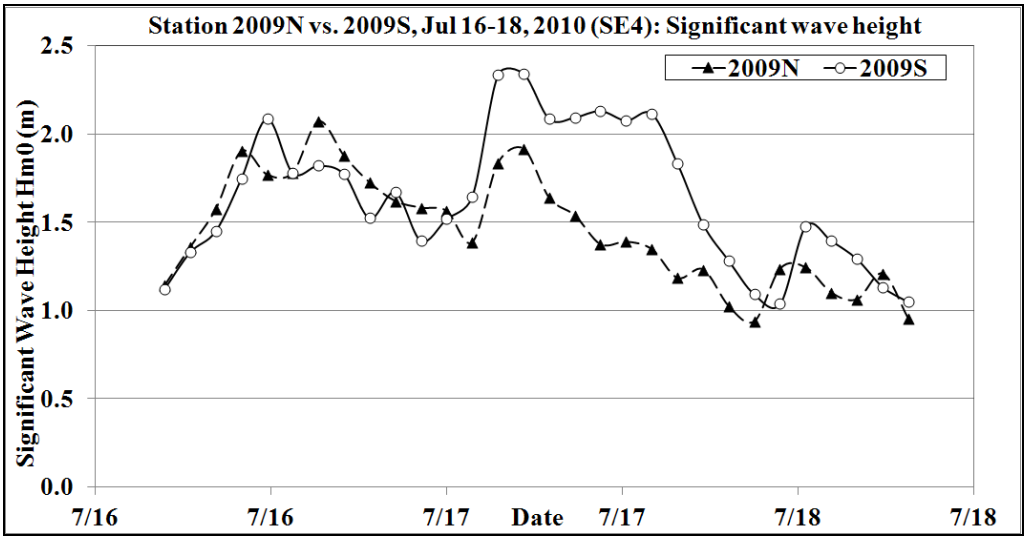

Figure 3.24 – SE4 significant wave height comparison

Comparison of Recording Doppler Current Profiler (RDCP) significant wave height (SWH) during wave record 16 – 18 Jul 2010 (SE4) for two different Stations: 1) Station 2009N, 67º38'17.76"N, 164º20'46.26"W, north location near Kivalina, AK, water depth 17m, and 2) Station 2009S, 67º10'33.30"N, 163º59'23.94"W, south location near Cape Krusenstern, AK, water depth 18m.

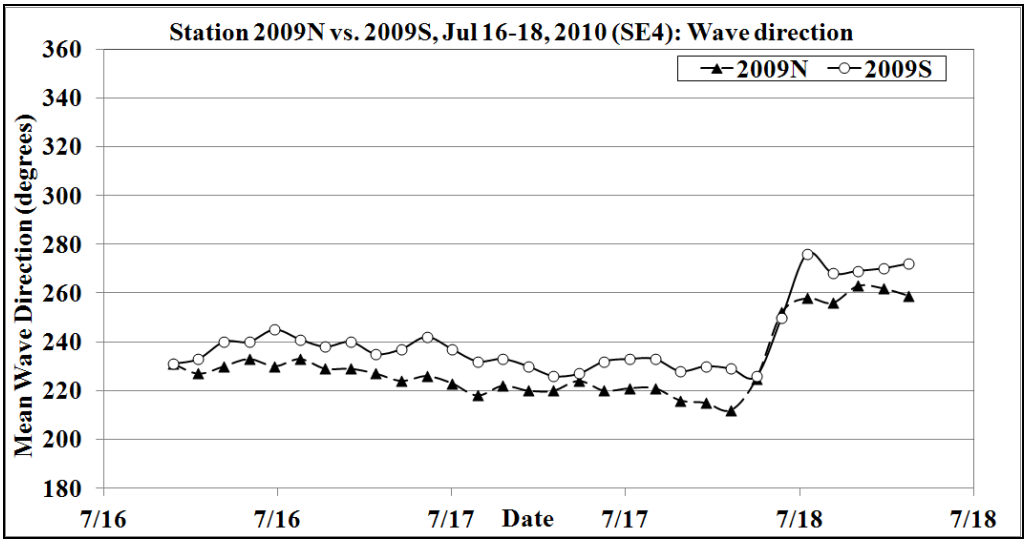

Figure 3.25 – SE4 wave direction comparison

Comparison of Recording Doppler Current Profiler (RDCP) mean wave direction during wave record 16 – 18 Jul 2010 (SE4) for two different Stations: 1) Station 2009N, 67º38'17.76"N, 164º20'46.26"W, north location near Kivalina, AK, water depth 17m, and 2) Station 2009S, 67º10'33.30"N, 163º59'23.94"W, south location near Cape Krusenstern, AK, water depth 18m.

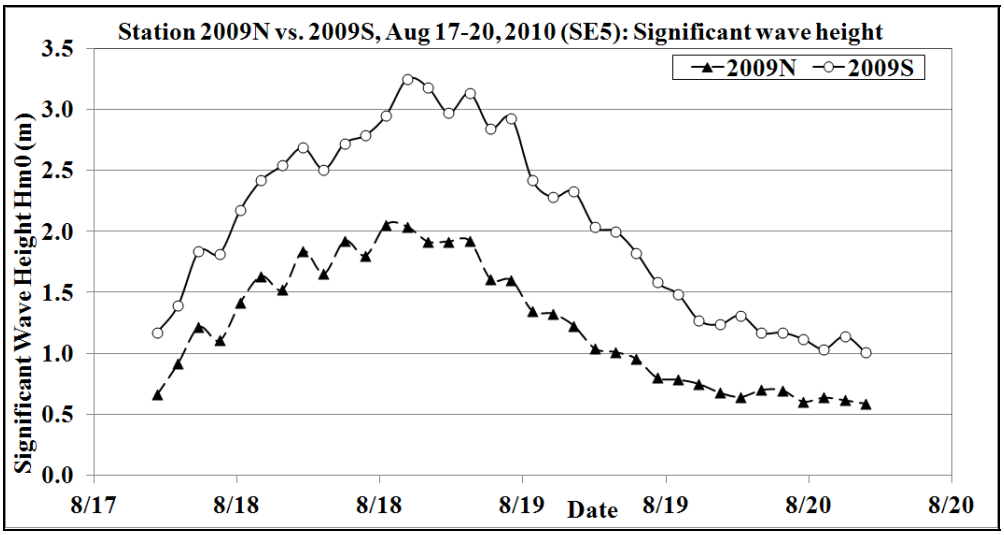

Figure 3.26 – SE5 significant wave height comparison

Comparison of Recording Doppler Current Profiler (RDCP) significant wave height (SWH) during wave record 17 – 20 Aug 2010 (SE5) for two different Stations: 1) Station 2009N, 67º38'17.76"N, 164º20'46.26"W, north location near Kivalina, AK, water depth 17m, and 2) Station 2009S, 67º10'33.30"N, 163º59'23.94"W, south location near Cape Krusenstern, AK, water depth 18m.

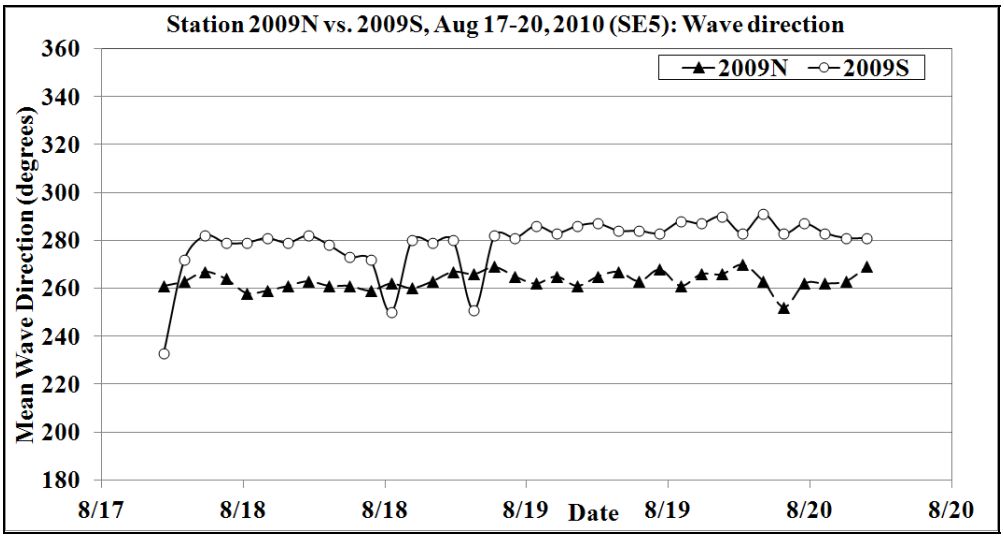

Figure 3.27 – SE5 wave direction comparison

Comparison of Recording Doppler Current Profiler (RDCP) mean wave direction during wave record 17 – 20 Aug 2010 (SE5) for two different Stations: 1) Station 2009N, 67º38'17.76"N, 164º20'46.26"W, north location near Kivalina, AK, water depth 17m, and 2) Station 2009S, 67º10'33.30"N, 163º59'23.94"W, south location near Cape Krusenstern, AK, water depth 18m.

Table 3.1 – Station 2009N significant wave height events ≥ 1m

Station 2009N significant wave height (SWH) events (1m-"minor" and 2m-"major" in *italics* to designate "SE"), (l to r) SWH duration, SWH, wave period, wave direction, fetch, wind speed, wind direction for wave record 3 Oct 2009 – 3 Sep 2010 at 67º38'17.76"N, 164º20'46.26"W, north location near Kivalina, AK, water depth 17m.

SWH Event	Date	SWH Duration (hrs)	Hm0 (m)	Tm02 (sec)	Wave Dir (deg)	Wind Spd (m/s)	Wind Dir (deg)
2009N-1m-1	10/9-10/10/2009	17.5	1.5	4.3	170	7.8	122
2009N-1m-2	10/11-10/11/2009	17.5	1.1	3.8	180	8.4	114
2009N-1m-3	10/22-10/22/2009	7	1.1	3.5	285	9.9	16
2009N-1m-4	10/27-10/27/2009	8.75	1.1	4.2	264	6.2	347
2009N-1m-5	11/9-11/9/2009	7	1.0	3.4	251	9.1	137
2009N-1m-6	12/6-12/6/2009	7	1.1	4.1	140	8.8	125
2009N-1m-7	12/21-12/22/2009	21	1.2	3.9	130	9.1	114
2009N-1m-8	5/21-5/22/2010	10.5	1.4	5.4	177	2.3	299
2009N-1m-9	7/12-7/13/2010	8.75	1.1	3.8	274	8.5	317
2009N-1m-10	7/14-7/15/2010	12.25	1.3	3.9	272	6.8	314
2009N-1m-11	7/16-7/18/2010	50.75	1.5	4.8	230	8.0	191
[1] 2009N-2m-12	*7/22-7/23/2010*	*38.5*	*1.6*	*5.0*	*234*	*6.5*	*225*
2009N-1m-13	8/1-8/3/2010	52.5	1.2	4.4	235	6.0	180
2009N-1m-14	8/16-8/17/2010	19.25	1.4	4.3	196	11.6	146
2009N-1m-15	8/17-8/19/2010	36.75	1.6	4.5	263	10.9	304
2009N-1m-16	9/2-9/3/2010	28	1.2	3.6	207	8.1	151

[1] 2009N-2m-12 (also known as SE3)

Table 3.2 – Station 2009S significant wave height events ≥ 1m

Station 2009S significant wave height (SWH) events (1m-"minor" and 2m-"major" in *italics* to designate "SE"), (l to r) SWH duration, SWH, wave period, wave direction, fetch, wind speed, wind direction for wave record 3 Oct 2009 – 9 Sep 2010 at 67º10'33.30"N, 163º59'23.94"W, south location near Cape Krusenstern, AK, water depth 18m.

SWH Event	Date	SWH Duration (hrs)	Hm0 (m)	Tm02 (sec)	Wave Dir (deg)	Wind Spd (m/s)	Wind Dir (deg)
2009S-1m-1	10/3-10/4/2009	19.25	1.2	3.9	147	5.7	86
2009S-1m-2	10/7-10/10/2009	61.25	1.7	4.3	150	7.3	97
2009S-1m-3	10/10-10/12/2009	38.5	1.2	3.8	156	8.0	116
2009S-1m-4	10/16-10/17/2009	26.25	1.2	4.0	285	5.0	300
2009S-1m-5	10/21-10/22/2009	29.75	1.3	3.9	303	8.3	23
2009S-1m-6	10/26-10/27/2009	26.25	1.3	4.7	278	2.6	332
2009S-1m-7	11/12-11/13/2009	22.75	1.3	6.2	280	3.8	180
2009S-1m-8	11/15-11/16/2009	29.75	1.2	7.4	280	2.2	178
2009S-1m-9	12/5-12/5/2009	7	1.4	3.8	95	12.7	112
2009S-1m-10	4/15-4/15/2010	7	1.7	5.8	182	2.3	184
2009S-1m-11	5/26-5/27/2010	45.5	1.3	4.7	179	3.2	140
2009S-1m-12	7/5-7/6/2010	31.5	1.4	4.4	284	7.1	169
2009S-1m-13	7/10-7/13/2010	64.75	1.4	4.0	287	5.1	306
2009S-1m-14	7/14-7/15/2010	24.5	1.4	4.0	288	4.0	293
[1] 2009S-2m-15	*7/16-7/18/2010*	*52.5*	*1.6*	*4.7*	*241*	*6.8*	*194*
2009S-1m-16	7/22-7/24/2010	45.5	1.7	4.7	254	4.8	214
2009S-1m-17	8/1-8/3/2010	56	1.2	4.2	243	6.3	211
2009S-1m-18	8/7-8/8/2010	7	1.2	3.6	280	3.8	305
2009S-1m-19	8/15-8/17/2010	50.75	1.5	3.8	158	9.4	130
[2] 2009S-2m-20	*8/17-8/20/2010*	*61.25*	*2.0*	*4.4*	*279*	*6.1*	*304*
2009S-1m-21	8/23-8/24/2010	21	1.1	3.7	259	4.0	301
2009S-1m-22	8/31-8/31/2010	14	1.2	3.8	292	3.3	306
2009S-1m-23	9/2-9/2/2010	22.75	1.2	3.8	223	6.7	147
2009S-1m-24	9/3-9/3/2010	14	1.3	3.8	149	5.7	122
2009S-1m-25	9/7-9/7/2010	7	1.3	3.5	158	6.9	100

[1] 2009S-2m-15 (also known as SE4)

[2] 2009S-2m-20 (also known as SE5)

Chapter 4 A description of one-dimensional wave spectra in the southeast Chukchi Sea location[1]

Abstract

The spectra of ocean wave data from the southeast Chukchi Sea obtained during open water season of 2007 and 2010 were calculated and analyzed to determine an idealized form for the spectrum of ocean surface waves for this region. Wind-generated waves were described using one-dimensional models driven by North American Regional Reanalysis (NARR) wind data fields. *In situ* wave measurements came from Recording Doppler Current Profilers (RDCP) situated at a single offshore position in (2007 UTC) and two near-shore positions (2009-2010 UTC). The wave steepness method presently in use by the US National Buoy Data Center was used to determine the separation frequency. From the wave steepness method and knowledge of the local wind speed, wave spectra were identified as either wind-sea or swell. It was shown that most of the single-peaked spectra observed were described best by the spectral forms of the JONSWAP and TMA. The highest significant wave heights at the offshore position (north of Shishmaref, Alaska) were a result of strong easterly winds forcing dominant wind-seas consistent in their mean wave directions. The largest significant wave heights at the northerly nearshore position (near Kivalina, Alaska) were forced by strong south wind and wave directions and were considered to be swell. The highest significant wave heights at the southerly nearshore position (near Cape Krusenstern, Alaska) were

[1] Francis, O.P., D.E. Atkinson, R.E. Jensen, and U. Bhatt (2012). A description of one-dimensional wave spectra in the southeast Chukchi Sea. *Ocean Engineering*, **in preparation for submission**.

comprised of strong west wind and wave directions and were considered to possess swell and wind-sea components. Agreement between JONSWAP and the observed data was greatest for the offshore region. For four events, there was good agreement between JONSWAP and the observed data, especially for the offshore region. Only one event differed significantly between the model and the *in situ* measurements.

4.1. Introduction

One-dimensional wave spectra are useful for describing wind-wave characteristics generated by storms. The shape of the spectra is determined by the type of incoming wave, i.e. wind-sea versus swell. Modern engineering practice uses the Pierson-Moskowitz (PM) spectrum (Pierson and Moskowitz, 1964), the Joint North Sea Wave Project (JONSWAP) spectrum (Hasselmann et al., 1973), and the TEXEL storm, MARSEN, ARSLOE (TMA) spectrum (Bouws et. al., 1985) to show the frequency distribution of waves, as applied to ocean settings. The PM, JONSWAP, TMA spectra were originally developed using data obtained from a large number of field measurements; these spectra were then fit to a set of parameters. The PM spectrum was designed for a fully developed sea and is independent of fetch and duration of the wind. The JONSWAP spectrum is a slightly modified PM spectrum with the inclusion of fetch limited wave spectra. The TMA spectrum is similar to the JONSWAP spectrum but modified for waves that are propagating toward a shallow water environment, where Kitaigordskii et al. (1975) showed that the Phillips (1958) f^{-5} can be modified for shallow water. Both PM and JONSWAP describe wind-waves which are characterized by random wave periods and random wave heights for deep water. The PM spectra (Pierson and Moskowitz, 1964) were designed for wind speeds between 10-20 m s^{-1} with unlimited fetch. The JONSWAP spectra (Hasselmann et al., 1973) were designed for wind speeds also up to a maximum of 20 m s^{-1} with a maximum fetch of 160km. However, the PM and JONSWAP spectra have been used for conditions far beyond their

original intended use such as the characterization of wave states during severe storm conditions and hurricanes (Rye, 1977; Lee 1980, Carter, 1982).

Today's understanding of wave characteristics in the southeast Chukchi Sea region comes from the Wave Information Study (WIS) (Jensen et al., 2002). WIS uses the numerical wave model WAM to estimate swell and wind-sea for various grid points along the Alaskan coastline. WAM was developed by the WAMDI Group (1988) and solves the energy balance equation, $S = S_{wind} + S_{nonlin} + S_{dissip}$ (Hasselmann et al., 1973). Similar to the JONSWAP and TMA, it shows the separation of wind-sea and swell and is able to generate directional wave spectra. However, despite the frequency limitations imposed by the RDCP instrument, described below, the JONSWAP and TMA will be shown to be more than adequate for categorizing wave spectra and distinguishing between wind-sea and swell. No other one-dimensional spectral characterization technique has ever been applied in this region.

In this region there is presently little work on the validation of wave models due to a lack of *in situ* measurements. Therefore, the ability to determine if models, such as WAM or JONSWAP and TMA, can be applied to the Chukchi Sea is important in order to show that these models can be considered accurate tools for future engineering and scientific applications in the Chukchi Sea. Our focus is phase-resolving models, focusing in particular on one-dimensional spectral models based on the energy balance equation (Hasselmann et al., 1973). Phase-resolving models are fully deterministic models based on hydrodynamics conservation laws, i.e. conservation of mass, momentum and energy

(Losada and Revilla, 2009). This study not only shows if these simple phase-resolving models can be used to accurately estimate wave spectra but also presents new *in situ* measurements in the southeast Chukchi Sea to validate these simple models and validates wind fields that can be used to force these models.

The overarching goal of this study is the characterization if wave states in the southeast Chukchi Sea using spectral models. This includes three tasks: 1) Apply wave theory and one-dimensional spectral models to *in situ* data in order to classify and describe the type of wave in offshore and nearshore regions of the southeast Chukchi Sea. 2) Obtain estimates of commonly used constants such as the JONSWAP and TMA peak enhancement factor γ for this region. 3) Cross-validate the JONSWAP and TMA one-dimensional wave spectral models with *in situ* wave measurements. *In situ* data comes from Recording Doppler Current Profilers (RDCPs) manufactured by Aanderaa Instruments, Bergen, Norway (AADI, 2006) that were placed in the southeast Chukchi Sea to gather wave measurements during July-December 2007 and October 2009-September 2010. Possible forcing mechanisms are investigated to understand the discrepancies between RDCP measurements and one-dimensional spectra models.

The analysis is presented in the following manner. First, previous work for one-dimensional wave spectra is presented in the context of how it fits into this study. Second, finite amplitude wave theory is used to describe the type of waves in the southeast Chukchi Sea. Third, a quantification of kinetic energy of the waves during identified storm forcing episodes is presented. Fourth, one-dimensional wave spectra

models were developed to estimate the expected wave spectrum generated by a particular storm are discussed. Fifth, the expected one-dimensional wave spectra and the RDCP spectra classifications as either swell or wind-sea are presented. Finally, a comparison of one-dimensional wave spectra with the RDCP wave spectrum of similar classification is presented.

4.2. Background and Methodology

Ewing (1980) analyzed wave states off the west coast of Scotland. Their study showed that east winds, which are fetch-limited, generated wave states described most accurately by the JONSWAP spectrum, whereas west winds produced swell-like conditions similar to the PM spectrum. From the wind and wave measurements collected for this study, we used only the JONSWAP and TMA spectrum models to describe our wave states. The JONSWAP and TMA were adequate in this study to describe the conditions because the region was not open ocean, due to the enclosed embayment of shoreline surrounding the southeast Chukchi Sea region, which was the direction from which the wind and wave propagated. The wind speeds observed in this region were also comparable to the JONSWAP experiment carried out in Hasselmann et al. (1973). The embayment generation region was also a shallow water environment of the nearshore *in situ* wave measurements. Therefore, the conditions were most favorable to the JONSWAP and TMA spectra.

Phillips (1958) originally proposed the first spectral form for the variance $E(f)$ using frequency, f^{-5}. Toba (1973) proposed an alternative to Phillips (1958) in using f^{-4} instead of f^{-5}. Hasselmann et al. (1973) who first proposed the JONSWAP model used the f^{-5} form. Donelan et al. (1985) proposed a modified JONSWAP with f^{-4}. In our analysis, we solve the one-dimensional wave spectrum using the f^{-5} form for the JONSWAP (Hasselmann et al., 1973) rather than the form f^{-4}, since the original

form of the JONSWAP using f^{-5} is still widely used and is a mainstay in many engineering references (Sorensen 1993, 2006).

Hasselmann et al. (1973) proposed to use constant values of σ_a and σ_b in the JONSWAP spectral form. The values, σ_a and σ_b, are the left and right-sided width of the spectral peak, respectively. Lewis and Allos (1990) stated that having σ_a and σ_b maintain constant values would give inconsistencies in the results. However Lewis and Allos (1990) results assumes the Pierson-Moskowitz (1964) form is correct, which disagrees with the Hasselmann et al. (1976) assessment of the Pierson-Moskowitz, a wave spectra model for fully developed seas. For this study, which uses the JONSWAP and TMA, the original constant values proposed by Hasselmann et al. (1973) will be applied.

Mitsuyasu et al. (1980) used ocean wave records taken near Japan to establish a peak enhancement factor for the JONSWAP. In their case, the analysis data was a subset of the entire data, partitioned by frequency. They used a separation frequency f_s<0.13 in order to focus on swell conditions. The *in situ* measurements of this study (RDCP) shared similar characteristics to the Mitsuyasu et al. (1980) study (cloverleaf buoy). Like a cloverleaf buoy, the RDCP gave a certain response due to its geometrical configuration. The cloverleaf buoy was accurate up to 0.3Hz before correction and 0.5Hz after correction. The RDCP wave spectra were considered up to 0.3Hz-0.4Hz (Section 4.7). Also, the RDCP spectral peak frequency lay in a similar range to that of the cloverleaf buoy, i.e. 0.1~0.2Hz, which enabled an analysis of possible swell occurrences as well as wind-sea occurring in lower frequency ranges (i.e. near the separation frequency).

Therefore, this study used Mitsuyasu et al. (1980) peak enhancement factor γ due to the same limitations imposed in our dataset as on theirs.

Although studies such as Hasselmann et al. (1976) and Young (1992) used significant wave height (H_{m0}), spectral peak frequency (f_p) and wind speed (U_{10}) to solve one-dimensional wave spectra, this method was not utilized here for two reasons. First, it was desired to compare theoretical waves generated using a wind field extracted from an atmospheric model. These wave data would be unrelated to the RDCP H_{m0} measurements so that model and RDCP spectra could be compared. Second, when RDCP H_{m0} measurements were considered and fetch was estimated, the values for fetch seemed unreasonable, especially for the highest SWH(s) in the SWH event, since fetch is influenced by f_p, and f_p is influenced by H_{m0}.

Estimating fetch was one of the biggest hurdles since defining where the wind generation field begins exactly is unknown. Therefore, estimating fetch as close to the wind generation boundary area as possible was attempted and was performed using peak wave frequency (f_m) (Wang and Hwang, 2001). Based on wind measurements and f_m, it was possible to then solve for fetch (F), which is needed for the fetch-limited JONSWAP and TMA spectral models we use in this study.

4.3. Wave and wind data

For this study wave and wind direction are taken to be of the same convention. Wind direction is defined as the direction *from which* the wind is coming and is given in degrees true bearing.

4.3.1. Site selection and RDCP instrument deployment

The observational location in southeast Chukchi Sea was chosen for several reasons: little work has been done north of the Bering Strait on the synoptic driving of sea states, the area has demonstrably strong wave forcing and possesses a complex regime that can include local wind waves and swell. In addition, there are various at-risk coastal inhabitants (several villages and an industrial operator), and a logistical arrangement was established with the industrial inhabitant, Teck Alaska Inc., whereby they availed to this project their contracted Foss Maritime tugs for deployment and retrievals.

The overall project entailed three data-gathering efforts using RDCP (Recording Doppler Current Profiler) deployments. One RDCP was deployed at an open-water location during the ice-free period, July-December 2007 UTC ("2007" in Figure 4.1), and two RDCPs were later deployed at coastal locations during ice-free and ice-covered periods October 2009-September 2010 UTC ("2009S" and "2009N" in Figure 4.1). These three deployments are termed "Stations" for the rest of the paper.

The onset of sea ice cover at Station 2007 was estimated to be December 8, 2007. Sea ice presence was estimated to be at Station 2009S from November 12, 2009 to July 1, 2010 and at Station 2009N from November 9, 2009 to July 2, 2010.

4.3.2. RDCP wave sampling

Two Recording Doppler Current Profilers (RDCP) were deployed to the southeast Chukchi Sea: one RDCP to an open-water location during the ice-free period, July-December 2007 UTC ("2007" in Figure 4.1), and two RDCPs to coastal locations during ice-free and ice-covered periods October 2009-September 2010 UTC ("2009S" and "2009N" in Figure 4.1). These deployments are termed "Stations" for the rest of the paper.

The sampling frequency of the RDCP was 2Hz. Each of the total number of observation sets (N) comprised of 15 minutes of individual wave observations which totaled 1800 samples (i =1800). Each observation i includes wave height H_i, wave period T_i and wave direction D_i. From the observed quantities, the RDCP yields the following: significant wave height, H_{m0}, mean wave period, T_{m01}, mean zero crossing, T_{m02} *or* $\bar{T}_z$, Energy wave direction, D_E, Mean direction, D_m, and Peak direction, D_p. For this study, significant wave height, H_{m0}, mean wave period, T_{m01}, mean zero crossing, T_{m02}, and mean wave direction, D_m were the focus of the analysis. The RDCP recorded individual wave heights H_i where the significant wave height (SWH) H_{m0} (i.e. $\sim H_s$) was estimated from the highest 33% of waves in a 15-minute wave record. H_{m0} is expressed as $4\sqrt{E}$ where E is the total variance of the wave field and expressed as $E = (1/16)\rho_w g {H_{m0}}^2$, and the terms ρ and g are dropped when expressing variance. The mean zero crossing parameter, T_{m02}, is the time obtained by dividing the record length by

the number of downcrossings (or upcrossings) in the record (AADI, 2006), compared to the mean wave period, T_{m01}, which is the wave period corresponding to the mean frequency of the spectrum (WMO, 1998).

Station 2007 recorded every 2.0h (i.e. the instrument was 2.0h at rest) for 3816h and 6 minutes, so the number of wave observations was N = 1704. Station 2009N recorded every 1.5h for 8041h and 15 minutes, for N = 4596. Station 2009S recorded every 1.5h for 8204h, for N = 4689.

4.3.3. Maximum significant wave height events established

An approach was needed to define when the seas were considered an "event". Therefore, significant wave height (SWH) (H_{m0}) was used to classify an "event". The approach used was defined similar to the approaches used in Hudak and Young (2002) and Francis-Chythlook (2004); that is, the wave magnitude exceeds and remains over a given threshold for a period of 6h or more in duration. Then the SWH event was considered to have ended when the wave magnitude dropped below the threshold for 6h or more. To better group and classify wave events, three threshold set-points were established: 1m, 2m, 3m. A threshold set-point is the minimum point that was considered. For example, a 2m threshold set-point would be a SWH event $\geq$ 2m (which includes SWH events $\geq$ 3m).

From these event datasets the largest events were retained for detailed analysis. To be retained, the NARR winds (see below) at the Station had to exceed 6.0 m s^{-1}, a condition stipulated by the observation that wave records showed that wind and wave direction were more likely to diverge for winds under 6.0 m s^{-1}.

There were 5 significant wave height events, identified as "SE1" through "SE5" evaluated in this paper. These events had the constraints 1) where they contained the maximum wave heights in the RDCP wave record, as mentioned in the previous paragraph, and 2) $U_{10} > 6.0$ m s^{-1}.

- SE1, September 18, 2007 0816 UTC - September 20, 2007 1416 UTC

- SE2, November 23, 2007 0552 UTC - November 24, 2007 0852 UTC; November 25, 2007 1152 UTC - December 2, 2007 0552 UTC
- SE3, July 22, 2007 0746 UTC - July 23, 2007 0301 UTC
- SE4, July 16, 2010 0446 UTC – July 17, 2010 1216 UTC
- SE5, August 17, 2010 2046 UTC – August 19, 2010 0416 UTC

4.3.4. Winds

Wind data for this study were extracted from the North American Regional Reanalysis (NARR) dataset (Mesinger et al., 2006). The NARR wind fields are taken from atmospheric weather forecast model simulations on a grid roughly 0.3° longitude x 0.3˚ latitude resolution that are informed by observational data. This system, a "reanalysis" data set, was developed and is maintained by the National Centers for Environmental Prediction (NCEP) of the US National Oceanic and Atmospheric Administration (NOAA). The analysis for the JONSWAP spectrum is based on winds at 10m (U_{10}) at each Station.

4.4. Wave theory and analysis

4.4.1. Finite amplitude wave theory

Due to the nature of the wind-wave interaction in the enclosed bay of the SE Chukchi Sea area, the simplest of phase-resolving models was applied. Phase-resolving models are fully deterministic models based on hydrodynamics conservation laws, i.e. conservation of mass, momentum and energy (Losada and Revilla, 2009). Although AADI (2006) classifies waves recorded by the RDCP under Linear Wave Theory and assumes the sea is deep if the absolute water depth is greater than 50 meters, linear wave theory is valid only for waves with small amplitude. However, due to the higher wave amplitude or considering the lower water depth of the RDCP deployments, Stokes wave theories should be used. Linear wave theory is an approximation of the Stokes theory, so finite amplitude wave theory is discussed and referenced from the U.S Army *Shore Protection Manual* (1984) and Sorensen (1993).

4.4.2. Linear wave theory

Finite amplitude wave theory was first developed by Airy (1845) and Stokes (1847). RDCP waves used in this study were evaluated and classified as Stokes' second-order and Stokes' third-order for deep water, and transitional water for one case scenario (see Table 4.1). However, solving and understanding Stokes' second-order and third-order equations means laying out the basis of Airy wave equations. The Airy wave theory, also known as linear or first-order wave theory, is the earliest and simplest. Despite this, it satisfactorily explains ~90% of all wave analysis situations and is in fact used for most engineering purposes; thus it will be used for this study.

Sorensen (1993) gives the general expression for water surface elevation (η) as

$$\eta = a\cos(\theta) + a^2 B_2(L,d)\cos(2\theta) + a^3 B_3(L,d)\cos(3\theta) + ...a^n B_n(L,d)\cos(n\theta) \qquad (4.1)$$

where a is the wave amplitude (m), θ is the phase function (radians), L is the wavelength (m), d is the depth (m), and B is a non-constant variable. The first term on the right side of Equation 4.1 describes Airy first-order (η_1) described in Equation 4.2, the first two terms on the right describes the second-order ($\eta_1+\eta_2$) described in Equation 4.5, and so on.

Airy (Linear) wave theory is based on the assumption that the wave amplitude is small (i.e. <<1m for the SE Chukchi Sea region as seen from RDCP data) and the contribution made to the solution by higher order terms in Equation 4.1 is negligible.

Therefore, the Airy wave equations (Airy, 1845) is solved for the water surface elevation (η_1), which is characterized by a sinusoidal waveform of wavelength L, height H and period T. The symbols x denotes the horizontal displacement of the water surface relative to the stillwater level, t denotes time, and the amplitude of the wave a is one-half of the wave height H and is given in the U.S Army *Shore Protection Manual*, (1984) as

$$\eta_1 = \frac{H}{2}\cos 2\pi\left(\frac{x}{L_1} - \frac{t}{T}\right) \tag{4.2}$$

where the wavelength L_1 for the first-order theory is

$$L_1 = \frac{gT^2}{2\pi}\tanh\left(\frac{2\pi d}{L_1}\right) \tag{4.3}$$

where d is the depth (m). For deep water, $(d/L > 1/2)$, as shown in the U.S Army *Shore Protection Manual*, (1984), Equation 4.3 reduces to

$$L_{1deep} = \frac{gT^2}{2\pi} \tag{4.4}$$

4.4.3. Higher order wave theory

For situations where wave steepness departs from a sinusoidal form, i.e., exhibiting increased steepness, higher-order wave theories are more appropriate; examples include Stokes (second-, third-, and fifth-order) and Cnoidal. Stokes (1847) second-order wave theory states that H/d not be large (i.e. ~1m for the SE Chukchi Sea region as seen from RDCP data), and therefore is applicable for deep water and most intermediate depth range. Skyelbreia (1959) presented third-order Stokes theory.

From Equation 4.1, $a = H/2$, for first (Airy) and second (Stokes 2nd) orders, or $a < H/2$ for third-order and higher, and B^2 , B^3 are specified functions of the wavelength L and depth d. Therefore, the water surface elevation, η_2 for second-order theory (Stokes, 1847) as reference in the U.S Army *Shore Protection Manual* (1984) would be the following, where all the variable are defined above

$$\eta_2 = \frac{H}{2}\cos 2\pi\left(\frac{x}{L}-\frac{t}{T}\right)+\frac{\pi H}{8}\left(\frac{H}{L}\right)\frac{\cosh\left(2\pi d/L\right)}{\sinh^3\left(2\pi d/L\right)}\left[2+\cosh\left(4\pi d/L\right)\right]\cos 4\pi\left(\frac{x}{L}-\frac{t}{T}\right) \quad (4.5)$$

For deep water, $(d/L > 1/2)$, as shown in the U.S Army *Shore Protection Manual*, (1984), Equation 4.5 reduces to

$$\eta_{2deep} = \frac{H}{2}\cos 2\pi\left(\frac{x}{L}-\frac{t}{T}\right)+\frac{\pi H^2}{4L}\cos 4\pi\left(\frac{x}{L}-\frac{t}{T}\right) \quad (4.6)$$

The wavelength (L_2) for second-order theory is identical to those obtained by first-order linear theory. Therefore, second-order theory (Stokes, 1847) wavelength, L_2 , as shown in the U.S Army *Shore Protection Manual*, (1984) is:

$$L_2 = \frac{gT^2}{2\pi}\tanh\left(\frac{2\pi d}{L_2}\right) \tag{4.7}$$

and the wavelength L_3 for third-order theory is given by:

$$L_3 = \frac{gT^2}{2\pi}\tanh\left(\frac{2\pi d}{L_3}\right)\left\{1+\left(\frac{\pi H}{L_3}\right)^2\left[\frac{5+2\cosh\left(4\pi d / L_3\right)+2\cosh^2\left(4\pi d / L_3\right)}{8\sinh^4(2\pi d / L_3)}\right]\right\} \tag{4.8}$$

4.4.4. Wave classification

For wave classification, Figure 4.2 is used to illustrate the approximate limits of validity for wave theories (Le Méhauté, 1969) to determine whether the RDCP Stations 2007, 2009S and 2009N were deep, transitional or shallow water waves, and what the appropriate Stokes analytical order was (i.e. second-order, third-order).

The wave period T is estimated from the mean zero crossing period T_{m02} of the RDCP wave record. To solve for T, the mean T_{m02} value was taken for each RDCP SWH "event", and then the mean T_{m02} value was taken again from all 1m, 2m or 3m SWH "events" (e.g. Station 2007 had two 3m SWH events, 5.7sec and 5.8 sec, therefore the mean value was 5.8 sec – see Table 4.1). The wave height (H) is the significant wave height parameter (H_{m0}) from the RDCP wave record. A threshold was needed for H_{m0} in establishing where the wave changed order number so that wavelength (L) could be solved with the correct Equation (i.e. Eqn. 4.7 or 4.8). Therefore, the bottom threshold of each SWH event 1m, 2m, 3m was used for H. The depth (d) is the bottom depth of where the RDCP was located. For RDCP station 2007, the average T_{m02} for 1m, 2m, and 3m SWH events were 4.6 sec, 5.2 sec, 5.8 sec, respectively. For RDCP station 2009N the average T_{m02} for 1m, 2m SWH events were 4.2 sec, and 4.8 sec, respectively. For RDCP station 2009S the average T_{m02} for 1m, 2m SWH events were 4.4 sec, and 4.8 sec, respectively. Table 4.1 lists these comparisons for RDCP Stations 2007, 2009N, and 2009S.

From Figure 4.2, the value d / gT^2 was used to classify the waves as deep, transitional, or shallow. Also from Figure 4.2, the value of H / gT^2 was used to classify the waves as Stokes' second-order, or Stokes' third-order. After classifying the order (e.g. Stokes' second order), wavelength L could be solved using Eqns. 4.7 and 4.8. For Stokes' second-order, T or T_{m02} and depth, d , were used to solve for wavelength, L_2 (Eqn. 4.7). For Stokes' third-order, T or T_{m02} , H or H_{m0} , and depth, d , were used to solve for wavelength, L_3 (Eqn. 4.8). After wavelength L was calculated, another check was performed to see if waves were deep, transitional, or shallow where d / L is estimated (Table 4.2).

4.5. Wave energy estimation

The frictional effect of winds moving over the ocean surface generates wave energy. The sum of the wave energy can be expressed as potential energy and kinetic energy. Potential wave energy is caused by its position above the wave trough. The kinetic wave energy is a function of the motion of the wave.

To find the potential energy, we can integrate the potential energy of a water column along the length of a wave (Equation 4.9). To find the kinetic energy, we can integrate the water velocity through a vertical plane over the length of the wave (Equation 4.10). These two components of energy have the same value, and can be added together to give the total energy (Equation 4.11). From Sorensen (2006) the energies E for a unit width of wave crest and for one wave length are expressed as

$$E_p = \frac{\rho g H^2 L}{16} \tag{4.9}$$

$$E_k = \frac{\rho g H^2 L}{16} \tag{4.10}$$

$$E = E_k + E_p = \frac{\rho g H^2 L}{8} \tag{4.11}$$

Kinetic energy, E_k, uses $\rho = 1027 \text{kg/m}^3$ for sea water density, g is gravity, H is significant wave height, H_{m0}. L is the wavelength defined in Equation 4.7 and 4.8 for Stokes' second-order and third-order theories. The wave period, T or T_{m02}, is the mean zero crossing period. So from a number of recorded RDCP observations for each SWH event, the significant wave height, H_{m0}, and wave period, T_{m02}, was taken to calculate wavelength, L and thus kinetic energy, E_k. In this study, Equation 4.10 is used to calculate kinetic energy of major SWH events at the RDCP Stations during 2007, and 2009-2010.

The energy of the wave is dependent on the wavelength, and the square of the wave height. Therefore, a wave twice as high as another of the same length will have four times as much energy.

4.6. One-dimensional spectral models and analysis

One-dimension spectral models were used to investigate the wave conditions in the southeast Chukchi Sea area. In this section an evaluation of wave theory is presented in terms of the archetypical spectral distributions that best describe wave states under different conditions. Following that, wave data from in situ observations and generated using atmospheric model winds are contrasted with JONSWAP (Joint North Sea Wave Project) and TMA (TEXEL storm, MARSEN, ARSLOE) spectra to assess what type of regime is present in the SE Chukchi Sea.

Equation 4.11 indicates that energy density may be expressed as $0.5\rho g a^2 / Hz$, which is a unit of energy per unit frequency interval, Hz. Frequency spectra are shown as energy density (m^2Hz^{-1}) versus frequency (Hz) where the units for ρ and g are not expressed for variance, leaving m^2Hz^{-1}.

4.6.1. JONSWAP spectrum

The fetch-limited JONSWAP spectrum is a result of the sum of processes $S = S_{in} + S_{nl} + S_{ds}$ representing energy input from the atmosphere S_{in}, the nonlinear spectral transfer due to conservative wave-wave interactions S_{nl}, and dissipation due to white capping S_{ds} (Hasselmann et al., 1973). This relationship predicts, among other things that as the spectral peak frequency f_m decreases, the fetch increases and therefore the energy of the wave increases.

The establishment of the JONSWAP spectrum was a major result from the Joint North Sea Wave Project (Hasselmann et al., 1973) that describes the expected spectral distribution for the case of fetch-limited, non duration limited, deep water. The JONSWAP spectra were designed for wind speeds up to a maximum of 20 m s^{-1} with a maximum fetch of 160km. The JONSWAP formula was obtained by multiplying the PM spectrum (Pierson and Moskowitz, 1964) (see Appendix) with the "peak enhancement" factor γ^a. From Hasselmann et al., (1973), the resulting spectrum is

$$E(f)_J = \frac{\alpha g^2}{(2\pi)^4 f^5} \exp\left[-\frac{5}{4}\left(\frac{f}{f_m} \right)^4 \right] \gamma^a \tag{4.12}$$

where f is the wave frequency. The Phillips constant α, (Phillips, 1958) and the peak frequency, f_m (Hasselmann et al., 1973), i.e. frequency where $E(f)_J$ is maximum on the spectrum is given respectively as

$$\alpha = 0.076\left(\frac{gF}{U_{10}^2}\right)^{-0.22} \tag{4.13}$$

$$f_m = \frac{3.5g}{U_{10}}\left(\frac{gF}{U_{10}^2}\right)^{-0.33} \tag{4.14}$$

where F is fetch, and U_{10} is wind at 10m.

The parameter γ is the ratio of maximum spectral energy to the maximum of the corresponding PM spectrum (Pierson and Moskowitz, 1964), also known as the peak enhancement factor. In the JONSWAP spectrum, γ values range from 1.6 to 6 but the value of 3.3 is recommended for general use. Mitsuyasu et al. (1980) however recommend γ as

$$\gamma = 7\left(\frac{gF}{U_{10}^2}\right)^{-0.143} \tag{4.15}$$

The parameter a from Hasselmann et al. (1973) is defined as

$$a = \exp\left[-(f - f_m)^2 / 2\sigma^2 f_m^2\right] \tag{4.16}$$

where $\sigma = 0.07$ when $f \leq f_m$ which defines the left sided width of the spectral peak, and $\sigma = 0.09$ when $f > f_m$ which defines the right sided width of the spectral peak.

4.6.2. TMA Spectrum

The TMA spectrum known as the TEXEL storm, MARSEN, ARSLOE spectrum (Bouws et. al., 1985) was developed to adjust for the effects of water depth. The TMA spectrum was developed for situations where wind waves are initially generated in deep water and then propagate into intermediate/shallow water depths. The spectral response for such situations is a period-dependent change in the shape of the spectrum. Bouws et al. (1985) defined the spectral form as

$$E(f)_T = E(f)_J \Phi(f,d) \tag{4.17}$$

which is the JONSWAP spectrum modified by a depth and frequency dependent factor $\Phi(f,d)$. Hughes (1984) proposed that α and γ in the JONSWAP spectral formulation are modified to

$$\alpha = 0.0078\left(\frac{2\pi W^2}{gL_p}\right)^{0.49} \tag{4.18}$$

$$\gamma = 2.47\left(\frac{2\pi W^2}{gL_p}\right)^{0.39} \tag{4.19}$$

for the TMA spectrum where L_p is the wave length, and W is wind speed at 10m.

4.6.3. Separation frequency, f_s

Separation frequency, f_s, is an estimate of the frequency which separates wave energies of wind sea and swell in a one-dimensional wave spectra. In this study, the separation frequency was estimated using the wave steepness method (Wang and Hwang, 2001) and is currently in use by the US National Data Buoy Center. The steepness function (Wang and Hwang, 2001) is expressed as follows, where all variables are defined earlier in the text.

$$\alpha(f_*) = \frac{8\pi\left[\int_{f_*}^{f_{\max}} f^2 E(f)df\right]}{g\left[\int_{f_*}^{f_{\max}} E(f)df\right]^{0.5}} \tag{4.20}$$

In the PM and JONSWAP spectral models, there is a close relationship between peak frequency of the steepness function f_m and the wind speed U. The relation between wind speed and peak frequency is given by Wang and Hwang (2001) as

$$U = a(f_m)^b \tag{4.21}$$

where U is wind speed (m s^{-1}), f_m is peak frequency of the JONSWAP spectra (Hz), and the two empirical constants determined from the regression analysis are a=0.379 and b = -1.746.

Ewing (1980) used wave phase speed $C = g/2\pi f$ to estimate separation frequency. Ewing (1980) stated that wave phase speeds (i.e. $g/2\pi f$) less than the local wind speed U_{10} were considered wind-sea. Wave phase speeds greater than the local wind speed U_{10} were considered swell.

Wang and Hwang (2001) uses the wave phase speed relation, $C = g/2\pi U$, to determine the separation frequency f_s as related to the wind speed given by the following.

$$f_s = \frac{g}{2\pi U} \tag{4.22}$$

From Equations 4.21 and 4.22 the relation between f_s and f_m (Wang and Hwang, 2001) is given as

$$f_s = A(f_m)^B \tag{4.23}$$

where A = 4.112 and B =1.746. These relations are based on the PM spectral model for fully developed seas. In our study, we use the JONSWAP spectral model for wind speed, similar to what Wang and Hwang (2001) did for their study. Comparison was performed using the RDCP spectral peak f_p , and the peak frequency of the steepness function f_m

for the JONSWAP spectral model. The RDCP spectral peak f_p is assumed to be more affected by the spectral irregularities than the peak frequency of the steepness function f_m for the JONSWAP spectral model (Wang and Hwang, 2001).

4.6.4. Application to one-dimensional spectral model and RDCP

Estimating fetch is one of the most difficult tasks in estimating wave spectra since it requires establishing the extent of the wind generation area, and the wind speed and direction are not uniform. Although the full wind generation boundary location was unknown, for the study area the generation area is functionally limited to the enclosed embayment of the SE Chukchi Sea; in this region, from the location of the 2007 RDCP, the maximum possible fetch ranged from 90-200km. To find fetch, F , in the JONSWAP spectral model, we use the relation in the Equation 4.14 proposed by Hasselmann et al. (1973) shown in Equation 4.24

$$F = \left(\frac{U_{10}^2}{g} \right) \left(\frac{U_{10} f_m}{3.5g} \right)^{1/-0.33} \tag{4.24}$$

where f_m is the JONSWAP peak frequency and U_{10} is the wind speed at 10m. The parameter f_m was calculated from the relation given by Wang and Hwang (2001) where $f_m = (U/a)^{1/b}$ and a =0.379 and b =-1.746.

The separation frequency f_s is defined as the separation between swell and wind-sea. To find the separation frequency for the JONSWAP spectra and then for the RDCP spectra, Equation 4.23 $f_s = A(f_m)^B$ was applied where the JONSWAP peak frequency f_m and the RDCP peak frequency f_p were substituted into Equation 4.23. For a

wave event where f_m or f_p was less than the separation frequency f_s, the wave event was considered swell. For a wave event greater than the separation frequency f_s, the wave event was considered wind-sea.

However, the RDCP spectra had a limited frequency range. The limited frequency range was due to the source level. The source level includes the transmitted power, the transducer efficiency, and the frequency. One consideration to be considered when utilizing this approach for the RDCP data is the fact that the RDCP outputs a truncated frequency range. This is a byproduct of instrument "source level" which is an aggregate measure integrating transmitted power, transducer efficiency, and emission frequency. Operating at 600Hz, the relatively small transducers are limited by non-linear behavior and cavitations (AADI, 2006). Therefore the transmitted power of a small transducer results in the limited transmitted power yielding a small propagation in linear wave propagation. Only an increased pulse length may increase the range by a small amount. Energy density (m^2Hz^{-1}) was given for a certain frequency range, $f_{\min}$ to $f_{\max}$ (Hz) which ranged as follows: 1) Station 2007: 0.03Hz - 0.3125Hz, 2) Station 2009N: 0.03Hz - 0.39Hz, and 3) Station 2009S: 0.03Hz - 0.375Hz. The RDCP $f_{\max}$ only allowed wind-seas where $f_p \leq$0.25Hz. Therefore wind-sea where the peak frequency (f_p) was greater than $f_{\max}$, was not observed. The $f_{\min}$ value for the RDCP appeared to be sufficient to identify the occurrence of swell.

Selection of the appropriate spectral model for analyzing significant wave events was based on assessment of water depth and fetch conditions at each station. Waves at Station 2007 were considered to be “deep water” (see Section 4.3). This fact, combined with the assumption of fetch limited conditions, suggests that the governing spectral form at this location is JONSWAP. Wave at Stations 2009N and 2009S were considered transitional, a function of shallower water at their more coastal locations, which meant the TMA spectrum was also utilized, in addition to JONSWAP.

4.7. Results

1) SE1 (2007-3m-3) at Station 2007 for wave record 18-20 September 2007 UTC, 67º3'29.94"N, 166º20'43.02"W, water depth 34m

Event SE1 consisted of 25 individual observations accumulated over a continuous period lasting 56.25h. Three distinct types of groups based on wave versus wind direction were identified. Two of three groups exhibited wave directions that differed from the wind directions, and the other group had similar wave and wind directions. The first group contained only three observations (SE1a) of wind versus wave directions; specifically, ESE winds were orientated about 177° clockwise (CW) to WNW waves, almost opposite in direction from each other. The JONSWAP and RDCP measurements for these both indicated swell. The largest group of 19 observations (SE1b) had similar wave and wind directions, where ESE winds were 15° CW from E waves. The JONSWAP and RDCP measurements showed that the higher SWHs (>2.4m) were located in the wind-sea region, while the lower SWHs (<2.4m) were located in the swell region. The third group also consisted of only three observations (SE1c); these exhibited E winds orientated about 70° CW from the primary NNE wave direction. The JONSWAP and RDCP measurements for these indicated swell. SE1b wave heights were considerably larger than groups SE1a and SE1c – significant wave height H_{m0} was 1.2m higher – and the mean period T_{m02} was about 0.8sec greater. Wind speed U_{10} was also on average 4 m s^{-1} higher than SE1a and SE1c. Therefore, spectral indications that a wind-sea state

prevailed during SE1b are supported by wind speed and direction observations, and wind-sea encompassed the largest SHWs in the record.

The SE1 wave record as a whole indicated that the JONSWAP included 15 swell observations and 9 wind-sea observations, while the RDCP included 10 swell and 6 wind-sea. The majority of observations were swell, but consisted of lesser wind speeds. The minority were wind-sea observations but were generated by higher wind speeds. When it was observed, swell tended to propagate from a SE direction. Wind-sea was situated in the same direction as the wind, an E direction. For significant wave height H_{m0}, wind-sea was about twice the height of swell (1.6m swell versus 3.3m wind-sea). The wind speed U_{10} was also about twice as high during wind-sea than during swell (8 m s^{-1} U_{10} swell versus 15 m s^{-1} U_{10} wind-sea). Swell observations were classified as 2nd order Stokes' waves with a wavelength of 34m and an overall energy of 60kJ m^{-1}. Wind-sea observations were 3rd order Stokes' waves with a longer wavelength of 48m and a much greater overall energy of 350kJ m^{-1}. Therefore, SE1 (as a whole) was considered a wind-sea event, since the greatest amount of observations was from wind-sea observations.

The JONSWAP peak enhancement factor γ was estimated to be 1.7 for swell, and 2.0 for wind-sea. The peak frequency f_m averaged much higher for swell (0.19Hz) than for wind-sea (0.12Hz), which corresponded to the low separation frequency f_s for the wind-sea (0.10Hz) than for swell (0.22Hz). JONSWAP spectral density peak, $E(f)_{\max}$

was at $1.3m^2Hz^{-1}$ for swell, and $15m^2Hz^{-1}$ for wind-sea. RDCP spectral density peak, $E(f)_{max}$ for swell ($2.0m^2Hz^{-1}$) was slightly higher than JONSWAP swell, while the RDCP spectral density peak, $E(f)_{max}$ for wind-sea ($12m^2Hz^{-1}$) was found to be slightly lower than the JONSWAP wind-sea.

Figures 4.3a, 4.3b shows a comparison of JONSWAP and RDCP spectra from the SE1b group during September 19, 2007, one of the highest SWH events during SE 1. Figures 4.3a, 4.3b shows the JONSWAP, RDCP peak frequencies in the wind-sea region. The JONSWAP peak energy is shown to be much higher than the RDCP peak energy. One of the possibilities may be due to the shortcomings of the JONSWAP formulation, however the most likely reason is due to the wind speeds that were used for estimating the JONSWAP were higher than the wind speeds that generated the wave state as recorded by the RDCP. This shows that estimating the exact magnitude and location of the generating wind field can be problematic.

2) SE2 (2007-3m-15) at Station 2007 for wave record 22 November – 2 December 2007 UTC, 67º3'29.94"N, 166º20'43.02"W, water depth 34m

There were 86 observations considered, for a total of 193.5h. There were five distinct groups of wave versus wind direction. The first group of 13 observations (SE2a) had similar directions, with NNW winds 20° clockwise (CW) to NW waves. The JONSWAP and RDCP measurements for these indicated swell. The second group of 7 observations (SE2b) had different wave and wind directions, where E winds were 135°

CW from NW waves. The JONSWAP and RDCP measurements for these were also swell. The third group of 3 observations (SE2c) also had different wind and wave directions, E winds orientated about 111° CW from SSW waves. Again, the JONSWAP and RDCP measurements for these were swell. The fourth group of 61 observations (SE2d) had the largest number of observations and similar wind and wave directions, ESE winds orientated about 20° CW from E waves. Again similar to SE1, the JONSWAP and RDCP measurements showed that the higher SWHs (>2.4m) were located in the wind-sea region, while the lower SWHs (<2.4m) were located in the swell region. The fifth group only had 2 observations (SE2e) with similar wind and wave directions, NE wind 37° CW from NNE waves. The JONSWAP and RDCP measurements for these were swell. Of these five groups, most of the observations (74 out of 86 observations) had similar wave directions with the majority of observations (SE2d) coming from the Kotzebue Sound, and the rest of these observations coming from the open Chukchi Sea (SE2a). Similar to the event during September 2007, the most dominant group (SE2d) also had E waves and ESE winds. The significant wave height H_{m0}, mean period T_{m02}, and wind speed U_{10} for SE2d when compared to the other wind/wave directions (SE2a,b,c,e) were also found to be similar to the event during September 2007, where they were higher by approximately the same order of magnitude.

The SE2 wave record overall, indicated that the JONSWAP encompassed 41 swell observations and 31 wind-sea observations, while the RDCP encompassed 38 swell observations and 14 wind-sea observations. The JONSWAP and RDCP results show that

SE2 was dominated by swell, which consisted of lower winds speeds. The observations with higher wind speeds were dominated by wind-sea. Some wave characteristics showed a greater difference for the RDCP than for the JONSWAP. For significant wave height H_{m0}, JONSWAP wind-sea was 1.0m higher than swell, compared to RDCP wind-sea which was 2.0m higher. The wind speed for swell was approximately 10m s^{-1} and for wind-sea it was 16m s^{-1}. Wind direction for swell was southerly and wind-sea was easterly. Swell was situated in a SSE direction and a SE wind direction. Wind-sea was situated E and an ESE wind direction. Swell observations for SE2 were classified as 2nd order Stokes' waves and wind-sea observations were 3rd order Stokes' waves. Swell observations had a wavelength of 37m and an overall energy of 100kJ m^{-1}. Wind-sea observations had a wavelength of 52m and a much greater overall energy of 390kJ m^{-1}. Therefore, SE2 (as a whole) was considered a wind-sea event, since the greatest impacts from waves were from wind-sea observations.

The JONSWAP peak enhancement factor γ was estimated to be 1.8 for swell, and 2.0 for wind-sea. The peak frequency f_m averaged higher for swell (0.16Hz) than for wind-sea (0.12Hz), which corresponded to the low separation frequency f_s for the wind-sea (0.10Hz) than for swell (0.16Hz). JONSWAP spectral density peak, $E(f)_{\max}$ was at 5.0m^2Hz^{-1} for swell, and 19m^2Hz^{-1} for wind-sea (higher than September 2007 observations). However RDCP spectral density peak, $E(f)_{\max}$ for swell (2.3m^2Hz^{-1}) was about half the JONSWAP swell. RDCP spectral density peak, $E(f)_{\max}$ for wind-sea

($14m^2Hz^{-1}$) was found to be lower than the JONSWAP wind-sea, similar to September 2007 observations.

3) SE3 (2009N-2m-12) at Station 2009N for wave record 22 – 23 July 2010 UTC, 67º38'17.76"N, 164º20'46.26"W, north location near Kivalina, AK, water depth 17m

For the next three SWH events (SE3, SE4, SE5), which were nearshore and at shallower depth, the number of observations and significant wave heights were lower than for the offshore observations. Also, wave and wind directions that the nearshore picked up varied greatly from the offshore, since the proximal coastline was to the east, most of the wave and wind action originated from an open fetch area to the west and south, depending on whether it was the northern 2009 station (2009N) or the southern 2009 station (2009S). Each of the SWH events (SE3, SE4, SE5) had one primary direction of impact, west or south where wave and wind direction were similar, which contrasts the varied wind and wave directions that the 2007 station experienced. Thus for these cases contrasting wind and wave directions did not constitute a reliable indicator of swell/wind-wave discrimination, which necessitated a greater reliance on spectral and frequency methods.

The SE3 wave record as a whole consisted of 12 observations, for a total of 21.0h. The JONSWAP encompassed 9 swell observations and 0 wind-sea observations, while the RDCP encompassed 7 swell and 1 wind-sea. Since the vast majority of the observations (including the highest wind speeds) for the JONSWAP and RDCP were

swell, the SE3 observations were considered to be swell. The swell wave direction was SW orientated about 29° clockwise (CW) to S wind direction. The wave characteristic of the swell were approximately H_{m0} = 1.8m, T_{m02} = 4.7sec, and U_{10} = 8.9m s^{-1}. The swell observations were classified as 2nd order Stokes' waves with a wavelength of 35m and a kinetic energy of 70kJ m^{-1}.

For swell observations, the JONSWAP and RDCP values were similar. The JONSWAP peak enhancement factor γ was estimated to be 1.8. The peak frequency f_m averaged 0.17Hz, and the separation frequency f_s averaged 0.19Hz. JONSWAP spectral density peak, $E(f)_{\max}$ was at 2.3m^2Hz^{-1}, and the RDCP spectral density peak, $E(f)_{\max}$ was at 2.2m^2Hz^{-1}. The TMA (3.6m^2Hz^{-1}) was found to be much higher than the RDCP value and did not agree as well as the JONSWAP.

4) SE4 (2009S-2m-15) at Station 2009S for wave record 16 – 18 July 2010 UTC, 67º10'33.30"N, 163º59'23.94"W, south location near Cape Krusenstern, AK, water depth 18m

The SE4 wave record as a whole consisted of 19 observations, for a total of 33.25h. The JONSWAP encompassed 19 swell observations and 0 wind-sea observations, while the RDCP encompassed 8 swell and 0 wind-sea. Since all observations (including the highest wind speeds) for the JONSWAP and RDCP were swell, the SE4 observations were considered to be swell. The swell wave direction was SW orientated about 39° clockwise (CW) from the SSW wind direction. The swell wave

characteristics included H_{m0} = 1.8m, T_{m02} = 4.7sec, and U_{10} = 7.9m s^{-1}. Swell observations were classified as 3rd order Stokes' waves with a wavelength of 34m and a kinetic energy of about 72kJ m^{-1}.

For swell observations, the JONSWAP and RDCP values were similar. The JONSWAP peak enhancement factor γ was estimated to be 1.7. The peak frequency f_m averaged 0.18Hz, and the separation frequency f_s averaged 0.20Hz. JONSWAP spectral density peak, $E(f)_{\max}$ was at 1.8m^2Hz^{-1}, and the RDCP spectral density peak, $E(f)_{\max}$ was at 1.8m^2Hz^{-1}. The TMA (2.7m^2Hz^{-1}) was found to be much higher than the RDCP value and did not agree as well as the JONSWAP.

5) SE5 (2009S-2m-20) at Station 2009S for wave record 17 – 20 August 2010 UTC, 67º10'33.30"N, 163º59'23.94"W, south location near Cape Krusenstern, AK, water depth 18m

The SE5 wave record as a whole consisted of 19 observations, for a total of 33.25h. The JONSWAP encompassed 19 swell observations and 0 wind-sea observations, while the RDCP encompassed 6 swell and 7 wind-sea. This was in contrast to SE3 and SE4, which observed primarily swell observations. However, since all of the JONSWAP and half the RDCP were characterized as swell, the SE5 observations were considered to be swell. The swell wave direction was west orientated about 15° counterclockwise (CW) to WNW wind direction. The swell wave characteristics included

H_{m0} = 2.6m , T_{m02} = 4.8sec, and U_{10} = 8.1m s^{-1}. Swell was classified as 3rd order Stokes' waves. The wavelength of swell averaged 33m and the kinetic energy was 130kJ m^{-1}.

For swell observations, the JONSWAP and RDCP values did not agree well with each other. For swell, the JONSWAP spectral density peak, $E(f)_{\max}$ was at 1.8m^2Hz^{-1}, and the RDCP spectral density peak, $E(f)_{\max}$ was at 4.0m^2Hz^{-1}. The TMA (2.6m^2Hz^{-1}) was found to be closer, but still much lower than the RDCP value. The discrepancy in JONSWAP/TMA and RDCP swell $E(f)_{\max}$ could be due to estimating the generating wind field incorrectly which the JONSWAP/TMA relies on for an accurate estimate of its spectra. The TMA peak enhancement factor γ was estimated to be 2.6 for swell. The peak frequency f_m averaged 0.17Hz, and the separation frequency f_s averaged 0.19Hz.

Figures 4.4a, 4.4b show a comparison of JONSWAP and RDCP spectrums from SE5 during August 18, 2010, one of the highest SWH events during SE 5. Figure 4.4a shows the JONSWAP peak frequency in the swell region, while Figure 4.4b shows the RDCP in the wind-sea region. The RDCP peak energy is shown to be much higher than the TMA/JONSWAP peak energies.

4.8. Discussion

After summarizing swell and wind-sea at each Station (i.e. SE1-5), it should also be mentioned that some of the highest SWHs at each Station were borderline 'swell+wind-sea'. This means that the peak frequency f_p or f_m was equal to the separation frequency f_s. Also many of the 'swell' or 'wind-sea' classifications examined in the previous sections were either just below (swell) or just above (wind-sea) the separation frequency f_s. The narrow frequency range of the RDCP only allowed a small range in this study.

Table 4.3 presents the highest SWH for each event (i.e. SE 1-5) and summarizes their wave spectra for the one-dimensional models (JONSWAP and TMA) and *in situ* (RDCP) measurements. Table 4.3 concentrates on the highest SWHs of each wave record only, and is useful for estimating what type of sea to expect at each given Station. The peak frequencies f_p, f_m and the separation frequency, f_s measured by the RDCP tended to be higher for the offshore SE1, SE2 compared to the JONSWAP. This was reversed for nearshore SE3, SE4, SE5 where JONSWAP peak frequencies f_p, f_m and the separation frequency, f_s were higher than RDCP. SE5 showed the largest difference in JONSWAP versus RDCP frequencies.

For the offshore RDCP, it was estimated that the highest wave states (+3m, +4m) for Station 2007 (SE1, SE2) were classified as wind-sea. The JONSWAP gave similar results. The +3m SE1 record (Event 1) had a large discrepancy between

energies $E(f)_{max}$, where the JONSWAP was much greater than the RDCP. This was due to the high wind speeds (+16 m s^{-1}) involved which would influence the JONSWAP compared to the SWHs (+3m) influencing the RDCP wave spectra. The +4m SE2 record (Event 2) saw a different outcome, where the JONSWAP and RDCP energies $E(f)_{max}$ were approximately the same. The JONSWAP, influenced by high wind speeds (+18 m s^{-1}), compared well to the RDCP wave spectra with high SWHs (+4m).

For the nearshore RDCP, classification of the highest wave states (+2m, +3m) for Stations 2009N and 2009S (SE3, SE4, SE5) included both swell and wind-sea. The JONSWAP, however remained similar to the classification previously found in the last section for the entire SE3,SE4, SE5 dataset, which was swell. For SE3 record, the JONSWAP and RDCP energies cross-correlated the best, compared to the TMA. For the SE4, SE5 records, the TMA cross-correlated the best with the RDCP. This difference between Station 2009N, showing the best cross-correlation between the JONSWAP and RDCP, and Station 2009S, showing the best cross-correlation between the TMA and RDCP, may be due to the bathymetry surrounding the Station. Waves propagating over the Station could be affected by bathymetry and close proximity to land, which would affect the direction of the wind/wave being measured.

4.9. Conclusions

From the comparisons given in Table 4.1, the conclusion drawn is that at Station 2007, all SWH events are deep water surface gravity waves. For Station 2009N and Station 2009S, 1m SWHs were classified as deep, and 2m or greater SWHs were classified as transitional. This result (see Table 4.1) implies that the cutoff depth between transitional and deep water for the southeast Chukchi Sea area is about 17-18m. This result from this study provides a modest assumption since wave periods T_{m02} do not vary much around the Kotzebue Sound/southeast Chukchi Sea region. For Station 2009S (18m), d / gT^2 and d / L suggested different classifications for the 2m SWH, deep and transitional. The wave period T_{m02} recorded by the RDCP was the same for 17m and also for 18m, so the cutoff between transitional and deep waters was also apparent. Upon further analysis, the 1m SWH for all Stations (i.e. 2007, 2009N and 2009S) were governed by Stokes' second-order wave theory. For 2m and 3m SWHs, all Stations were governed by Stokes' third-order wave theory. This shows that Southeast Chukchi Sea waves are not merely Linear (Airy) waves, so higher order wave processes are needed to describe these waves accurately.

The JONSWAP and TMA one-dimensional wave spectra models were used to describe storm-generated wave states. The JONSWAP and TMA spectrums provided an accurate fit for the given dataset and conditions. Five different datasets, two located offshore (SE1, SE2), and 3 nearshore (SE3, SE4, SE5) were evaluated. The two offshore

(SE1, SE2) and the two nearshore (SE3, SE4) were best described with the JONSWAP wave spectrum. According to Stokes' wave theories (Table 4.1), the two offshore datasets were classified as deep water waves so were best explained by JONSWAP. However, the nearshore datasets varied depending on wave height. For 1m SWH nearshore datasets waves were considered deep water waves. For +2m SWH nearshore, these were located in the transitional zone. Therefore, for the +2m SWH nearshore, both the TMA and JONSWAP spectrum were used to see which one was the best fit. Only the nearshore (SE5) with +3m SWH were best described by the TMA spectrum. The other two nearshore (SE3, SE4) did not contain +3m SWH in their dataset, which may explain why those wave heights corresponded best with the JONSWAP.

At the offshore location, Station 2007, the RDCP and JONSWAP were classified as "wind-sea". At the nearshore location, Stations 2009N and 2009S, the RDCP and JONSWAP were classified as "swell". This was applied to each dataset in its entirety. For highest SWHs only in each dataset (Table 4.3), these classifications became altered slightly for the RDCP, where some of the highest SWHs the RDCP recorded nearshore were classified as "wind-sea". For wind-sea observations, wind speeds would directly influence the outcome. However, discrepancies for SE1 were observed, in which the JONSWAP had much larger energies influenced by wind speed, than the RDCP influenced by SWH (Table 4.3). This inaccuracy could be due to the wind speed being overestimated. The nearshore RDCPs results also differed from the JONSWAP. This was due to the wind speeds being lower for the nearshore, therefore the JONSWAP produced

a lower $E(f)$. Since the wave source was swell, perhaps the wind field impacted the wave state more than what was assumed to create the wind-sea, which is reflected by the RDCP's highest SWHs.

The fetch length for the five datasets was found to range between 100-150km. SE1 and SE2 wind-sea states (i.e. highest SWH states) had wind and wave directions which originated from the enclosed embayment to the east of the RDCP location, towards Kotzebue Sound. SE3 and SE4 swell states were also fetch-limited; originating from the south and from the southwest the northern Seward Peninsula shoreline was a hundred or so kilometers away. However, SE5 swell (and wind-sea) states had wind and wave directions from an open fetch area. The SE5 fetch was estimated between the 100-150km range, but it is possible that there was another forcing mechanism present which was shown when comparing the higher RDCP spectrum to the JONSWAP/TMA spectrums. This difference in spectra could be due to the inaccuracy of locating the generating wind boundary field, which influences an accurate estimate of fetch. Estimating the exact location of the generating wind field was extremely difficult, especially during certain periods when wind fields were constantly changing.

Overall, the one-dimensional wave spectra using the JONSWAP and TMA agreed very well with the RDCP wave spectra. The only discrepancy was shown in the nearshore SE5 were both the JONSWAP and TMA fell short of the much higher RDCP value. Although the RDCP captured the wave energy, which is apparent from the +3m SWH measured, the JONSWAP/TMA was unable to capture it since JONSWAP/TMA relied

on winds to describe its spectra. Therefore, accurately estimating boundary wind fields at the exact time and location which, generate waves proved to be problematic, especially for SE5.

At the offshore Station 2007 and the nearshore Station 2009S, the wind direction was 15°-20°clockwise from the wave direction. For the nearshore Station 2009N, the wave direction was 30°-39°clockwise from the wind direction. The orientation of wind and wave directions could be due to a slanted fetch effect. This happens when offshore wind blows at an angle to the shoreline so that fetch becomes asymmetrical with respect to the wind direction. The waves then align with the longer fetch direction instead of with the wind direction (Walsh et al. 1989, Donelan et al. 1985). This was likely seen in some cases, where the fetch F estimated to be necessary to result in the observed waves was slightly longer than the available measured straight-line fetch to the shoreline. This wave versus wind direction effect was also documented and discussed in Wang and Hwang (2001).

The difference between wave direction and wind direction was also thought to be due to the strong current flow in the SE Chukchi Sea. There is a strong current prominent in the southeast Chukchi Sea region, traveling eastward over Station 2007 (offshore), and traveling eastward and northward over Stations 2009N and 2009S (Coachman and Tripp, 1970; Overland and Roach, 1987; Woodgate et al., 2005; Panteleev et al., 2010). Wind-sea states, especially the highest wind-seas such as SE1 and SE2 wind-seas, did not see this discrepancy. SE1 and SE2 wind-sea was easterly, and currents in the opposite

direction (flowing from the west). However the swell states, such as SE3, SE4, and SE5 swells, were influenced by current flow since wave direction was similar current direction rather than wind direction. At Station 2009S, prevailing current flow direction is eastward and northward, which corresponds to the westerly and southwesterly wave direction, and northward at Station 2009S, which corresponds with the southerly wave direction.

North American Regional Reanalysis (NARR) winds proved to be sufficient in estimating the wind fields of the JONSWAP and TMA wave spectral models as demonstrated for 4 out of 5 events, as validated against the observed RDCP spectra. The results showed a good agreement in the spectral shape, energy density, and frequency.

Values used to solve for γ were consistent with Mitsuyasu et al. (1980) where γ=1.7 for the SE Chukchi Sea region. Using the peak enhancement factor γ proposed by Mitsuyasu et al. (1980) would contribute to similar results.

In our analysis, we use the original frequency form of f^{-5} based on Phillips (1958) and used in the JONSWAP by Hasselmann et al. (1973). Further analysis using the frequency form of f^{-4} proposed by Donelan et al. (1985) could be investigated.

In conclusion, this study quantitatively describes the wave states affecting the southeast Chukchi Sea. This study also points out the shortcomings and difficulties of estimating the boundary generating wind field. Properly identifying the boundary generating wind field is most important when describing wind-waves. With these tools used in this study in hand, one can use this type of analysis for their own purpose in

describing the wave state to their particular case, or use the results from this study to estimate wave conditions that can be expected in the southeast Chukchi Sea region, both onshore and offshore.

Acknowledgements

This publication is the result in part of research sponsored by the Cooperative Institute for Arctic Research (CIFAR) with funds from the National Oceanic and Atmospheric Administration (NOAA) under cooperative agreement NA17RJ1224 with the University of Alaska. Funding also provided by NOAA projects, NA06OAR4600179 and NA08OAR4600856. Generous logistical support from Teck Alaska Incorporated and Foss Maritime Company has been provided to this project from its beginning.

References

AADI (Aanderaa Data Instruments) (2006). *RDCP Primer TD 220c*, 70 pp.

Airy, G.B. (1845). Tides and waves. *Encyc. Metrop.*, 192, 241–396.

Bouws, E., H. Gunther, W. Rosenthal, and C.L. Vincent (1985). Similarity of the Wind Wave Spectrum in Finite Depth Water 1. Spectral Form. *Journal of Geophysical Research*, Vol. 90, No. C1, pp. 975-986.

Carter D.J.T. (1982), Prediction of wave height and period for a constant wind velocity using the JONSWAP results. *Ocean Engineering*, 9 (1), 17–33.

Coachman, L. K. and R. B. Tripp (1970). Currents North of Bering Strait in Winter. *Limnology and Oceanography*, Vol. 15, No. 4, 625-632

Donelan, M.A., J. Hamilton, and W.H. Hui (1985). Directional spectra of wind-generated waves. *Phil. Trans. Roy. Soc. London* A315, 509-562.

Ewing, J.A. (1980). Observations of Wind-waves and Swell at an Exposed Coastal Location . Estuarine and Coastal Marine Science, 10, pp. 543-554.

Francis-Chythlook, O. (2004) Coastal Processes in Elson Lagoon, Barrow, Alaska. MS Thesis, University of Alaska Anchorage, Anchorage, Alaska.

Hasselmann, K., T.P. Barnett, E. Bouws, H. Carlson, D.E. Cartwright, K. Enke, J.A. Ewing, H. Gienapp, D.E. Hasselmann, P. Kruseman, A. Meerburg, P. Müller, D.J. Olbers, K. Richter, W. Sell and H. Walden (1973). Measurements of wind-wave growth and swell decay during the Joint North Sea Wave Project (JONSWAP). *Deutsche Hydrographische Zeitschrift* A8 (12), 95pp.

Hasselmann, K., D.B. Ross, P. Müller and W. Sell, (1976). A parametric wave prediction model. *Journal of Physical Oceanography*, 6**,** pp. 200–228.

Hudak DR and JMC Young (2002) Storm climatology of the southern Beaufort Sea. *Atmosphere Ocean,* 40, 145–158.

Jensen, R., N. Scheffner, S.J. Smith, D. Webb, and B. Ebersole. (2002). *Engineering Studies in Support of Delong Mountain Terminal Project ERDC/CHL TR-02-26*, September 2002, Vicksburg, MS.

Kitaigorodskii, S.A., V.P. Krasitskii, and M.M. Zaslavskii, 1975. On Phillips' theory of equilibrium range in the spectra of wind-generated gravity waves. *J. Phys. Oceanography*, v. **5**, p. 410-421.

Lee, Y.K. (1980). Hurricane Eloise wave spectra. *Coastal Engineering*, 4, 151-156.

Le Méhauté, B. (1969). An introduction to hydrodynamics and water waves. *ESSA Tech. Rep.* ERL 118-Pol 3-2.

Lewis, A.W. and R.N Allos (1990). JONSWAP's parameters: sorting out the inconsistencies. *Ocean Engineering*, 17, 409-415.

Losada, I.J. and J.A. Revilla (2009). Applications to Fluid Mechanics: Water Wave Propagation, in Continuum Mechanics, (eds. Jose Merodio), in Encyclopedia of Life Support Systems (EOLSS), Developed under the Auspices of the UNESCO, Eolss Publishers, Oxford, UK, [http://www.eolss.net]

Mesinger, F., G. DiMego, E. Kalnay, K. Mitchell, P.C. Shafran, W. Ebisuzaki, D. Jovic, J. Woollen, E. Rogers, E.H. Berbery, M.B. Ek, Y. Fan, R. Grumbine, W. Higgins, H. Li, Y. Lin, G. Manikin, D. Parrish, and W. Shi (2006). North American Regional Reanalysis. Boulder, CO NOAA.OAR/ESRL PSD:42.

Mitsuyasu, H., F. Tasai, T. Suhara, S. Mizuno, M. Ohkusu, T. Honda, and K. Rikiishi (1980). Observation of the Power Spectrum of Ocean waves Using a Cloverleaf Buoy. *Journal of Physical Oceanography*, 10, pp. 286-296.

Overland, J.E. and A.T. Roach (1987). Northward flow in the Bering and Chukchi Seas. *Journal of Geophysical Research*, Vol.92, No.C7, 7097-7105.

Panteleev, G., D.A. Nechaev, A. Proshutinsky, R. Woodgate, and J. Zhang (2010). Reconstruction and analysis of the Chukchi Sea circulation in 1990-1991. *Journal of Geophysical Research*, 115, C08023, doi:10.1029/2009JC005453.

Phillips, O.M. (1958). The equilibrium range in the spectrum of wind-generated waves. *J. Fluid Mech.*, 4, 426-434.

Pierson W.J. and L. Moskowitz (1964). A proposed spectral form for fully developed wind seas based on the similarity theory of S. A. Kitaigorodskii, *Journal of Geophysical Research* Vol. 69, No. 24, pp. 5181–5190.

Rye, H. (1977). The stability of some currently used wave parameters. *Coastal Engineering*, 1, 17-30.

Skjelbreia, L. (1959). *Gravity waves Stokes third-order approximation.* Tables of functions, Council on Wave Research, University of California, Berkeley.

Sorensen, R.M. (1993). *Basic Wave Mechanics for Coastal and Ocean Engineers*. John Wiley & Sons, Inc. ISBN 0-471-55165-1. 284 pp.

Sorensen, R.M. (2006). *Basic Coastal Engineering, Third Edition.* Springer Science. ISBN 0-387-23332-6. 324 pp.

Stokes G.G. (1847). On the theory of oscillatory waves. *Trans Cambridge Philos Soc*, 8, 441-473.

Toba, Y. (1973). Local balance in the air-sea boundary process III. *J. Oceanog. Soc. Japan*, 29, 209-220.

U.S. ARMY ENGINEER WATERWAYS EXPERIMENT STATION, (1984). *Shore Protection Manual*, 4th ed., 2 vols., Washington, D.C: U.S. Government Printing Office.

Walsh, E.J., D.W. Hancock, D.E. Hines, R.N. Swift, and J.F. Scott (1989). An observation of the directional wave spectrum evolution from shoreline to fully developed. *J. Phys. Oceanogr*., 19, 670-690.

WAMDI Group (1988). The WAM model—A third generation ocean wave prediction model. *J. Phys. Oceanogr.,*18**,** 1775–1810.

Wang, D.W. and P.A. Hwang (2001). An Operation Method for Separating Wind Sea and Swell from Ocean Wave Spectra. *Journal of Atmospheric and Oceanic Technology*, 18, pp. 2052-2062.

Woodgate, R.A., K. Aagaard, and T. Weingartner (2005). A year in the physical oceanography of the Chukchi Sea: Moored measurements from autumn 1990-91, *Deep-Sea Research, Pt. II*, 52 (24-26): 3116-3149.

World Meteorological Organization (WMO) (1998). *Guide to Wave Analysis and Forecasting, Second Edition*. WMO-No. 702, Secretariat of the World Meteorological Organization – Geneva Switzerland. ISBN 92-63-12702-6. 159 pp.

Young, I.R. (1992). The determination of spectral parameters from significant wave ehight and peak period. *Ocean Engineering*, 19, 5, 497-508.

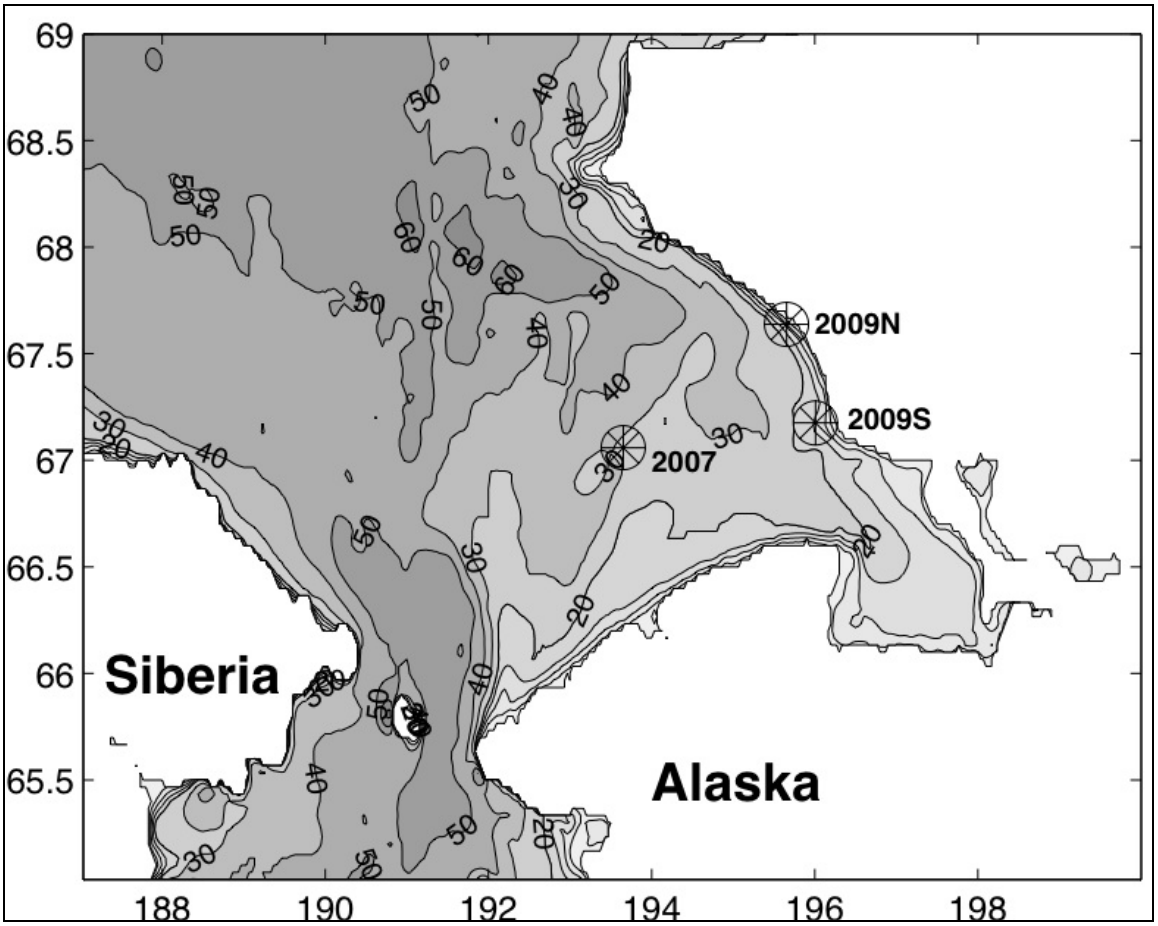

Figure 4.1 – *In situ* measurement locations on bathymetry map
Bathymetry map of south-eastern Chukchi Sea showing Stations 2007 (34m depth), 2009N (17m depth) and 2009S (18m depth).

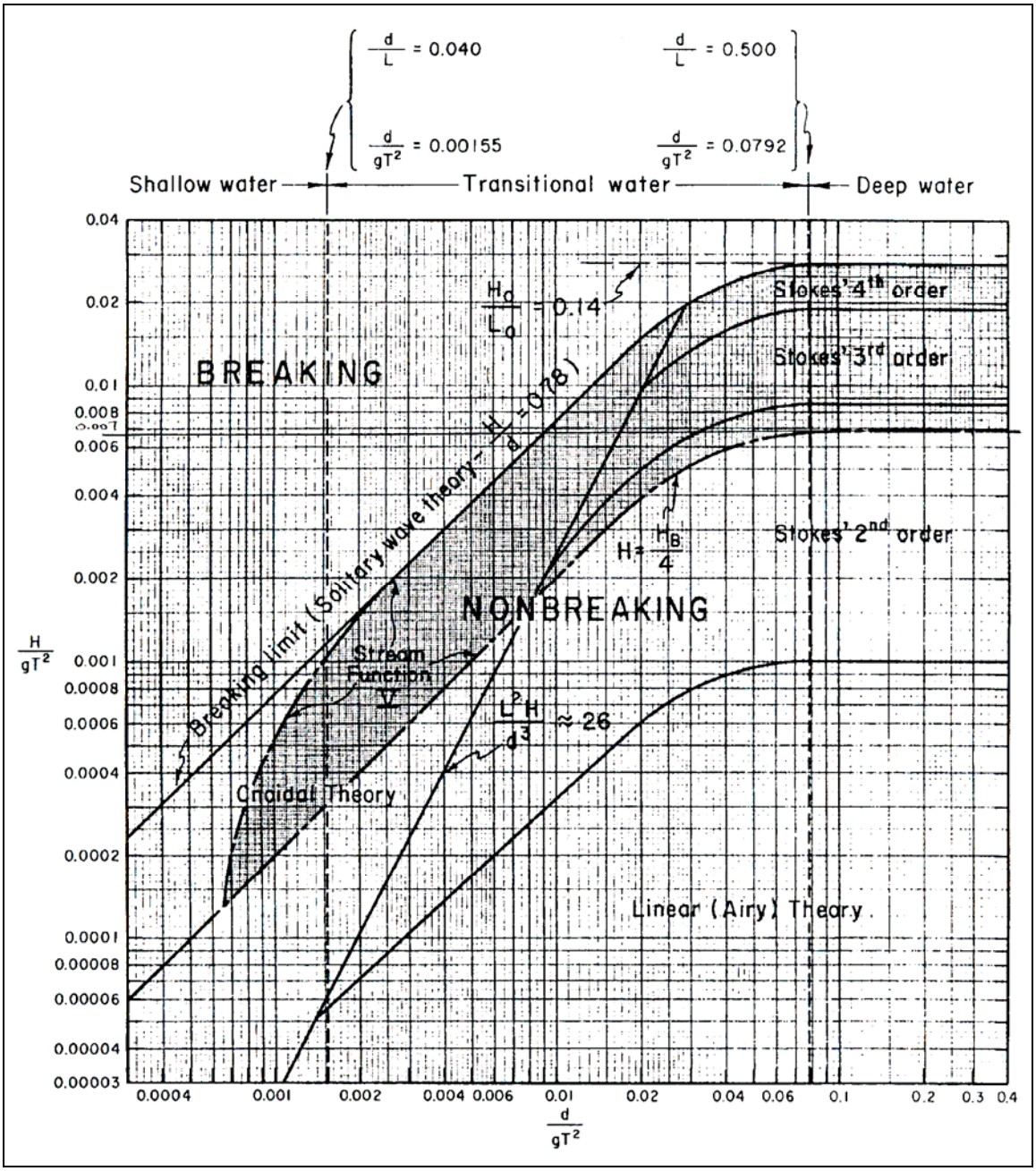

Figure 4.2 – Wave theory limits
Approximate limits for various wave theories. Le Méhauté (1969).

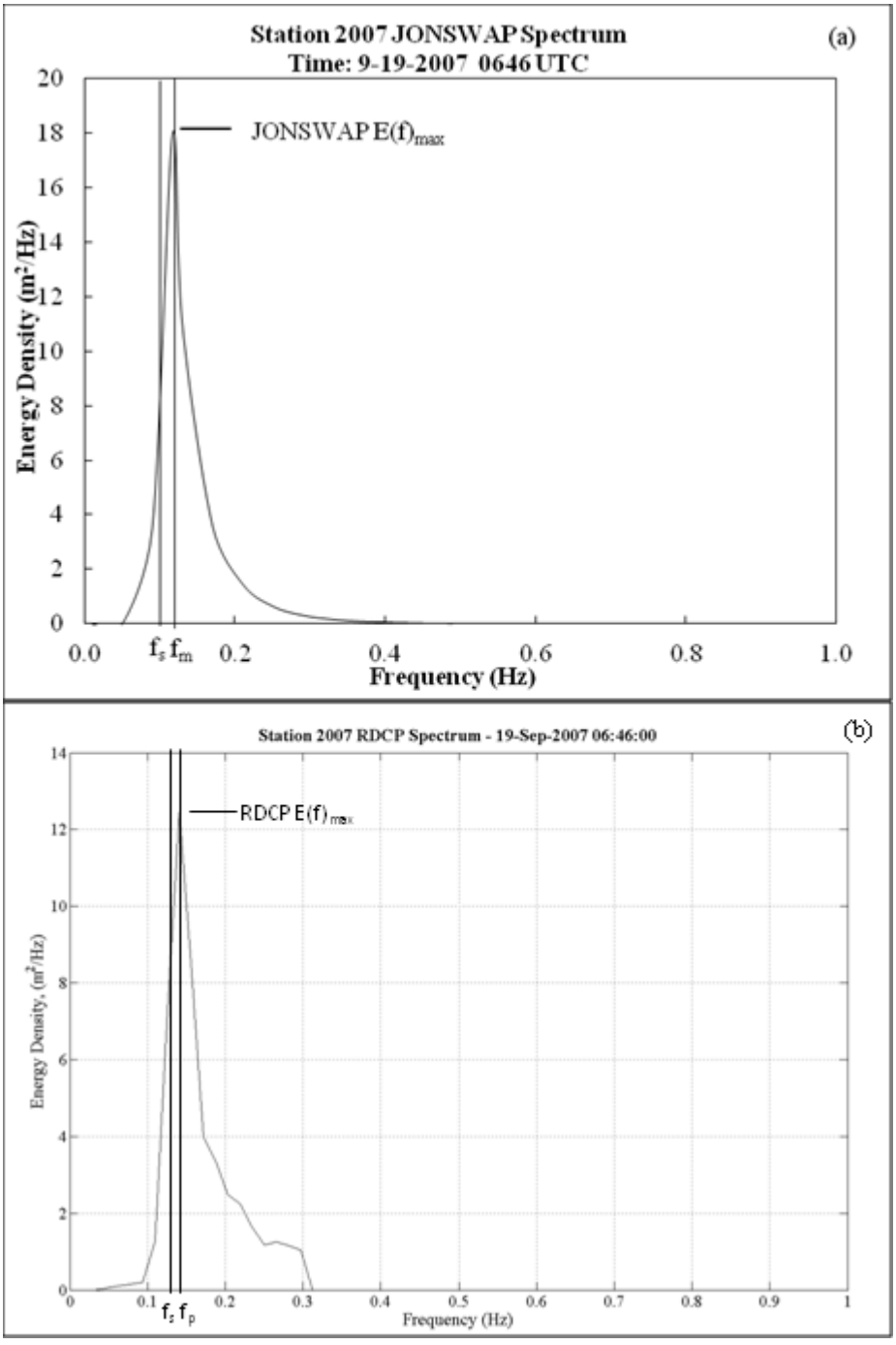

Figure 4.3 – SE1 JONSWAP versus RDCP spectrums
Comparison of JONSWAP spectrum ((a)-left) versus RDCP spectrum ((b)-right) for September 19, 2007, Station 2007, 67º3'29.94"N, 166º20'43.02"W, water depth 34m, SWH = 3.5m, U10=16.2 m s^{-1}.

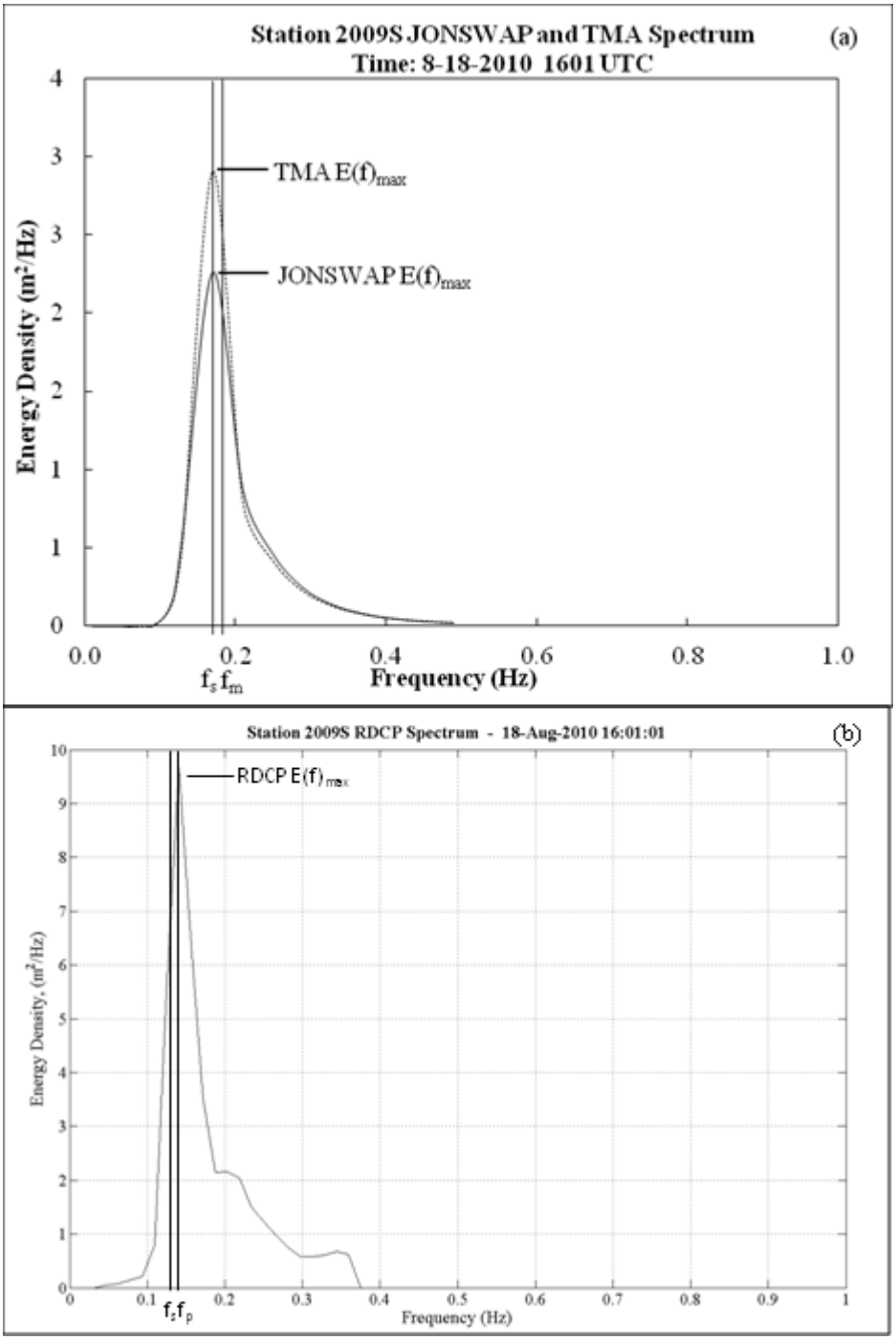

Figure 4.4 – SE5 JONSWAP/TMA versus RDCP spectrums
Comparison of JONSWAP, TMA spectrums ((a)-left), versus RDCP spectrum ((b)-right) for August 18, 2010, Station 2009S, 67º10'33.30"N, 163º59'23.94"W, water depth 18m, SWH = 3.2m, U10=8.8 m s^{-1}.

Table 4.1 – Wave theory classification of *in situ* measurements
Wave theory classification for RDCP Stations 2007, 2009N, and 2009S according to RDCP significant wave height thresholds, H_{m0} = 1,2,3m, with respective wave period, T_{m02}, averaged for each and depth, *d*.

Station 2007 (d=34m)			
Category	1m	2m	3m
T (sec)	4.6	5.2	5.8
d/gT^2	0.164	0.128	0.103
Wave classification for d/gT^2	deep	deep	deep
H/gT^2	0.00482	0.00754	0.00909
Order	Stoke's 2nd	Stoke's 3rd	Stoke's 3rd
L (m)	33	43	54
d/L (m/m)	1.029	0.789	0.629
Wave classification for d/L	deep	deep	deep
Station 2009N (d=17m)			
Category	1m	2m	3m
T (sec)	4.2	4.8	n/a
d/gT^2	0.098	0.075	n/a
Wave classification for d/gT^2	deep	transitional	n/a
H/gT^2	0.00578	0.00885	n/a
Order	Stoke's 2nd	Stoke's 3rd	n/a
L (m)	28	37	n/a
d/L (m/m)	0.618	0.462	n/a
Wave classification for d/L	deep	transitional	n/a
Station 2009S (d=18m)			
Category	1m	2m	3m
T (sec)	4.4	4.8	n/a
d/gT^2	0.095	0.080	n/a
Wave classification for d/gT^2	deep	deep	n/a
H/gT^2	0.00527	0.00885	n/a
Order	Stoke's 2nd	Stoke's 3rd	n/a
L (m)	30	37	n/a
d/L (m/m)	0.596	0.488	n/a
Wave classification for d/L	deep	transitional	n/a

Table 4.2 – Classification of gravity waves
Classification of gravity waves by water depth. From US Army Shore Protection Manual (1984).

Classification	***d/L***	***2πd/L***	**tanh (*2πd/L*)**
Deep water	> 1/2	> π	≈ 1
Transitional	1/25 to1/2	1/4 to π	tanh (*2πd/L*)
Shallow water	< 1/25	< 1/4	≈ *2πd/L*

Table 4.3 – Wave spectrum comparisons
Comparison of JONSWAP, TMA, and RDCP for highest SWHs in wave records SE1-5.

				JONSWAP				TMA	RDCP			
SE	No. Obs.	SWH (m)	U_{10} (m/s)	E(f)max (m^2/Hz)	fs (Hz)	fp (Hz)	Type	E(f)max (m^2/Hz)	E(f)max (m^2/Hz)	fs (Hz)	fp (Hz)	Type
1	7	3+	16+	17	0.10	0.12	wind-sea	-	12	0.13	0.14	wind-sea
2	3	4+	17+	21	0.09	0.11	wind-sea	-	20	0.11	0.13	wind-sea
3	4	2+	9+	3.4	0.16	0.15	swell	6.4	3.4	0.15	0.15	swell+ wind-sea
4	6	2+	7+	1.7	0.20	0.18	swell	2.6	3.4	0.17	0.16	swell
5	4	3+	8+	2.1	0.18	0.17	swell	2.7	9.5	0.13	0.14	wind-sea

Notes:
SE 1: September 18, 2007, Station 2007, 67º3'29.94"N, 166º20'43.02"W, water depth 34m
SE 2: December 1, 2007, Station 2007, 67º3'29.94"N, 166º20'43.02"W, water depth 34m
SE 3: July 22, 2010, Station 2009N, 67º38'17.76"N, 164º20'46.26"W, water depth 17m
SE 4: July 17, 2010, Station 2009S, 67º10'33.30"N, 163º59'23.94"W, water depth 18m
SE 5: August 18, 2010, Station 2009S, 67º10'33.30"N, 163º59'23.94"W, water depth 18m

Appendix

A.4.1. Summary of one-dimensional wind wave spectra (Phillips, 1958)

A one-dimensional frequency spectrum is the wave energy plotted as a function of frequency. Sorensen (1993, 2006) provide a good summary for one-dimensional wind wave spectra in coastal engineering practice. The energy density of a wave is $E = \rho g H^2 / 8$. Frequency f and period T share the following relationships $f = 1/T$ and $df = -dT / T^2$. The wave energy density at a particular frequency is denoted as $S(f)$. This yields the following expression for one-dimensional wave spectrum $S(f)$ (Phillips, 1958):

$$S(f)df = \sum_{f}^{f+df} \frac{H^2}{8} \tag{4.25}$$

where the units for $S(f)$ would be m^2Hz^{-1}.

The shape and scale of the wave spectrum will vary depending on the wind speed, position within the fetch, and other factors. Phillips (1958) found that for deep water waves should have the form for $S(f)$ as

$$S(f) = \frac{\alpha g^2 f^{-5}}{(2\pi)^4} \tag{4.26}$$

Phillips (1958) found α to be $\alpha = 0.0074$ from measured wind wave spectra.

A general spectral form of the modified Phillips (1958) formula for the equilibrium range is

$$S(f) = \frac{A}{f^5} \exp\left[-B / f^4\right] \tag{4.27}$$

where A and B adjust the scale of the spectrum. A and B are dependent on wave height and frequency (i.e. H_s and f_p) which are influenced by wind speed, fetch, and duration. f_p is the peak spectral frequency.

A.4.2. Pierson-Moskowitz spectrum (Pierson and Moskowitz, 1964)

The PM spectrum known as the Pierson-Moskowitz spectrum (Pierson and Moskowitz, 1964) was developed for a fully developed sea for deep water. Pierson and Moskowitz analyzed wave and wind records, for a fully developed sea for wind speeds between 10-20 m s^{-1}, from British weather ships operating in the North Atlantic. The form of this spectrum (Pierson and Moskowitz, 1964) is

$$E(f)_P = \frac{\alpha g^2}{(2\pi)^4 f^5} \exp\left[-0.74(g / 2\pi U_{19.5} f)^4\right] \tag{4.28}$$

where the wind speed $U_{19.5}$ is measured at an elevation of 19.5m and f is the wave frequency. The Phillips constant α is 8.1×10^{-3}.

Chapter 5 Ocean wave conditions in the Chukchi Sea from satellite and in situ observations[1]

Abstract

In situ observation of significant wave heights (SWHs) conducted from three fixed bottom-mounted Recording Doppler Current Profiler (RDCP) instruments in the south-eastern Chukchi Sea in 2007 and 2009 were compared with corresponding satellite observations from Envisat. A strong correlation (0.96) was indicated between satellite and *in situ* observations for the off-shore RDCP located approximately 82 km to the nearest coastline in the region with uniform topography. However, the corresponding cross-correlations are much lower (0.79 and 0.58) for the RDCPs located within 3.5km and 10.8 km, respectively, of the nearest coastline probably due to a strong spatial topography gradient and an insufficient number of satellite data points for validation. Cross-validated satellite observations were used for the analysis of wave conditions in the Arctic during the years 1993-2011. We found approximately a 0.020m/year increase of SWH for the SE Chukchi Sea and a 0.025m/year increase for the Pacific-Arctic, which correlates well with gradual ice retreat observed in the Arctic during the last two decades.

[1] Francis, O.P., G.G. Panteleev, and D.E. Atkinson (2011). Ocean wave conditions in the Chukchi Sea from satellite and in situ observations. *Geophys. Res. Lett.*, 38, L24610, doi:10.1029/2011GL049839.

5.1. Introduction

Satellite altimeter radar observations offer clear advantages of studying the sea state. They allow homogeneous, global, and continuous coverage, at improved resolution while *in situ* observations only offer localized coverage. Past studies have been done which compare the two methods (e.g. Young, 1994; Janssen et al., 2007; Li and Holt, 2007; Zieger et al., 2009) including the systematic calibration and cross-validation of the SWH data from different sensors. Recently, Young et al. (2011) analyzed data from all seven available altimeter missions and showed that global wind speeds and wave heights were increasing during the last 23 years, and assumed that the increase of the wind speed is the major factor contributing to the increase of the waves. However, all these studies did not include the Arctic Ocean where wave data is lacking for both satellite and in situ measurements due to the unavailability of several satellites (e.g. Topex/Poseidon and Jason -1 where the maximum northern extent ends at +66°, compared to ERS-1/2 and Envisat where the maximum northern extent ends at +81.5°) and due to sea ice coverage and remoteness. Also, in the North Pacific region, nearest to the area this paper focuses on, Young et al. (2011) showed in some analyses they conducted that there was a slight decrease in the wind speed and wave height trend. So, further examination is warranted for regions near the North Pacific. Our study focuses on the Pacific Sector of the Arctic Ocean and thus partly closes the existing gap in the analysis of the inter-annual variability of the wave conditions of the World Ocean. The paper is organized as follows: In the next section we describe the utilized RDCP data sets and available satellite observation.

In section 3 we provide a cross-validation between RDCP and satellite observation. In section 4 we analyze interannual variability of the wave conditions in the south-eastern part of the Chukchi Sea and in the Pacific Sector of the Arctic Ocean. Section 5 summarizes the results of the study.

5.2. Data

In this paper we utilize the following significant wave height (SWH) datasets.

5.2.1. SWH from Recording Doppler Current Profilers (RDCPs) in the SE Chukchi Sea

Recording Doppler Current Profiler (RDCP) (AADI, 2006) measurements collected in the southeast Chukchi Sea for 2007 and 2009-*2010* were used for this study. There were three RDCP deployments mounted at the bottom of the sea floor in a fixed upright position, one RDCP was deployed to an open-water location during the ice-free period, July-December 2007 ("2007" in Figure 1), and two RDCPs were later deployed to coastal locations during ice-free and ice-covered periods October 2009-September 2010 ("2009S" and "2009N" in Figure 1). Motivation for deployment was due to the lack of *in situ* measurements where instrument deployment and retrieval in this remote and ice-covered area is problematic. Freeze-up periods were estimated from RDCP recorded sea surface temperature (SST) as follows: 1) Station 2007 freeze up began December 8, 2007, 2) Station 2009S freeze up began November 12, 2009 and ended July 1, 2010, 3) Station 2009N freeze up began November 9, 2009 and ended July 2, 2010.

The RDCP sampled at a frequency of 2Hz. Each N observation was comprised of 15 minutes of individual wave observations i. The RDCP recorded individual wave heights H_i for 15 minutes where the significant wave height (SWH) H_{m0} (i.e. $\sim H_s$) was estimated from the highest 33% of waves in its 15-minute wave record. H_{m0} is expressed

as $4\sqrt{E}$ where E is the total variance of the wave field and expressed as $E = (1/16)\rho_w g H_{m0}{}^2$, and the terms ρ and g are dropped when expressing variance. Station 2007 recorded every 2.0 hours (i.e. the instrument was 2.0 hours at rest) for 3816 hours and 6 minutes, so the number of wave observations was N = 1704. Station 2009N recorded every 1.5 hours for 8041 hrs and 15 minutes, for N = 4596. Station 2009S recorded every 1.5 hours for 8204 hours, for N = 4689. Estimates of the RDCP SWH comes from a quartz pressure sensor with accuracy ranging between 0.001 m and 0.005 m for the installations in 2007 and 2009-2010, respectively. High accuracy of the pressure center and set-up of the RDCP observation ensure the high accuracy (no more than 1%) of the SWH estimates.

5.2.2. Satellite along-track observations from Aviso (http://www.aviso.oceanobs.com/)

Satellite along track altimeter radar observations from ERS-1/2 and Envisat satellites (www.aviso.oceanobs.com) from 1993-present were used in our study. The ERS-1, ERS-2, and Envisat radar altimeter have a foot print of 7km. The significant wave height is defined as $H_s = 4\sqrt{\sigma^2}$, where σ^2 is the variance of the sea surface elevation defined by the returned wave form detected by the satellite sensor (Chelton et al., 2001). Typically, altimeter measurements of H_s have an accuracy (rms error) within σ_{track} =0.5m (Zieger et al., 2009) which was assumed for this study. ERS-1/2 and Envisat satellites have a period of 35 days. During this period, these satellites provide wave observations along the tracks separated by approximately 40km in the Chukchi Sea (Figure 1).

5.3. Cross-validation RDCP and satellite observations

The location of the satellite tracks (Figure 1) and relatively high period (35 days) of the available satellites does not allow one to conduct point-by-point cross validation between satellite and RDCP SWH estimates. Because of this, we compared RDCP data with satellite observations within spatial-temporal domain defined by temporal and spatial scales. For satellite comparison to the RDCP, only ENVISAT is shown because it was the only satellite flown during the years 2007, 2009-2010, the years of the RDCP measurements. ENVISAT replaced the decommissioned ERS-2 satellite. The temporal scale was defined as equal to the temporal resolution of the wave observations in 2007 (1.5 hour) and 2009 (2 hours). The spatial scale was estimated by the distance that the wave travels for a corresponding time scale.

Taking into account that larger waves have a higher travelling speed we provide comparison for two different spatial scales (~30 and 50 km) defined by the traveling distance for small (<1.5m) waves and large (>1.5m) waves, respectively, based on RDCP SWH. The corresponding spatial scales are shown in Figure 1. We also excluded from consideration all satellite observations located closer than 10km to the coast and located in the shallow (< 10 m) regions.

As seen from Figure 1, each satellite track intersects the spatial domains in several locations. The satellite SWH observations for each spatial domain were estimated as a mean over all k satellite observations within the chosen temporal-spatial domain. Treating individual satellite observation as independent observation of the SWH with standard

deviation (STD) σ_{track}, we estimated the corresponding standard deviation of the SWH for the binned areas as $\sigma_{sat} = 1/\sqrt{k/\sigma_{track}^2}$. We found that this approach to estimating satellite STD is robust and gives similar results for large and small domains (Figure 2). The mean RDCP SWH was estimated as a mean over the chosen temporal window (usually 1-2 available values). We used a double temporal window to get estimates of the corresponding STD.

Figures 2a,b shows results of cross–validation in the large and small domain for Station 2007. We found that the linear fit between Envisat and the RDCP (Figure 2a) is almost ideal. Our results also show a very high mean correlation of approximately 0.96 between the RDCP and satellite data both for the large (Figure 2a) and small (Figure 2b) domains. This indicates the robustness of the cross-validation between RDCP and Envisat data in the 2007. We also would like to note that according to Figure 2a, the correlation should be higher for the larger waves (>1.5m), which is closer to the central diagonal than the waves with a smaller height. This indicates a higher accuracy for satellite observations of larger waves.

Figures 2c,e shows results of the cross-validation between the RDCP and satellite data for the large domains for Stations 2009N and 2009S. The linear fit and the cross-correlation (0.79) is not as high for Station 2009N as for Station 2007, but these results are still significant. The correlation (0.58) for Station 2009S is even smaller. We speculate that we obtained relatively low cross-correlations for Stations 2009N and 2009S due to two basic reasons. First, is that because of the near-shore location, much of

the domain is covered by land (Figure 1). Second, is the sharper topography gradient from the shoreline to Stations 2009N and 2009S therefore only Envisat depths greater than 10m were considered which eliminated much of the coastal region in the domain.

A similar cross-validation for the small domains (Figures 2d,f) gives a higher correlation. Unfortunately, the number of available data pairs of RDCP and Envisat are too low to state whether this cross-validation is statistically significant. However, it gives us ground to believe that if we had more data pairs for the small domain, we could obtain similar results we achieved for Station 2007. Overall, despite the fact that the results of the cross-validation for Stations 2009N and 2009S were not robust, we would like to note that all cross-correlations were rather high. Therefore, we propose that satellite SWH observations can be successfully used for the analysis of wave conditions in the Chukchi Sea, and probably in the Arctic Ocean.

5.4. SHW for a period 1993-2010

Satellite SWH observation from ERS-1/2 and Envisat allows analyses of wave conditions in the Chukchi Sea from 1993-present. Figure 3a shows all available satellite SWH observation within the square domain that occupies a major part of the south-eastern Chukchi Sea (Figure 1) while simultaneously excluding the shallow regions. The analysis of Figure 3a shows that over the 17-year satellite SWH record (1993-2010) for the southeast Chukchi Sea, there was a 0.02m/year increase which equates to a 0.34m increase over 17 years (Figure 3a). There is also an increase of the maximum SWH. In particular, according to Figure 3a there were at least 5 events when SWH exceeded 4m during the last decade (2002, 2004, 2005, 2006, 2010) compared to only two events in the 1990's.

As we mentioned above, Young et al. (2011) reported that wind conditions over the North Pacific and Bering Sea were relatively stable and there was no increase in the wind speed over the Northern Pacific and Bering Sea. The mean wind speed in the eastern Chukchi Sea derived from NCEP/NCAR reanalysis (Figure 3b, Kistler et al., 2001) agrees well with Young et al., (2011). It does not reveal significant trend and has insignificant (0.31) correlation with SWH.

In order to identify physical mechanisms that control the SWH increase in the south-eastern Chukchi Sea, we analyzed the ice concentration (Comiso and Nishio, 2008) in the region limited to 66.6°-67.7°N and 192°-195°E. When ice concentration was < 0.15, the ocean was considered ice free. The ice free area was calculated in (km^2). The

annual mean ice-free area for this region is shown in Figure 3a and reveals a relatively high mean correlation of 0.58 with observed SWH. Interestingly, for the period of 1993-2005, the correlation was even higher at 0.77. We speculate that is due to the relatively stable wind conditions during 1993-2005 and significant decrease of the wind speed after 2005 (Figure 3b). In the absence of other physical mechanisms we assume that diminishing ice in the Arctic (Comiso et al., 2008; Screen and Simmonds, 2010; Perovich and Richter-Menge, 2009; Zhang, 2010) is the primary cause responsible for the identified SWH changes.

We suggest two possible mechanisms affecting ice decrease. First, is the increase of the fetch that allows the growth of higher waves under the same winds. Second, is the increase duration of the ice-free season in the Arctic Ocean. This may allow generation of high waves due to strong storms in the late fall and early winter, and favorable ice free conditions. The identified increase of SWH in the Chukchi Sea is not a local phenomenon. The analysis of the satellite SWH data for the Pacific Sector of the Arctic Ocean shows that this effect is global and also that the mean annual SWH significantly increases in almost every part of the Arctic Ocean (Figure 4). The regions with maximum SWH that reaches up to 0.03-0.04 m/year are usually located 100-200 km offshore. Figure 4a, shows that the highest growth of the SWH is near the northern Alaskan Coast. Taking into account, that 1993-2010 mean SWH for this region is about 1.5m (Figure 4b), we find that SWH in this region has doubled (i.e. increased up to 2 times) during the

last two decades. Our analysis of the ERS-1/2 and Envisat data shows similar SWH growth rates for the all regions north from 66°N.

5.5. Conclusions

The analysis of the Envisat satellite data shows high correlations with the wave data from the RDCP obtained in 2007 and 2009. The correlation is very high for the offshore observation (2007) and lower for the coastal observations (2009N and 2009S) probably due to inhomogeneity of wave conditions and an insufficient amount of data for cross-validation.

Using the ERS-1/2 and Envisat SWH data we found the mean SWH significantly increases during the last two decades with an averaged rate of 0.02 m/year for the south-eastern Chukchi Sea. The result shows that satellite data has excellent coverage for global oceans, but not for nearshore locations. Until better methods can be developed for obtaining satellite nearshore data, in situ measurements for coastal applications is recommended.

Given the mean SWH for the SE Chukchi Sea and Pacific-Arctic regions, the 17-year trends were shown both shown to increase, with a larger increase over the Pacific-Arctic. However, the SWH is not increasing everywhere proportionately over the Pacific-Arctic region as seen in the comparison between the averaged rate and the mean of the SWH. This higher increase in SWH in some areas over others is likely due to longer open water season and therefore shorter periods of first-year sea ice. Also the higher increase results from some areas of the Pan-Arctic region may be due to more synoptic-scale meteorological activity than other regions, causing larger wind-waves to form.

The 17-year trend in the mean SWH was explained by ice decline. However, internannual variability would be more related to the wind conditions. Taking that into account, it is important to analyze waves and atmospheric conditions in a potentially ice-free ocean in the future.

Acknowledgements

This publication is the result in part of research sponsored by the Cooperative Institute for Arctic Research (CIFAR) with funds from the National Oceanic and Atmospheric Administration (NOAA) under cooperative agreement NA17RJ1224 with the University of Alaska. Oceana Francis was supported and *in situ* measurements funded by NOAA projects NA06OAR4600179 and NA08OAR4600856 through David Atkinson's projects. Logistical support for *in situ* measurements was provided by Teck Alaska Incorporated and Foss Maritime Company. Gleb Panteleev was supported by the Japan Agency for Marine-Earth Science and Technology (JAMSTEC) through their sponsorship of research activities at the International Arctic Research Center, by North Pacific Research Board 828 award, and by National Science Foundation award 1107925.

References

AADI (Aanderaa Data Instruments) (2006). *RDCP Primer TD 220c*, 70 pp.

Chelton, D.B., J.C. Ries, B.J. Haines, L.-L. Fu, and P.S. Callahan (2001). Satellite altimetry. *Satellite Altimetry and Earth Sciences: A Handbook of Techniques and Applications*, L.-L. Fu and A. Cazenave, Eds., Academic Press, 1-131.

Comiso, J. C., C.L. Parkinson, R. Gersten, and L. Stock (2008). Accelerated decline in the Arctic sea ice cover. *Geophys. Res. Lett*. 35 doi:10.1029/2007GL031972.

Comiso J.C. and F. Nishio, (2008). Trends in the sea ice cover using enhanced and compatible AMSR-E, SSM/I, and SMMR data. J. Geophys. Res., 113, C02S07, doi:10.1029/2007JC004257.

Janssen, P., S. Abdalla, H. Hersbach, J-R. Bidlot (2007) Error Estimation of Buoy, Satellite, and Model Wave Height Data. *J. Atmos. Oceanic Technol.*, 24, 1665–1677. doi:10.1175/JTECH2069.1

Kistler, R., E. Kalnay, W. Collins, S. Saha, G. White, J. Woollen, M. Chelliah, W. Ebisuzaki, M. Kanamitsu, V. Kousky, H. van den Dool, R. Jenne, and M. Fiorino, (2001). The NCEP-NCAR 50-Year Reanalysis: Monthly Means CD-ROM and Documentation. *Bull. Amer. Meteor. Soc*., 82, 247-267.

Li, J-G. and M. Holt (2007). Validation of a regional wave model with Envisat and Buoy observations. Proc. 'Envisat Symposium 2007', Montreux, Switzerland, 23–27 April 2007 (*ESA SP-636, July 2007)*.

Perovich D.K., J.A. Richter-Menge (2009). Loss of sea ice in the Arctic. *Annu Rev Mar Sci* 1:417–441.

Screen, J. A. and I. Simmonds (2010). The central role of diminishing sea ice in recent Arctic temperature amplification. *Nature* 464*,* 1334–1337*,* doi:10.1038/nature09051, 2010

Young, I.R., S. Zieger, A.V. Babanin (2011). Global trends in wind speed and wave height. *Science* 332, pp. 451-455. DOI:10.1126/science.1197219.

Young I.R. (1994). Global ocean wave statistics obtained from satellite observations. *Appl. Ocean Res.* 16*,* 235.

Zhang, X. (2010). Sensitivity of Arctic summer sea ice coverage to global warming forcing: Toward reducing uncertainty in Arctic climate change projections. *Tellus* A. 62:220-227.

Zieger, S., J. Vinoth, I. R. Young (2009). Joint calibration of multiplatform altimeter measurements of wind speed and wave height over the past 20 years. *J. Atmos. Ocean. Technol.* 26, 2549.

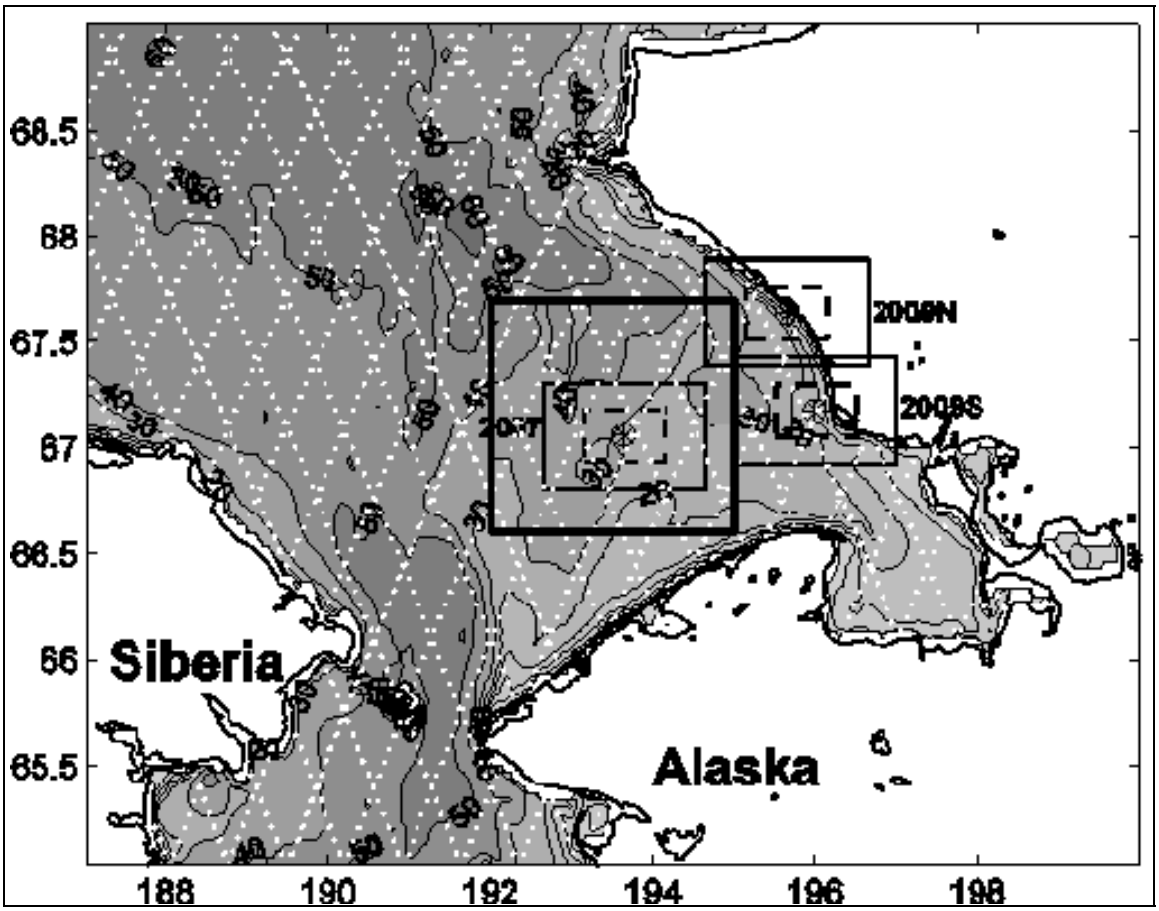

Figure 5.1 – Satellite tracks map
Region, satellite tracks (ERS-12, Envisat), locations, squares.

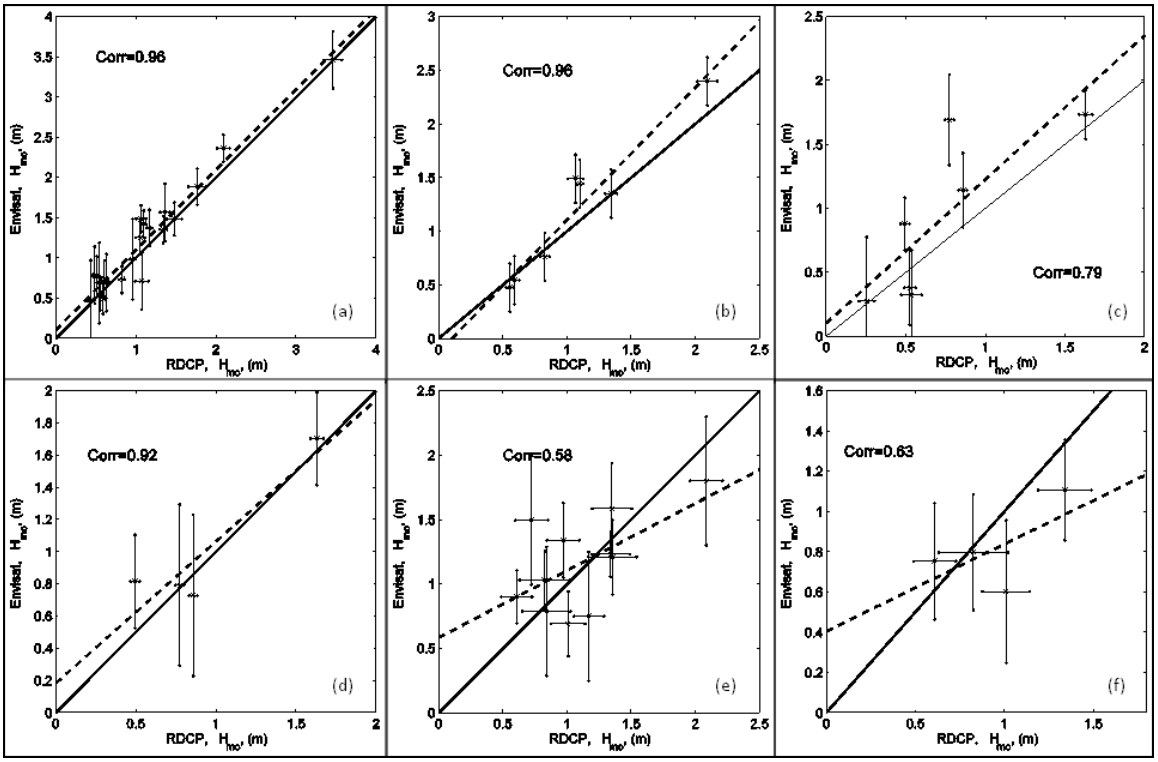

Figure 5.2 a-f – Satellite versus RDCP

(top left, clockwise). Significant wave height H_{m0} linear comparison from Recording Doppler Current Profiler (RDCP) dataset (x-axis) versus Envisat satellite altimeter dataset (y-axis) for (a) Station 2007 large domain (solid line, Fig 5.1), (b) Station 2007 small domain (dashed line, Fig 5.1), (c) Station 2009N large domain (solid line, Fig 5.1), (d) Station 2009N small domain (dashed line, Fig 5.1), (e) Station 2009S large domain (solid line, Fig 5.1), (f) Station 2009S small domain (dashed line, Fig 5.1).

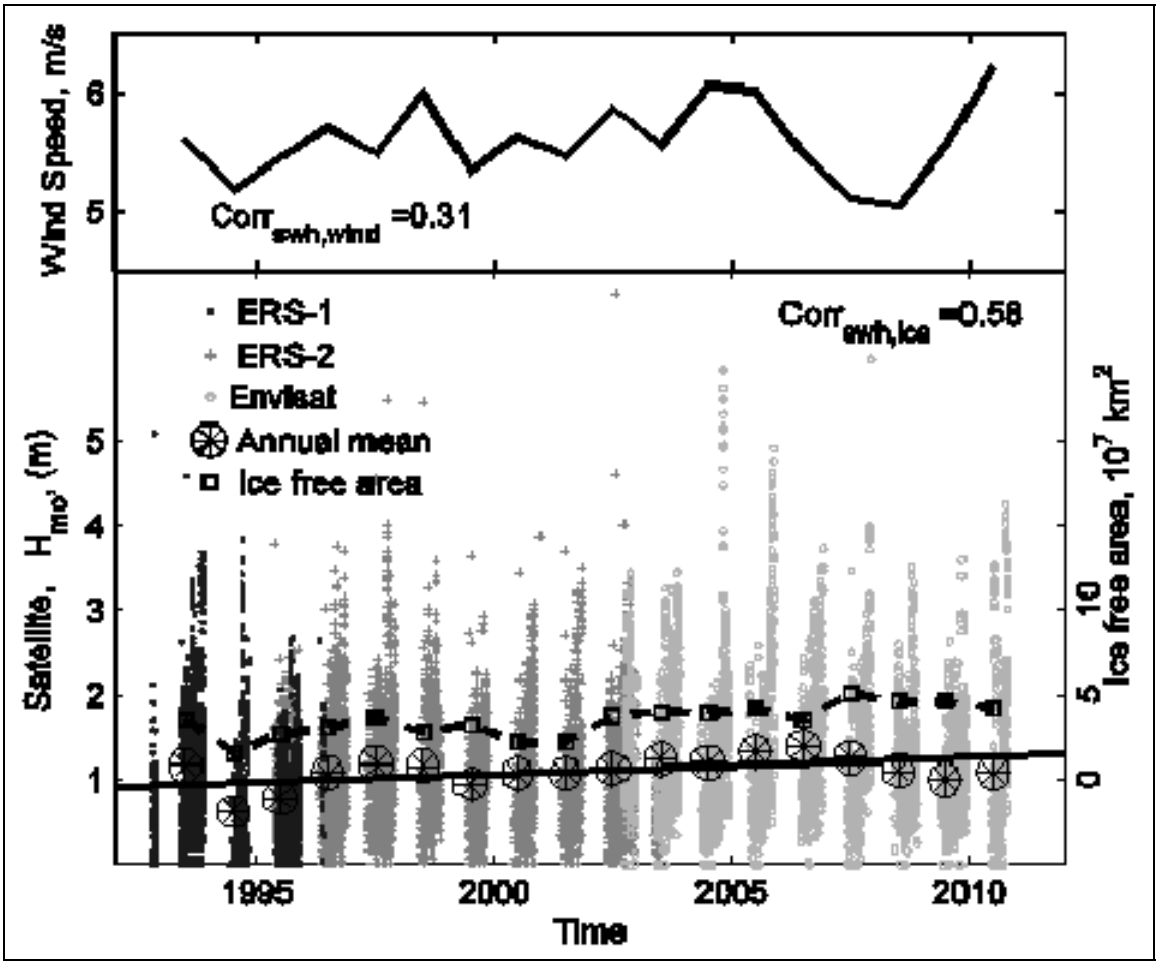

Figure 5.3 – Satellite trend for Chukchi Sea

Significant wave height (SWH) for the period 1993-2010 for the southeast Chukchi Sea around Station 2007 (i.e. largest domain around Station 2007 in Fig 1) showing (Top): NCEP NCAR Reanalysis I wind (Kistler et al., 2001) trend and correlation to SWH. (Bottom): Satellite data and its mean value (stars) with solid line showing SWH mean trend. Dashed line is the ice-free area over the Chukchi Sea (Lat 65-74ºN, Lon 170-210°E) for the period May 1 - Nov 1 for each year (Comiso and Nishio 2008), and the correlation of sea ice concentration to SWH. The linear fit to the satellite data has a positive increment of 0.02 m/year with 80% and 90% confident intervals 0.008-0.03m/year and 0.005-0.033 m/year, respectively.

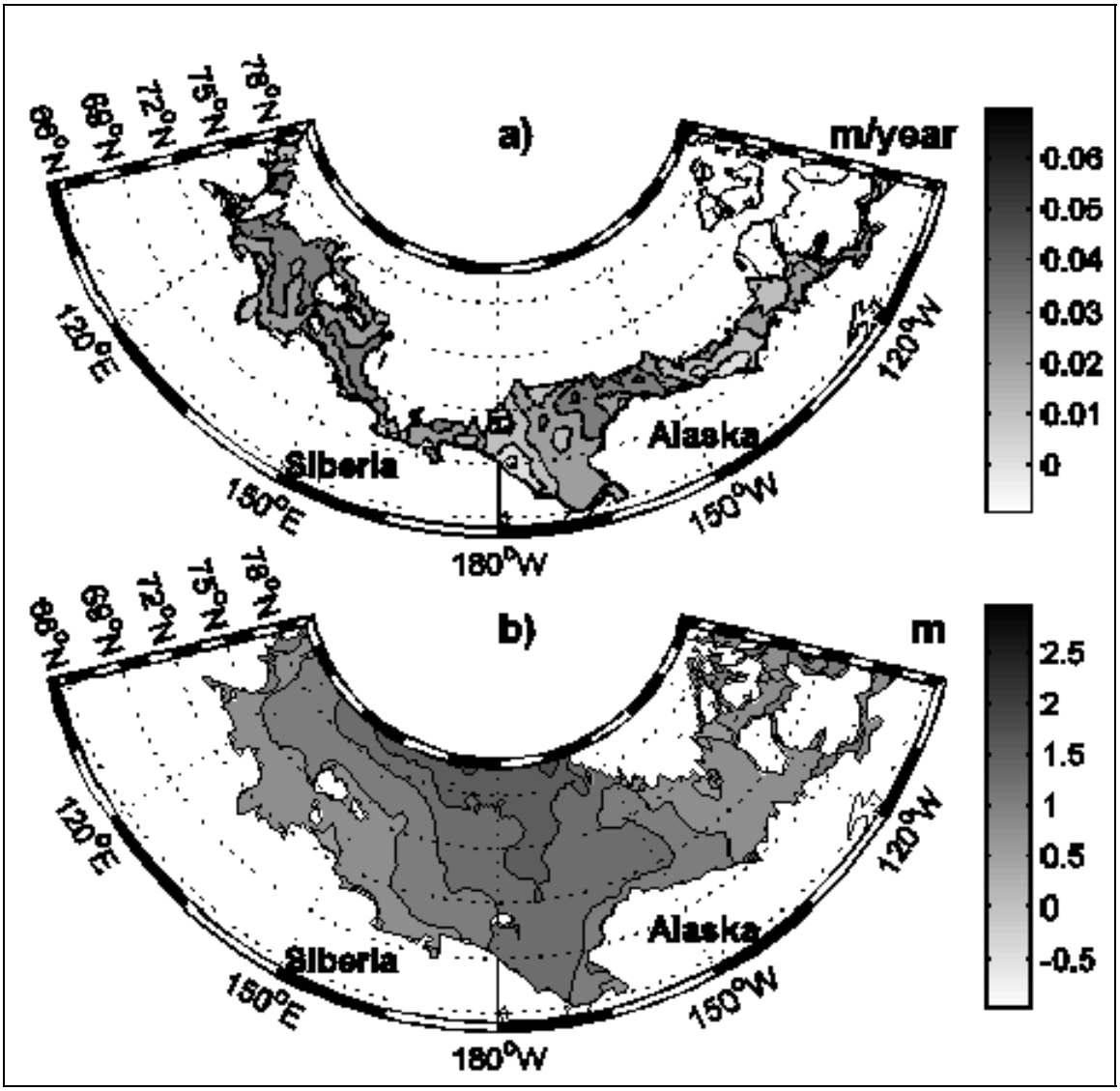

Figure 5.4 – Satellite trend for Pacific-Arctic
Significant wave height (SWH) for the period 1993-2010 for Pacific-Arctic region showing (a) SWH incremental change (m/year) (top fig) and, (b) SWH mean value (bottom fig)

Chapter 6 Summary and Conclusions

One of the overarching goals for this PhD dissertation was to develop an ocean wave synthesis for the southeast Chukchi Sea, Alaska through investigation of *in situ* measurements, modeling, and long term satellite data. The second overarching goal was to evaluate if these *in situ*, satellite, modeling, and wind tools are suitable for this region. *In situ* observations were used for two main purposes: to perform wave analysis and provide linkages to meteorological conditions. These observations were also used for cross-validation with one-dimensional wave models and satellite altimetry data, the other two tools in this study. Wave data derived from satellite altimeter were also used to identify recent wave state trends.

The efforts of this dissertation were guided by the following research hypothesis which was: "Wave states in the Chukchi Sea, Bering Sea, and Pacific Arctic regions have displayed change throughout the last few decades, which can be attributed to environmental parameters such as sea-ice variability, and can be shown by the tools for analyzing waves used in this study, i.e. *in situ* and satellite measurements, and modeling."

6.1. Research Question 1

What is the best characterization of present wave states in the southern Chukchi Sea?

Using simple phase-resolving methods, the waves in the southeast Chukchi Sea were classified as surface gravity wind waves of Stokes' 2nd order (1m SWH). For larger SWHs (>2m) the waves are dominated by 3rd order Stokes' waves. The transition from deep to intermediate waves began at 18m.

The wave states were further classified as swell or wind-sea from one-dimensional frequency spectra using *in situ* (RDCP) measurements and models (JONSWAP and TMA). This was performed using the wave steepness method, where separation frequency was determined from the peak frequency of the RDCP and the JONSWAP. Wind speed was used to find peak frequency and then fetch, which are needed parameters for the JONSWAP and TMA models. The JONSWAP/TMA frequency spectrums were then compared to the RDCP spectrum. For the highest significant wave heights, the spectra showed only one peak indicating a strong presence of wind-sea or swell. These single peak wave states were what were evaluated in our study due to the frequency limitations of the RDCP.

The results from these studies demonstrated that for offshore regions of the southeast Chukchi Sea, the highest significant wave heights were from the east wind/wave direction. The results also implied that the highest significant wave heights offshore were wind-sea. The fetch-limited high winds generated from the Kotzebue Sound seem to contribute all of the energy imparted to the observed significant wave

heights of +3m to +4m. This implied a strong wind-sea presence. This was verified by the JONSWAP spectrum and the RDCP spectrum, as the peak frequency of the spectrum was greater than the separation frequency which implied wind-sea. Swell was also observed for offshore wave records, but this was for lower significant wave heights and an open fetch coming from a west direction, such as the Bering Strait or Chukchi Sea.

For the nearshore regions of the southeast Chukchi Sea, the highest significant wave heights were from the south and west wind/wave directions. The results showed that the highest significant wave heights were swell, with the exception of a wind-sea state for one of the wave records.

The north nearshore location (near Kivalina, Alaska) experienced swell conditions. A broader synoptic assessment indicated strong south-southwest wind fields (+15m s^{-1}) in the vicinity of the Bering Strait. These winds were thought to contribute to a major part of the energy imparted to the waves since local wind was southerly at only +9m s^{-1}. The JONSWAP and RDCP wave spectra also confirmed that these waves are swell.

For one of the events at the south nearshore location (near Cape Krusenstern, Alaska) the wave states were also found to be swell, with similar conditions to the north nearshore location (near Kivalina, Alaska). A synoptic assessment again indicated strong southwest wind fields (+18m s^{-1}) in the vicinity of the Bering Strait. These winds appeared to be a major energy source affecting the wave state again since local wind was

south-southwesterly at only +9m s^{-1}. The JONSWAP and RDCP wave spectrums also confirmed this as swell.

For the other event at the south nearshore location the results showed swell for the JONSWAP/TMA spectrum, and wind-sea for the RDCP spectrum. The difference between the two spectrums was thought to be due to several different locations of wind fields, which generated waves in different locations. These large regions of west-northwest wind fields (+16m s^{-1}) were located in the south Chukchi Sea. One of these regions of wind fields may have imparted energy that the RDCP picked up as wind-sea. This would not have been accounted for in the estimation of the wind field (where wind field was estimated using the North American Regional Reanalysis, Mesinger et al., 2006, and the Global Reanalysis, Kistler et al., 2001) for the JONSWAP if a different pocket of wind field was used. This shows that determining the exact fetch of the wind field is not trivial.

6.2. Research Question 2

What are the atmospheric drivers responsible for the observed wave state in this region?

Synoptic activity was analyzed and low pressure systems were linked to RDCP wave parameters (height, period, direction). Two types of identification were used to identify atmospheric drivers responsible for the observed wave states. This included identifying a 1) significant wave height (SWH) event, and 2) the atmospheric driver which created the SWH event. A significant wave height (SWH) event was defined as a wave height that remained over a given threshold (i.e. 1m, 2m, or 3m) for a period of 6 hours or more in duration. (Hudak and Young, 2002; Francis-Chythlook, 2004). The atmospheric driver, i.e. "storm" was manually done by identifying several key features: 1) any closed low feature on a chart of 925mb with geopotential height less than 700 m, 2) wind magnitude greater than 10m/s at 925mb, and 3) wind direction directed into southern Chukchi Sea.

Upon performing the linkage of atmospheric drivers to *in situ* wave observations, it was found that for creation of highest SWH events (i.e. wind-waves) neighboring high and low pressure systems over the Chukchi, and cyclones over the Bering were responsible. Storms that have moved in which formed in the North Pacific, take them through the Strait and into the Chukchi Sea. Another storm pathway runs roughly east-west across the north Russian/Alaska coast. Since storms often stall when positioned over the eastern Bering Sea, they allow wind duration to be maximized which can simulate a near fully developed sea state for the given fetch. If the storm did not stall, a near fully-

developed sea-state would be unlikely to be attained since maximum wind speeds rarely exceed 40m s^{-1}.

Offshore (Station 2007) results showed a strong agreement between wind direction and wave direction. Although there is a strong current prominent in the southeast Chukchi Sea region, traveling eastward (Coachman and Tripp, 1970; Overland and Roach, 1987; Woodgate et al., 2005; Panteleev et al., 2010), current flow coming from the west over Station 2007 was found to be overcome by strong easterly winds. This was seen for the higher significant wave heights (1-2m). Lower significant wave heights (<1m) had a westerly wave direction, i.e. the same direction as the current flow. Therefore, current flow and swell were believed to play a part in lower significant wave heights (<1m).

Nearshore (2009N/S) results showed a strong agreement between wind direction and wave direction. Station 2009N displayed more south winds/waves compared to Station 2009S which displayed southwest to west-northwest winds/waves, which was thought to be due to wave refraction. There is a strong current traveling eastward and northward (Coachman and Tripp, 1970; Overland and Roach, 1987; Woodgate et al., 2005; Panteleev et al., 2010). At Station 2009S, this current is found to travel eastward and northward, which corresponds with the westerly and southwesterly wave direction. At Station 2009S, this current is found to travel northward, which corresponds with the southerly wave direction. Therefore, westerly waves that would have been present at Station 2009N may have been refracted due to the strong current traveling northward.

The southerly wave direction at Station 2009N was also possible due to longer southerly fetch than Station 2009S. The westerly wave direction at Station 2009S was also believed to be attributed to an open westerly fetch. Station 2009N also exhibited SWHs that were smaller in magnitude and fewer in number than those recorded at Station 2009S due to its proximity to an enclosed embayment north of Station 2009N. Besides current flow and fetch, shore-fast sea ice was also shown to play a role in wave activity. This early ice breakup is thought to be caused by extra-tropical cyclonic activity later and earlier in the seasons (Sienkiewicz et al., 2005), and less available sea ice (Comiso et al., 2008).

6.3. Research Question 3

What has been the trend of the wave states in the Chukchi Sea over the last few decades, and what is the largest contributor to observed change: sea ice retreat or a change in the synoptic wind regime?

The consequences of these findings are shown with satellite data. The satellite data displays a linear trend where the mean significant wave height was found to increase significantly over the last two decades with an average rate of 0.020m yr^{-1} in the southeastern Chukchi Sea. In the Pacific-Arctic region, the significant wave height was shown to increase at a faster rate (0.025m yr^{-1}). When extrapolating the linear satellite trend of 0.020m yr^{-1} in the southeast Chukchi Sea, in 50 years the significant wave height is likely to increase by 1m from its present state. It is speculated that the increase in SWH is due to longer open water season due to ice decline, which was shown by a 0.58 correlation of SWH to the ice-free area. Increased synoptic activity, which would affect wind conditions may also play a role but to a much lesser extent since there was a weak correlation between SWH and wind speed (0.31).

Unlike *in situ* measurements which only cover recent years, remotely sensed significant wave height data are available for at least 17 years for Chukchi Sea and Pacific-Arctic regions. Because of the proven high accuracy of satellite significant wave height measurements (Young, 1994; Janssen et al., 2007; Li and Holt, 2007; Zieger et al., 2009), we were not only able to produce an accurate record for the last 17 years, but also able to cross-validate RDCP *in situ* measurements with satellite measurements.

6.4. Final Summary

In summary, the results from the dissertation include:

- The area is dominated by **surface gravity wind waves** of Stokes' 2nd order (1m SWH). For larger SWHs (>2m) the waves are dominated by 3rd order Stokes' waves. Transition from deep to intermediate waves begins at 18m.
- Strong pressure gradients, caused by juxtaposed high and low pressure regions, or powerful transient cyclones, generated the winds responsible for the highest SWH events (i.e. wind-waves).
- For the **offshore** region, the available fetch was from all directions. Highest SWHs & winds were easterly and "wind-sea". Lower SWHs & winds were from various directions and "swell".
- For the **nearshore** region, the available fetch was from the westerly direction. All SWHs & winds were westerly and southerly and "swell" (occasionally "wind-sea").
- There was a **strong correlation** for the offshore region compared to nearshore region when dealing with satellite and other wave analysis performed in this study.
- Significant wave height has increased by **0.38m over the past 20 years** for the SE Chukchi. This correlates with the **gradual ice retreat** and to a lesser extent, wind speed.

- Significant wave height **will increase to 1m in 50 years** (from a simple extrapolation).
- Significant wave height increase was found not only in the Chukchi Sea, but also in the **Pacific Arctic** as well.
- North American Regional Reanalysis (**NARR**) winds should be considered a **reliable** wind forcing tool for estimating waves states.
- The **models** used in this study should be considered **accurate tools** for evaluating the Chukchi Sea.

Understanding how atmospheric forcing affects wave states in the southeast Chukchi Sea has been a longstanding need and has received little focus until now. This study has explored this issue from several perspectives: direct linkage of observed wave data to its synoptic forcing events; detailed analysis of wave spectral structure to distinguish between likely wave source; and examination of satellite data to identify trends in wave activity in this region. This involved selecting significant wave height events of at least +2m lasting for 6h or more from wave records and linking these events to their synoptic activity. Several methods of analysis were then performed to understand the present wave state in this region and the recent trends in order to lay the groundwork needed to make future trend projections.

The wave measurements were recorded acoustically with several Recording Doppler Current Profilers (RDCPs) located in offshore and nearshore locations. These

RDCP measurements were able to capture wave height, wave period and wave direction. These results were used to produce one-dimensional wave spectrum. Engineering practice also uses one-dimensional wave spectrum to describe wave states by use of wind-generated models. With the powerful tools of both *in situ* measurements and models, we could compare the one-dimensional wave spectrums for each, and also were able to utilize wave direction from the *in situ* measurements. This established a framework by which synoptic linkages to resultant wave states could be explored. This included the linkage between low pressure storms, winds created as a result of these low pressure systems, the limited fetch in which the wind was able to create these wave states, and the wave states themselves.

From the increasing significant wave height trend, global warming trend, and the failing conditions (eroding bluffs, outdated marine ports) already in place in the southeast Chukchi Sea, the need for better preparedness is clearly evident. Impacts have already been felt in this region where Alaska communities have had to evacuate their homes due to severe and ongoing erosion. Given the permafrost degradation in this region, the rate of sea ice decline in the Arctic, and intense storm activity, the significant wave height increase is expected to continue and lead to more damage. The area which we consider key for our future Arctic infrastructure, Delong Mountain Terminal, could become inoperable unless new engineered modifications are performed to the existing infrastructure. Also, communities will need to be relocated unless attention toward better shore protection is given. Also shipping activity, for one of the biggest northern ports in

the US, is in need of continuous real-time wave observations in coastal locations (since satellite measurements fall short), can be implemented at different locations. Shipping activity is already delayed by the large wave heights that occur in this region due to storm activity. Better monitoring of wind and wave conditions will allow shipping activity to be better prepared and continue activities. Permanent wind and wave observations will also help the infrastructure in the southeast Chukchi Sea region to be better prepared for the next large storm.

References

Coachman, L. K. and R. B. Tripp (1970). Currents North of Bering Strait in Winter. *Limnology and Oceanography*, Vol. 15, No. 4, 625-632

Comiso, J. C., C.L. Parkinson, R. Gersten, and L. Stock (2008). Accelerated decline in the Arctic sea ice cover. *Geophys. Res. Lett*. 35 doi:10.1029/2007GL031972.

Francis-Chythlook, O. (2004). Coastal Processes in Elson Lagoon, Barrow, Alaska. MS Thesis, University of Alaska Anchorage, Anchorage, Alaska.

Hudak DR and JMC Young (2002). Storm climatology of the southern Beaufort Sea. *Atmosphere Ocean,* 40, 145–158.

Janssen, P., S. Abdalla, H. Hersbach, J-R. Bidlot (2007). Error Estimation of Buoy, Satellite, and Model Wave Height Data. *J. Atmos. Oceanic Technol.*, 24, 1665–1677. doi:10.1175/JTECH2069.1

Kistler, R., E. Kalnay, W. Collins, S. Saha, G. White, J. Woollen, M. Chelliah, W. Ebisuzaki, M. Kanamitsu, V. Kousky, H. van den Dool, R. Jenne, and M. Fiorino, (2001). The NCEP-NCAR 50-Year Reanalysis: Monthly Means CD-ROM and Documentation. *Bull. Amer. Meteor. Soc*., 82, 247-267.

Li, J-G. and M. Holt (2007). Validation of a regional wave model with Envisat and Buoy observations. Proc. 'Envisat Symposium 2007', Montreux, Switzerland, 23–27 April 2007 (*ESA SP-636, July 2007)*.

Mesinger, F., G. DiMego, E. Kalnay, K. Mitchell, P.C. Shafran, W. Ebisuzaki, D. Jovic, J. Woollen, E. Rogers, E.H. Berbery, M.B. Ek, Y. Fan, R. Grumbine, W. Higgins, H. Li, Y. Lin, G. Manikin, D. Parrish, and W. Shi (2006). North American Regional Reanalysis. Boulder, CO NOAA.OAR/ESRL PSD:42.

Overland, J.E. and A.T. Roach (1987). Northward flow in the Bering and Chukchi Seas. *Journal of Geophysical Research*, Vol.92, No.C7, 7097-7105.

Panteleev, G., D.A. Nechaev, A. Proshutinsky, R. Woodgate, and J. Zhang (2010). Reconstruction and analysis of the Chukchi Sea circulation in 1990-1991. *Journal of Geophysical Research*, 115, C08023, doi:10.1029/2009JC005453.

Sienkiewicz, J.M, J.M. Von Ahn, and G. M. McFadden (2005). Hurricane Force Extratropical Cyclones. *American Meteorology Society* (2005-07-18).

Woodgate, R.A., K. Aagaard, and T. Weingartner (2005). A year in the physical oceanography of the Chukchi Sea: Moored measurements from autumn 1990-91, *Deep-Sea Research, Pt. II*, 52 (24-26): 3116-3149.

Young I.R. (1994). Global ocean wave statistics obtained from satellite observations. *Appl. Ocean Res.* 16, 235.

Zieger, S., J. Vinoth, I. R. Young (2009). Joint calibration of multiplatform altimeter measurements of wind speed and wave height over the past 20 years. *J. Atmos. Ocean. Technol.* 26, 2549.

Appendices

Appendix A – Contributions to the Dissertation Chapters

A.1 Chapter 2

The text re-editing and guidance provided by Dr. David. E. Atkinson. The writing, literature search, organizing *in situ* data for processing, and the work of corresponding author were conducted by Oceana P. Francis. Funding to support Oceana P. Francis and funding for obtaining *in situ* measurements were provided by Dr. David. E. Atkinson.

A.2 Chapter 3

The text re-editing and guidance provided by Dr. David. E. Atkinson. The writing, literature search, organizing *in situ* data for processing, and the work of corresponding author were conducted by Oceana P. Francis. Funding to support Oceana P. Francis and funding for obtaining *in situ* measurements were provided by Dr. David. E. Atkinson.

A.3 Chapter 4

All work for this paper, and the work of corresponding author were conducted by Oceana P. Francis. Technical text review before submission provided Dr. Robert E. Jensen. Linguistic text review before submission provided by Dr. David. E. Atkinson and Dr. Uma Bhatt. Funding to support Oceana P. Francis and funding for obtaining *in situ* measurements were provided by Dr. David. E. Atkinson.

A.4 Chapter 5

The Matlab codes, the satellite data processing, guidance, and text re-editing were provided by Dr. Gleb G. Panteleev. The writing, literature search, organizing *in situ* data for processing, and the work of corresponding author were conducted by Oceana P. Francis. Funding to support Oceana P. Francis and funding for obtaining *in situ* measurements were provided by Dr. David. E. Atkinson.

Appendix B – Further qualitative reading on atmospheric conditions affecting the southeast Chukchi Sea

The storms that affect the southern Bering Sea are extra-tropical cyclones, and are well documented in the scientific literature (Blier et al., 1997; Swanson, 2002; Charles and Colle, 2009; Ulbrich et al., 2009). These cyclones form within the extra-tropical regions of the Earth (30° and 60° latitude from the equator). An extra-tropical cyclone is a mass of inward spiraling winds driven by a low pressure system. Due to the Coriolis effect, the wind flow is counterclockwise in the northern hemisphere. Extra-tropical cyclones are classified as baroclinic since they form along zones of temperature and dewpoint gradient under favorable upper air conditions. Thus, they are common in the fall and winter when the jet stream is still a little farther north and where cold air moving southeast off the Asian continent encounters warm air over the Pacific Ocean. There are many more extratropical cyclones that form in the Northern Hemisphere (234 cyclones) compared to the Southern Hemisphere (37 cyclones) (Simmonds and Keay, 2000; Gulev et al., 2001). In the Arctic, the average pressure for cyclones is 988 hPa during the winter, and 1,000 hPa during the summer (Brummer et al., 2000). In the northern Pacific Ocean, the strongest extra-tropical cyclones (hurricane force) are most likely to form in December and January (Sienkiewicz et al., 2005).

These storms often have a long fetch, i.e. the length of the wind blowing in a single direction over water, so the stronger and longer the fetch length, the larger the waves it creates. However, the Bering Strait buffers these Bering Sea wave states. In the

southeast Chukchi Sea region, some of this wave energy does progress through the Bering Strait. However, most of the southeast Chukchi Sea region wave energy is from the extra-tropical cyclone winds where they are typically on the cold/poleward side of the low pressure center where the pressure gradient force is highest. The high winds over the Kotzebue Sound produce waves, which have a fetch around 160km. The most active extra-tropical cyclones are found over ice-free maritime areas (such as the Aleutians) during the winter. Extra-tropical cyclones in the north Gulf of Alaska and Bering and Chukchi Sea regions tend to loiter, thus, even though wind speeds may only be moderate, they have enough duration to allow fully-developed wave sates to be realized in the Kotzebue Sound area. Despite the shorter fetch in the Kotzebue Sound area where the RDCPs in this study were placed, these storms are able to generate wave heights greater than 3m in the SE Chukchi Sea.

Identification of location of high wind speeds globally can be found in Silvester (1974). Silvester (1974) shows a global wind pattern where high winds occur predominantly between the latitude range of 40° to 60° in both hemispheres. These are the northern latitudes where the cyclones form that affect our area of interest (SE Chukchi Sea). Kamphuis (2010) summarizes this global wind pattern by stating that warm air flowing from the equator toward the poles and cold air flowing away from the poles meet there to form the polar front. The earth's rotation then causes depression-type storms that move along this front. These storms occur throughout the year and at short intervals (i.e. hours to days); wave conditions can be expected to vary from hour to hour

throughout the year and in unpredictable patterns because this polar from shifts north-south as a result of small pressure and temperature changes. These shifts are a combination of short term, annual, and longer-term changes (e.g. El Nino). Most of the sea state is generated along this polar front. This does not include wave generation by tropical storm activity. On the polar fronts, the sea near the coasts is usually locally generated due to the regularly occurring storms near these coasts. Swell-dominated coasts are found closer to the equator where few local storms occur. On swell-dominated coasts, the wave parameters are usually constant for weeks or months.

B.1 References

Blier, W., S. Keefe, W.A. Shaffer, and S.C. Kim (1997). Storm Surges in the Region of Western Alaska. *Monthly Weather Review*, 125, 3094-3108.

Brummer, B., S. Thiemann, and A. Kirchgassner (2000). A cyclone statistics for the Arctic based on European Centre re-analysis data. *Meteorology and atmospheric physics* 75 (3–4): 233–250.

Charles M.E. and B.A. Colle (2009). Verification of Extratropical Cyclones within the NCEP Operational Model. Part I: Analysis Errors and Short-Term NAM and GFS Forecasts. *Weather and Forecasting*, 24, 1173-1190.

Gulev, S.K., O. Zolina, and S. Grigoriev (2001). Winter Storms in the Northern Hemisphere (1958–1999). *Climate Dynamics* 17, 795–809.

Kamphuis, J.W. (2010). *Introduction to Coastal Engineering and Management, Second Edition. Advance Series on Ocean Engineering – Vol. 30*, World Scientific Publishing Co. Pte. Ltd. ISBN 981-283-485-0. 525 pp.

Sienkiewicz, J.M, J.M. Von Ahn, and G. M. McFadden (2005). Hurricane Force Extratropical Cyclones. *American Meteorology Society* (2005-07-18).

Silvester, R. (1974). *Coastal Engineering: Generation, propagation and influence of waves*. Elsevier Scientific & Technology. ISBN 0444411011

Simmonds, I. and K. Keay (2000). Variability of Southern Hemisphere Extratropical Cyclone Behavior, 1958–97. *Journal of Climate*, 13 (3): 550–561.

Swanson, Kyle L. (2002). Dynamical Aspects of Extratropical Tropospheric Low-Frequency Variability. *J. Climate*, 15, 2145–2162.

Ulbrich, U., G.C. Leckebusch, and J.G. Pinto (2009). Extra-tropical cyclones in the present and future climate: a review. *Theor Appl Climatol*, 96, 117-131.

Appendix C – Further qualitative reading on wind-wave interaction

C.1 Surface winds and wave generation

Wave initiation and growth theory is well established in numerous textbooks and articles (e.g. Thoresen 2010, Sorensen 1993, 2006, Phillips 1957, 1960; Miles 1957). Theoretical discussion of waves is limited here to pointing out that they are depth, fetch and duration limited.

The significant wave height (H_s), defined to be the average wave height of the one-third largest waves, and period (T_s) depend primarily on fetch (F – the distance over which the wind blows), wind speed, (W_s – commonly measured at the 10m elevation), and the duration of the wind (t_d). Wind speed of greater magnitude results in greater wave height. The duration, which is the time the wind blows in one direction, results in greater wave height with longer duration. The fetch, which is the distance the wind blows in one direction, results in greater wave height with longer fetch. When maximum fetch and maximum duration are reached then significant wave height becomes a function only of wind speed. This is the definition of a "fully-developed sea".

Sorensen (2006) sums up the difference between fetch- versus duration-limited conditions. The growth of the significant wave height and period is a function of distance along a fetch. Fetch-limited waves are generated by a wind of constant velocity, blowing over a constant fetch and having different durations. If the wind duration exceeds the time required for waves to propagate down the entire length of fetch (i.e., $t_d > F/C_g$; where C_g is group celerity) the waves will grow in H_s and T_s but not attain their fully-developed states; their characteristics at the end of the fetch will depend on the fetch

length and the wind velocity. This is known as a "fetch-limited" condition. If the duration is less (i.e. $t_d < F/C_g$) the waves will not grow in H_s and T_s, and wave generation is "duration-limited". If both the fetch and duration are sufficiently large, maximum H_s and T_s are reached at the downwind end and a fully developed sea will be realized for that wind velocity. As the waves grow, the periods, and thus the group celerities (velocities), continually increase along the fetch so an average group celerity would have to be used to determine if waves are fetch or duration limited.

For a fully developed sea, water depth, wind duration and fetch are unlimited. As the wind velocity, fetch, and/or duration of the waves increase, the height and period of the resulting downwind waves will increase. However, there is a fixed limit to which the average height and period can grow after the wind speed has reached a certain limit, given unlimited fetch and duration. At this limiting condition the rate of wind energy input to the waves is balanced by the rate of energy dissipation due to wave breaking and surface water turbulence. This condition usually occurs in the deep open sea and is commonly not reached even in large storms (Sorensen, 2006). For the SE Chukchi Sea fetch must be considered more carefully because this is an enclosed embayment region; it is also seasonally limited by the presence of sea ice, which can act to dampen wave activity (Squire 2007).

C.2 Description of wind-sea and swell

Kinsman (1965) classified waves by their periods and heights, ranging from capillary waves that have very short wave periods (0.1 sec of less) and heights (few millimeters) to gravity waves with long periods (minutes or hours) and heights (10s of meters). Gravity waves are wind-generated waves and account for most of the available wave energy in the ocean. Gravity waves have periods ranging 1 to 30 sec and wave heights that are usually less than 10m and mostly around 1m (Kamphuis, 2010). Gravity waves, which can be subdivided either as *locally generated waves* or *swell*, are measured by the RDCP instrument.

Thoresen (2010) defines wind waves, also known as locally generated waves, to be waves generated by winds that are acting on the sea surface in the immediate vicinity of a measuring station. Swell, also known as ocean waves, are also wind-generated waves, but are created in depth unlimited conditions at a distance from the measuring station. The winds that drove the swell may be too distant to be felt at the wave measuring station, may have stopped blowing, or changed direction by the time the waves reach the station.

A local wind wave (sometimes called wind-sea) is a wave generated and influenced by the local wind field. In form, wind waves are normally relatively steep (high and short), short-crested, and are often irregular and directional, so it is difficult to distinguish wave fronts. A “wave front” is set of points, forming a continuous line or surface, in space reached by a wave at the same instant as the wave propagates. The local wind-wave state consists of many different wave heights and periods combined together

within a particular time series signal. These waves form two different wave trains which propagate at a small angle away from the dominant wind direction (Kamphuis, 2010). An irregular wave state occurs when two wave trains are superimposed upon each other. Strongly exaggerated peaks and troughs in wave height can occur, along with other variations of wave height, in accordance with general principals of destructive and constructive interference observed during superposition of waves.

A swell wave is a wave that travels out from an area of wind-wave generation. Swell is more orderly than the local wind-wave, smaller wave heights, and more pronounced wave grouping (Kamphuis, 2010). After leaving the active wind generation area, energy dissipation and lateral spreading of the waves will decrease the wave height. This preferentially affects shorter period waves so the significant period will increase (Sorensen, 2006) as the shorter period waves dampen out of the overall signal. The swells with longer wavelengths do not have steep wave heights (i.e. wave steepness is the ratio of the wave height H to the wavelength λ) and are more symmetrically shaped than local wind waves. The longest wavelengths propagate with greatest velocity and move out of the generating area first, with wave groups of progressively shorter wavelengths following.

Locally generated wind-waves are often mixed with swells. However, enclosed bodies of water, such as inland seas, often experience only locally generated wind-waves because there is no access from a larger ocean area. Wave direction is an important parameter because it allows identification of the progenitor strong-wind event that caused

the observed wave response. Sorensen (2006) summarizes that waves are generated with propagation directions aligned at a range of oblique angles (<90°) to the direction of the wind. The range of directions decreases with an increase in wave period as waves grow while propagating along the fetch. Thus, the smaller the fetch length, the lower the chance those waves will remain in the generating area and grow to appreciable size.

Less important factors controlling wave height are atmospheric stability, temporal and spatial variations in the wind field during wave generation, fetch length and, for depth-limited conditions, water depth and bottom characteristics (Sorensen, 2006). The water depth affects the transfer of energy from the wind to the waves and limits the non-breaking wave heights. Frictional interaction with an absorbing bottom material dissipates wave energy and therefore retards the rate of wave growth and wave size. However, the RDCP station was found to be in "deep-water" so bottom friction was not a factor in this study.

Accurate calculations of the wave heights at the end of a fetch require a detailed knowledge of the fetch and the wind field (Thoresen, 2010). There are two types of fetch, "effective fetch" and "straight line fetch". To find "effective fetch", an angle of 45° on either side of the wind direction needs to be constructed and divided into 6° intervals to the shoreline. These radials are extended from the measurement site until they first intersect the shoreline. The length component of each radial in the direction parallel to the wind direction is measured and multiplied by the cosine of the angle. The resulting values for each radial are added together and divided by the sum of the cosines of all the

individual angles. The “straight line fetch” is merely the straight line distance along the wind direction from the mooring to the shoreline. Thoresen (2010) recommends that straight line fetch should be used to define fetch length for applications. Fetch analysis in this paper subscribes to this recommendation.

Therefore for simple applications, we can consider a wave field simply defined by a selected constant wind speed and straight fetch length having a specified duration (Sorensen, 2006).

C.3 References

Kamphuis, J.W. (2010). *Introduction to Coastal Engineering and Management, Second Edition. Advance Series on Ocean Engineering – Vol. 30*, World Scientific Publishing Co. Pte. Ltd. ISBN 981-283-485-0. 525 pp.

Kinsman, B. (1965). *Wind Waves*. Prentice-Hall, Englewood Cliffs, NJ, 676 pp.

Miles, J.W., (1957). On the generation of surface waves by shear flows. *J. Fluid Mech*. 3, 185-204.

Phillips, O.M., (1957). On the generation of waves by turbulent wind. *J. Fluid Mech*., 2, 417-445.

Phillips, O.M. (1960) On the dynamics of unsteady gravity waves of finite amplitude. Part l.The elementary interactions. *J. Fluid Mech*., 9, 193-217.

Sorensen, R.M. (1993). *Basic Wave Mechanics for Coastal and Ocean Engineers*. John Wiley & Sons, Inc. ISBN 0-471-55165-1. 284 pp.

Sorensen, R.M. (2006). *Basic Coastal Engineering, Third Edition.* Springer Science. ISBN 0-387-23332-6. 324 pp.

Squire, V.A. (2007). Of ocean waves and sea-ice revisited, Cold Regions Science and Technology, 29, 110-133.

Thoresen, C.A. (2010). *Port designer's handbook, Second edition.* Thomas Telford Ltd. ISBN 978-0-7277-4086-1. 554 pp.

Appendix D - Further quantitative reading on one-dimensional wave spectra

The statistical variability of the water surface elevation can be modeled in terms of the Fourier series. Waves appear in a confused state with successive heights, periods and wave length varying significantly. The actual direction of propagation is also often difficult to define. Instead of an orderly sinusoidal form (WMO, 1998) given by

$$\eta = a\sin(kx - \omega t) \tag{D.1}$$

the typical water surface is confused so representation is done by the use of spectral or Fourier model. Under this approximation, the water surface elevation is approximated by the linear superposition of sinusoidal forms as defined by Equation D.1 (WMO, 1998) as

$$\eta(t) = \sum_{i=1}^{N} a_i \sin(\omega_i t + \phi_i) \tag{D.2}$$

where a_i, ω_i, and ϕ_i are the amplitude, frequency and phase of the *i*th component in the summation. From Equation D.2, a complex water surface record can be constructed from the summation of a number of sinusoids. The average energy of the wave profile (WMO, 1998) can be represented as

$$\overline{E} = \frac{\rho_\omega g}{8} \sum_{i=1}^{N} H_i^2 \tag{D.3}$$

which also describes the variance of the record, σ^2 (WMO, 1998) as

$$\frac{\overline{E}}{\rho_\omega g} = \frac{1}{2N} \sum_{i=1}^{N} a_i^2 = \sigma^2 \tag{D.4}$$

Therefore, the amplitude components, a_i^2 are related to the energy of the record, the distribution of which as a function of frequency could be represented by plotting a_i^2 versus frequency. This amplitude spectrum is discrete, represented only at the frequencies ω_i of the summation (Equation D.2). As $N \to \infty$, the amplitude spectrum can be transformed into the continuous spectrum, $F(f)$ (WMO, 1998) where

$$F(f)\Delta f = \frac{a_i^2}{2} \tag{D.5}$$

The spectrum, $F(f)$ is called the frequency, omni-directional (no direction is associated with the spectrum) or variance (as the area under the spectrum is the variance f the record) spectrum (WMO, 1998)

$$\sigma^2 = \int_0^\infty F(f)\mathrm{d}f \tag{D.6}$$

The choice of the values of ϕ_i will influence the resulting water surface elevation, but have no influence on the spectrum.

Typical spectra of wave systems have a form where the squared amplitudes for each component are plotted against their corresponding frequencies. In this study, wave spectra were computed by Fast Fourier transform (FFT), developed by Cooley and Tukey (1965). The FFT size was selected to be 128. Wave spectrum plots are expressed in terms of Energy density ($\mathrm{m^2Hz^{-1}}$) versus Frequency (Hz). The wave energy E equals $\rho_w g H^2/8$ or $\rho_w g a^2/2$ ($H = 2a$). The term $\rho_w g$ is dropped and $a^2/2$ or, a^2, is plotted along the vertical axis. The wave-energy spectrum is therefore synonymous to the variance spectrum $S(f)$. The wave spectral plots give a continuous curve connecting the discrete points found from the Fourier analysis.

The curves and peaks from the wave spectral plots describe the sea state. Irregular seas give rise to broad spectra which may show several peaks. These may be clearly separated from each other or merged into a very broad curve with several humps. Swell will generally give a very narrow spectrum concentrating the energy in a narrow range of frequencies (or wavelengths) around a peak value. Such a narrow spectrum is associated with the relatively “clean” appearance of the waves.

Wave direction is not represented on the frequency spectral plots, only "energy" distribution over wave frequencies, $E(f)$. On the vertical axis, a measure for the wave energy is plotted in units of $\mathrm{m^2Hz^{-1}}$. This unit is usual for "frequency spectra". We have seen earlier that, although spectrum may be continuous in the theory, in practice the variances (or energies) are computed for discrete frequencies. An example for obtaining a^2 is where a frequency of 0.16 Hz is considered to be a mean value in an interval which could be 0.155 to 0.165 Hz. The value, divided by the width of the interval, is a measure for the energy density and expressed in units of $\mathrm{m^2Hz^{-1}}$ (again omitting the factor $\rho_w g$). Therefore, the wave spectrum is often referred to as the *energy-density spectrum*.

D.1 References

AADI (Aanderaa Data Instruments) (2006). *RDCP Primer TD 220c*, 70 pp.

Cooley, J.W. and J.W. Tukey (1965). An algorithm for the machine calculation of complex Fourier series. *Math. Comput.* 19, 297–301.

WMO (1998). Bouws E, Draper L, Shearman EDR, Laing AK, Feit D, Mass W, Eide LI, Francis P, Carter DJT, Battjes JA. Guide to Wave Analysis and Forecasting, 2nd edn, *WMO - No.702. World Meteorological Organization:* Geneva; Switzerland

Appendix E – Recording Doppler Current Profiler

E.1 Acoustic-based measurements

The Recording Doppler Current Profiler (RDCP) uses the Doppler principle (Doppler, 1842) to measure water velocity which relates the change in frequency of a source to the relative velocities of the source and the observer (AADI, 2006). There are two methods of measuring the Recording Doppler Current Profiler (RDCP) employs: pressure-based and acoustic-based. The method of measuring in this study was done acoustically where the RDCP measured significant wave height, wave period, and wave direction.

For acoustic-based measurements, the RDCP applies the Doppler principle by acting both as a source and receiver while bouncing short pulses of acoustic energy off small particles, plankton and air bubbles (e.g. scatterers) that are usually present in the sea. When the scatterers move towards the source, the sound shifts to a higher frequency, and then part of it is backscattered towards the source. For the RDCP, the sound is shifted one time as perceived by the scatterers and a second time as perceived by the current profiler transducers.

The RDCP consisted of 4 transducers in a Janus configuration that act as both transmitters and receivers. The transducers are orientated 90º in azimuth from each other and with a 20-30º angle to the vertical mounted on a cylindrical shaped housing contacting the electronics. This configuration of beams looks forwards and backwards. The four transducers transmit short pulses (pings) of acoustic energy along narrow beams, acoustically imaging a water volume determined by the distance along the beam,

the width of the beam and the pulse duration. Due to the presence of scatterers in the water, a fraction of the transmitted energy is backscattered towards the instrument at successive times after transmission representing successively increasing distances from the transducers.

The sampling occured at a 2Hz rate (2 samples per second) so therefore 1800 samples were recorded within the 15-minute duration of the RDCP wave record.

The wave motion at the sea surface causes a dynamic pressure that can be measured by use of a pressure sensor attached to the RDCP. To obtain RDCP wave data, the RDCP instrument applies several steps. The total water pressure = atmospheric pressure + hydrostatic pressure due to the weight of the water + a dynamic pressure due to surface wave motion. The atmospheric pressure to the absolute pressure is subtracted from the samples and a fixed atmospheric pressure from RDCP is used (101.3 Pa). The hydrostatic pressure is calculated and subtracted from the time series samples, and is used to calculate deployment depth. The dynamic pressure depends on the surface wave period and the sensor deployment depth and is used to calculate the wave spectrum. Calculation of the wave spectrum involves Fourier transformation of the time series using a Fast Fourier Transform (FFT) algorithm and scaling of the power spectrum to compensate for the damping of the dynamic pressure.

The damping of the dynamic pressure can be described by Linear Wave Theory. We elaborate on the Stokes' Wave Theory in detail in the dissertation. As the damping factor approaches 1, the observed dynamic pressure approaches the true dynamic

pressure. To compensate for the damping of the dynamic pressure, the power spectrum is multiplied with a transfer function that is the inverse of the function describing the damping of the dynamic pressure. The deeper the sensor is deployed the more is the dynamic pressure damped. The shorter the surface wave period, the faster the damping of the dynamic pressure will be. Hence, the power spectrum must be scaled to correct for the difference between the true dynamic pressure and then observed dynamic pressure before the wave parameters can be calculated.

E.2 RDCP wave parameters

The RDCP recorded a number of wave observations which we will denote here as N. Each N is composed of 15 minutes of individual wave observations i, which records every cycle when the RDCP awakens. In essence, the RDCP wave observations N are a summary of the individual wave observation i. The individual wave observations i that the RDCP records are wave height H_i, wave period T_i and wave direction D_i. From wave height H_i, wave period T_i and wave direction D_i, the RDCP estimates the following: significant wave height, H_{m0}, mean wave period, T_{m01}, mean zero crossing, T_{m02} *or* $\overline{T}_z$, Energy wave direction, D_E, Mean direction, D_m, and Peak direction, D_p. Depending on the length which the RDCP is set up to record or its battery life, determines the number of observations, N. For our purposes in this study, we use significant wave height, H_{m0}, mean zero crossing (i.e. mean wave period), T_{m02}, and mean wave direction, D_m.

The RDCP measured the significant wave height, H_{m0} from 15 minutes of wave height H_i observations. H_{m0} in general terminology is approximately equal to $\overline{H}_{1/3}$ which is the average height of the highest 33% of waves in a wave record measured from the highest point of a wave (crest) to the lowest point (trough). So the RDCP recorded the wave heights H_i for 15 minutes and computed highest 33% of waves in its 15-minute wave record, and gave a significant wave height H_{m0}.

The RDCP measured mean zero crossing (i.e. mean wave period), T_{m02}, from 15 minutes of individual wave period T_i observations. The average (or mean) of the individual wave periods T_i were taken to compute T_{m02}. The average or mean wave period, also called zero-crossing wave period T_{m02} or $\overline{T}_z$, is the time obtained by dividing the record length by the number of downcrossings (or upcrossings) in the record, where $T_{m02} = \sqrt{m_0 / m_2}$. The mean zero crossing T_{m02} is used because it is commonly used in wave record analysis for height and period (Sorensen, 2006) and is also used in the zero-upcrossing method (Pierson, 1954).

The RDCP measured mean wave direction, D_m from 15 minutes of individual wave direction D_i observations. The average (or mean) of the individual wave direction D_i were taken to compute D_m. Mean wave direction, D_m is the direction corresponding to the angle of the vector arising when all contributions in the spectrum are summed. Since the purpose of our study is to correlate wind and wave direction, and the mean wind direction is used (Mesinger et al., 2006), the mean wave direction D_m is used. RDCP wave direction is defined as the direction from which the wave is coming from. Wave direction is given in degrees, with 0º (North), 90º (East), 180º (South), and 270º (West). So for example, a wave having a direction of 135º is coming from a south-eastward direction and going in a north-westward direction.

E.3 RDCP Setup

A recording time of 20 minutes was set for all 3 RDCPs (Stations 2007, 2009N, and 2009S) with acoustic waves being measured for 15 minutes out of this 20 minutes, and ocean currents being measured for 5 minutes. This means that the duration of N was 20 minutes long comprised of 15 minutes of wave recording + 5 minutes of currents recording. The frequency was 2 Hz. Station 2007 recorded every 1.5h (i.e. the instrument was 1.5h at rest) for 3816h and 6 minutes. The number of wave observations was N = 1704. Station 2009N recorded every 2.0h for 8041h and 15 minutes. The number of wave observations was N = 4596. Station 2009S recorded every 2.0h for 8204h. The number of wave observations was N = 4689.

As stated in AADI (2006), the RDCP 600 transducers are tilted 25° off the vertical axis. Therefore, the distance to the surface/bottom along the vertical axis is shorter than along the main lobe axis. As a result, strong signals backscattered off the surface/bottom originating from the pressure field outside the main lobe arrive at the same time as the backscattered signal from the main lob pressure field and may obscure these cells. AADI (2006) estimates that for a 25º beam angle about 10% of the water volume closest to the surface may hold inaccurate data. This was seen with the surface cell wave data. So for wave measurements in this study, Cell 1 (i.e. cell directly below the surface cell) was used instead of the surface cell due to strong scatterers in the surface cell.

The recorded data by the RDCP600 indicated very good signal strength. Signal strength above -45 is considered good. Signal strength below -45 is considered bad (i.e.

noisy). The signal strength for all three Stations was well above -45 which indicated very good signal strength. This was assumed to be due to the higher accumulation of small particles in the water which are especially prevalent in southeast Chukchi Sea region. This also accounts for good wave direction recorded by the RDCP at a deeper depth than the recommended 20m for acoustic reading (AADI, 2006) since acoustic energy requires small particles which it can bounce off of to measure.

E.4 RDCP Profiles (Columns)

The RDCP 600 was configured to deal with several profiles (columns) simultaneously. Each column was setup as either instrument referred or surface referred, cell overlap or no cell overlap, and individual cell size. The three different column types are:

- *Instrument referred column* starts at a certain distance from the instrument and extends above the instrument to a certain range. Instrument referred columns are not influenced by tidal variations. This type of application is good for deep waters or when bottom currents are to be monitored.
- *Surface referred column* starts at a certain distance from the surface and extends down in the sea. The instrument utilizes the high accuracy pressure sensor to measure the distance from the instrument to the surface and uses this information to maintain the column starting position. A surface referred column will automatically compensate for tidal variations. Surface referred columns that extend below the instrument are skipped and padded with zeros in the data. This type of application is good for measuring currents and waves close to the surface or monitoring current speeds at a certain depth.
- *Surface cell* is a surface referred column that is one single cell aligned so that the center of the cell is located at the surface.

Cell overlap is the overlap of one cell to its neighboring cells. This feature improves the vertical resolution of the sea column without sacrificing data quality. By using a cell overlap, you can achieve improved near surface measurements.

Table E.1. RDCP Profile (column) setup for Stations 2007, 2009N, and 2009S

Category	**Column 1**	**Column 2**	**Column 3**	**Column 4**	**Surface**
Surface referred	Yes	No	Yes	No	Yes
Distance to column (m)	1	2	1	2	-1
Cell size (m)	2	2	2	2	2
Number of cells	10	9	15	15	1
Cell overlap (%)	0	0	40	40	0
Column size (m)	20	18	18	18	2

For the wave analysis of the RDCP, all columns are taken into consideration and there is a choice to use either the top Surface cell or Cell 1. The Surface cell was found to have a noisy signal and on occasion produced a significant wave height that was deemed unreasonable for this area (i.e. 12m). Cell 1 however produced a reasonable significant wave height (i.e. 3m) typical for the southeast Chukchi Sea region during a storm, so Cell 1 was used in this study.

E.5 References

AADI (Aanderaa Data Instruments) (2006). *RDCP Primer TD 220c*, 70 pp.

Doppler, J. C. (1842). Über das farbige Licht der Doppelsterne und einiger anderer Gestirne des Himmels. In *Versuch einer das Bradley'sche aberrations-theorem als integrirrenden Theil in sich schliessenden allgemeineren Theorie* (p. 465). Prague: K. Böhm Gesellschaft der Wissenschaften.

Mesinger, F., G. DiMego, E. Kalnay, K. Mitchell, P.C. Shafran, W. Ebisuzaki, D. Jovic, J. Woollen, E. Rogers, E.H. Berbery, M.B. Ek, Y. Fan, R. Grumbine, W. Higgins, H. Li, Y. Lin, G. Manikin, D. Parrish, and W. Shi (2006). North American Regional Reanalysis. Boulder, CO NOAA.OAR/ESRL PSD:42.

Pierson, W.J. (1954) An electronic wave spectrum analyzer and its use in engineering problems. New York Univ NY Report Date : OCT 1954.

Sorensen, R.M. (2006). *Basic Coastal Engineering, Third Edition.* Springer Science. ISBN 0-387-23332-6. 324 pp.